NOVA SCHOOL OF SCIENCE & TECHNOLOGY

DEPARTMENT OF PHYSICS

MARTA FILIPA CASTRO NUNES CRISPIM DOS SANTOS

BSc in Materials Engineering Science

NANO-ENGINEERED PLATFORMS FOR IMAGING AND TARGETING OF THE BREAST CANCER MICROENVIRONMENT

MASTER IN BIOMATERIALS AND NANOMEDICINE

NOVA University Lisbon

November, 2023

NOVA SCHOOL OF SCIENCE & TECHNOLOGY

DEPARTMENT OF PHYSICS

NANO-ENGINEERED PLATFORMS FOR IMAGING AND TARGETING OF THE BREAST CANCER MICROENVIRONMENT

MARTA FILIPA CASTRO NUNES CRISPIM DOS SANTOS

BSc in Materials Engineering Science

Adviser: João Miguel de Oliveira Conniot
Post-Doctoral Researcher, NMS-NOVA University

Co-adviser: Paula Isabel Pereira Soares
Principal Researcher, FCT-NOVA University

Examination Committee

Chair: Jorge Alexandre Monteiro de Carvalho e Silva
Associate Professor, FCT-NOVA University

Rapporteur: Gabriela Araújo da Silva
Associate Professor with Aggregation, NMS-NOVA University

Adviser: João Miguel de Oliveira Conniot
Post-Doctoral Researcher, NMS-NOVA University

MASTER IN BIOMATERIALS AND NANOMEDICINE

NOVA University Lisbon
November, 2023

Nano-engineered platforms for imaging and targeting of the breast cancer microenvironment

This document was created with the (pdf/Xe/Lua)LaTeX processor and the NOVAthesis template (v7.1.5) [1].

For my dear grandpa, without whom I would not have been
inspired to pursue a degree in science and engineering.
To my mom, for everything in life.
To my boyfriend, "sic parvis magna"

Acknowledgements

First and foremost, I would like to express my sincere gratitude to all those who have contributed to the completion of this master thesis. Without their support and guidance, I would not stand here today with such work.

I am deeply thankful to my thesis adviser, João Miguel de Oliveira Conniot for his support and expertise, and for always pushing me to do my best. I want to thank my co-adviser, Professor Paula Isabel Pereira Soares, for her assistance and availability throughout the year. I also want to extend my gratitude to NOVA Medical School Research, specially Dr. João Conde and Dr. Bárbara Mendes, and all the Conde NanoLab's team for the opportunity to do my master thesis with them, sharing their knowledge and experience. Qualities that I will carry with me into my future professional and personal lives.

I am also grateful to NOVA School of Science and Technology, the Departments of Materials Science, Life Sciences, Physics and Chemistry for the past six years that were filled with knowledge, experiences, and memories. Thanks to Professor Jorge de Carvalho e Silva, it was an honour to be able to belong to the first edition of the masters in Biomaterials and Nanomedicine. I welcome the new opportunities this Master will bring in the upcoming future.

A special thanks to my lab partners and dear friends, Mariana Pereira, Jhenifer Oliveira, and Diana Sousa for all the support you gave me throughout the year, all the lunches we've shared, late evenings around DLS, all the laughter and the love you gave me. To many more "spheoids", "polipipetações" and "rodamonas". Without you this thesis would not have been the same.

Thank you, Margarida, Rita, and Carolina, for putting up with me since the beginning of college, for your guidance and affection. To my darling friends Inês, Matilde, and Marta, I could not have asked for a better friend trio for the last two years. Thank you for all the moments we have shared, I count on sharing many more in the future.

I also owe a big thanks to my long-time loving friends for always being by my side, listening to my worries and achievements. You have been a pilar through many important moments in my life. I also want to thank everyone that has crossed paths with me, has given me advice and helped me become a better person.

To my uncle, Miguel, I thank you for helping me continuing my studies and for believing that I would achieve anything.

I also want to thank my caring and supportive boyfriend, Guilherme. Your love and devotion have been everything to me for the nine years of our relationship. Your commitment throughout the years has been extremely important. Your sense of humour and laughter has made me cope with the bad moments in my life and inspired me to keep going when I feel like giving up. You bring out the best in me and I treasure every single moment we share as we journey through life together. I love you very much.

To my dear furr friends, Meggie, Batman, Mr. Tom and Mikas, thank you for all the invasion of personal space, allowing me to cuddle you even when you want to jump out of my lap and for being my all-time companions. Meggie, thank you for our philosophi-cat conversations. Batman, thank you for your extreme need of attention in the meowrnings. Mr. Tom, thank you for your high-and-might looks, but I still love you anyways. Mikas, thank you for your yellow cat crazy but loving energy. You are all purr-fect.

Lastly, but most importantly, thank you mom for everything. Thank you for always being an inspiration of strength, knowledge, and power. For giving me all the love you have and more. Thank you for always having my back every step of the way. I am all grown up now, but I still learn from you every day. As we always say, I love you to the moon and back.

”

“Is tu fuil ‘o mo chuislean, is tu cnaimh de mo chnaimh. Is leatsa mo bhodhaig, chum gum bi sinn ‘n ar n-aon. Is leatsa m’anam gus an criochnaich ar saoghal.”

— J.F., Out
(my coping mechanism)

Abstract

Breast cancer, a highly heterogeneous disease, remains a challenge in oncology. It includes distinct subtypes (luminal, HER2-enriched, and triple-negative breast cancer), each with unique clinical features and treatment responses. Despite advances in conventional therapies, improving outcomes for breast cancer patients still require innovative approaches. This project aimed to improve breast cancer treatment by developing targeted nanosystems for gene delivery, to address the complexities of the tumour microenvironment. The primary objective was to formulate poly-(lactic acid) (PLA)-based nanoparticles (NP)s, optimising their physical characteristics. The resulting NPs displayed hydrodynamic diameters around 200 nm, positive zeta potential +8 mV and low polydispersity index (<0.2), ensuring excellent stability and suitability for further functionalisation. Significantly, these PLA-based nanoparticles exhibited notable versatility. They efficiently complexed with nucleic acids (NA) (plasmid DNA (pDNA) and miR-125b), forming NP complexes whose properties depended on N/P ratios. Importantly, this study demonstrated the biocompatibility of these PLA-based NPs. They exhibited negligible toxicity across various breast cancer cell lines (BT-474, SK-BR-3 and MDA-MB-231), rendering them promising candidates for safe and effective drug delivery. Furthermore, these NPs were efficiently taken up by 2D cell cultures, indicating their potential for intracellular drug delivery. Additionally, a robust 3D cell culture model using BT-474 spheroids was established, providing a more physiologically relevant system for studying the breast cancer microenvironment. The incubation of BT-474 spheroids with the NA complexed PLA-based NPs exhibited limited transfection efficiency which might be due to the spheroids morphology. In conclusion, this study presents a promising platform of PLA-based NPs for the possible treatment of breast cancer. These NPs offer precise targeting capabilities and adaptability for gene therapy applications, addressing the challenges posed by breast cancer's molecular diversity. In the future, this research opens doors to advanced nano-based therapies and personalised treatments in the fight against breast cancer.

Keywords: Breast cancer, polymeric nanoparticles, miRNA, gene therapy, poly-(lactic acid), tumour microenvironment, miR-125b

The research work described in this dissertation was carried out in accordance with the norms established in the ethics code of NOVA University of Lisbon. The work described and the material presented in this dissertation, with the exceptions clearly stated, constitute original work carried out by the author.

Resumo

O cancro da mama, uma doença altamente heterogénea, continua a ser um desafio oncológico. Inclui vários subtipos distintos: luminal, HER2 amplificado e triplo negativo, cada um com características clínicas e respostas terapêuticas únicas. Apesar dos avanços nas terapias convencionais, melhorar os resultados para pacientes com cancro da mama requer abordagens inovadoras. Este projeto visou aprimorar o tratamento do cancro da mama desenvolvendo nanossistemas direcionados para entrega de material genético. O objetivo principal envolveu a formação de nanopartículas (NP) de ácido polilático (PLA) otimizando as características físicas. As NP resultantes tinham aproximadamente 200 nm de diâmetro hidrodinâmico, potencial zeta positivo (8 mV) e baixo índice de polidispersão (<0,2), garantindo excelente estabilidade e funcionalização adicional. As NP baseadas em PLA complexaram eficientemente com ácidos nucleicos (AN) (DNA plasmídico e miR-125b), formando complexos cujas propriedades dependiam das proporções de rácios amina/fosfato. Este estudo demonstrou a biocompatibilidade das NP baseadas em PLA, com baixa toxicidade em várias linhas celulares de cancro da mama (BT-474, SK-BR-3 e MDA-MB-231), tornando-as candidatos promissores para a administração segura de fármacos. As NP entraram eficientemente em culturas de células 2D, demonstrando potencial para administração intercelular de fármacos. Além disso, estabeleceu-se um robusto modelo de cultura celular 3D usando esferoides BT-474, fornecendo um sistema mais relevante para estudar o microambiente tumoral. A incubação de esferoides BT-474 com as NP complexadas com NA exibiu eficiência de transfeção limitada, possivelmente devido à morfologia dos esferoides. Em conclusão, este estudo apresenta uma plataforma promissora de NP baseadas em PLA para o tratamento do cancro da mama, colmatando os desafios da diversidade molecular. Esta investigação abre portas a terapias avançadas de nanomedicina e tratamentos personalizados na luta contra o cancro da mama.

Palavras-chave: Cancro da mama, nanopartículas poliméricas, microRNA, terapia genética, ácido polilático, microambiente tumoral, miR-125b

O trabalho de investigação descrito nesta dissertação foi realizado de acordo com as normas estabelecidas no código de ética da Universidade Nova de Lisboa. O trabalho descrito e o material apresentado nesta dissertação, com as exceções claramente indicadas, constituem trabalho original realizado pela autora.

Contents

List of Figures

List of Tables

Acronyms

AC	Acoustic *(p. 21)*
AFM	Atomic force microscopy *(pp. 16, 21, 29, 31, 32, 35)*
ASOs	antisense oligonucleotides *(p. 14)*
AuNP	Gold NP *(p. 8)*
BC	Breast cancer *(pp. 1–9, 11, 14–16, 18, 22, 42, 48, 49)*
BRCA	Breast Cancer gene *(p. 4)*
CFM	Confocal fluorescence microscopy *(p. 25)*
CME	Clathrin-mediated endocytosis *(p. 28)*
CMV	Cytomegalovirus *(p. 17)*
CRISPR	Clustered Regularly Interspaced Short Palindromic Repeats *(p. 13)*
CRISPR-Cas9	CRISPR associated protein 9 *(p. 13)*
CTLA-4	Cytotoxic T lymphocyte-associated protein 4 *(p. 6)*
DAPI	4',6'-diamino-2-fenil-indol *(pp. 26, 41)*
DCM	Dichloromethane *(pp. 18, 19)*
DLS	Dynamic light scattering *(pp. 16, 20, 27–29, 31–35)*
ECM	Extracellular matrix *(pp. 2, 4–6, 12)*
EDTA	Ethylenediaminetetraacetic acid *(pp. xvii, 21, 22, 25)*
ELS	Electrophoretic light scattering *(p. 20)*
EPR	Enhanced permeability and retention *(pp. 8, 28)*
ER	Oestrogen receptor *(pp. 1, 2)*
FBS	Foetal Bovine Serum *(pp. 22, 25)*
FDA	US Food and Drug Administration *(p. 10)*
HA	Hyaluronic acid *(pp. 9, 10)*

HER Epidermal Growth Factor *(pp. 1, 2, 6, 15)*
HIF-1 Hypoxia inducible factor 1 *(p. 3)*
HR Hormonal receptors *(p. 2)*
HS Hydrodynamic size *(pp. 16, 20, 27, 29, 31–36)*
HT Hormonal therapy *(pp. 1, 6, 13)*

IHC Immunohistochemistry *(p. 1)*
INP Inorganic NP *(p. 8)*
iRFP713 infrared fluorescent protein 713 *(pp. 17, 46)*
IT Immunotherapy *(p. 6)*
ITH Intra-tumoral heterogeneity *(pp. 2, 4)*

LB Luria Broth *(p. 17)*
LbNp Lipid-based NP *(p. 8)*

MA Metabolic activity *(pp. 24, 43–45)*
mcDNA minicircle DNA *(p. 13)*
miR microRNA *(pp. 14–24, 33–41, 44–49)*
miRNA microRNA *(pp. 11, 14, 15, 28)*
mRNA Messenger RNA *(pp. 13, 15)*
MTT 3-(4,5-dimethylthiazol-2-yl)-2,5-diphenyltetrazolium bromide *(pp. 24, 43–45, 48)*

NA Nucleic acid *(pp. 9–14, 16, 18–24, 28, 31, 33, 43, 47, 48)*
NADPH Nicotinamide adenine dinucleotide phosphate *(p. 24)*
NMR Nuclear Magnetic Resonance *(p. 18)*
NP Nanoparticle *(pp. 3, 7–16, 18–25, 27–49)*

PAMAM Poly-amidoamine *(pp. 10, 11)*
PARP Poly ADP ribose polymerase *(pp. 3, 4)*
PBS Phosphate-buffered Saline *(pp. 19, 23–26)*
PCL poly(ϵ-caprolactone) *(pp. 10, 11)*
PD-1 Programmed death-1 *(p. 6)*
pDNA plasmid DNA *(pp. 11, 13, 16, 21, 31–39, 41, 44–49)*
PEG Polyethylene glycol *(pp. 8, 11, 12, 18)*
PEI Polyethylenimine *(p. 10)*
Pen-Strep Penicillin streptomycin *(p. 22)*
PFA Paraformaldehyde *(p. 25)*
PI Polydispersity index *(pp. 16, 20, 27–29, 31, 33, 34)*
PLA Poly-(Lactic Acid) *(pp. 10–12, 16, 18, 19, 23, 27–33, 45, 47–49)*

PLGA poly(lactic-co-glycolic acid) *(pp. 10, 11)*
PLL poly-L-Lysine *(pp. 10, 12)*
PNB para nitro benzyl *(p. 18)*
PNP Polymeric NP *(pp. 8–11, 14)*
PR Progesterone receptor *(p. 1)*
PVA Polyvinyl alcohol *(pp. 12, 19)*

RNAi RNA interference *(p. 13)*
RT Room temperature *(pp. 18, 20, 21, 24, 25, 29)*

saRNA self-amplifying RNA *(p. 14)*
shRNA short hairpin RNA *(p. 14)*
siRNA Small interfering NP *(pp. 8, 10, 14)*
SPIONS Superparamagnetic iron oxide NP *(p. 9)*

TBE Tris-Borate EDTA *(pp. 21, 22)*
TC Tissue culture *(pp. 22, 23)*
TEA triethylamine *(p. 18)*
TLC thin layer chromatography *(p. 18)*
TME Tumour microenvironment *(pp. 2–5, 11, 42)*
TNBC Triple Negative Breast Cancer *(pp. 1, 2, 6)*
TPGS D-alpha-Tocopherol polyethylene glycol 1000 succinate *(pp. 16, 18, 19, 23, 27–29, 31–34, 47–49)*
TT Targeted therapy *(pp. 6, 7)*

UV Ultraviolent *(pp. 22, 23, 25)*

WHO World Health Organization *(p. 1)*

ZP Zeta potential *(pp. 16, 20, 27–29, 31, 33–35, 48, 49)*

1 Introduction

1.1 Breast Cancer

1.1.1 Definition and risk factors

Breast cancer (BC) is the most common type of diagnosed cancer among women and the number one cause of cancer-related deaths among women globally [2, 3, 4]. According to the World Health Organization (WHO), 2.3 million women having been diagnosed with BC in 2020 resulting in 650 000 deaths globally. Although BC is usually associated as a women's disease, it is not exclusive. It may also occur in men. However, the diagnosed cases of BC in men account for less than 1% [2].

Several risk factors play a role in BC occurrence and progression. Factors such as physical traits (gender and age), genetic factors and ethnicity are inherent to each individual and differently influence the expression of the disease. Other factors as demographic distribution, lifestyle, and long-term Hormonal therapy (HT) are extrinsic and can be modified to prevent the development or slowdown the progression of BC [5, 6, 7].

BC classification is still ongoing and evolving by integrating new findings and knowledge from advances in research and the clinic [8]. Despite this, it is a disease that is generally regarded as highly heterogeneous [2, 9, 10, 11] with substantial genetic and clinical variability [2], which translates to various different presentations among the patients [12].

The WHO has updated the 2012 classification of BC tumours which divides them by major tumour groups. The groups are breast carcinoma, neuroendocrine tumours and other types and newly recognised entities [8]. Regardless of this classification, factors such as invasiveness, morphology, expression of Immunohistochemistry (IHC) markers and, recently, genetic panels are frequently used to classify BC [2]. A very common and important classification of BC is based on the expression of hormone receptors (oestrogen and progesterone) and Epidermal Growth Factor (HER)2 status [11, 9, 12, 13]. According to the different expression levels, BC can thus be classified as Oestrogen receptor (ER) positive, Progesterone receptor (PR) positive, HER2 positive, or Triple Negative Breast Cancer (TNBC), which lacks expression of the three mentioned receptors. Based on the

Hormonal receptors (HR), BC tumours can be further classified as Luminal A (HR positive and HER2 negative) or Luminal B (HR positive and HER2 positive or negative) [14, 10, 11, 12, 9]. These subtypes are further exemplified in Figure 1.1.

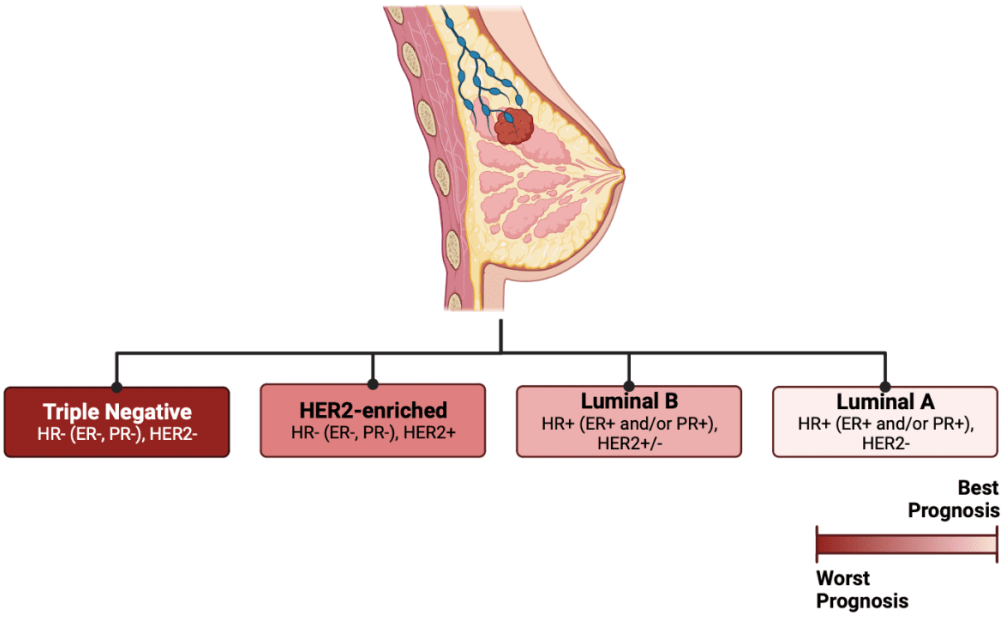

Figure 1.1: BC subtypes, expression profiles and associated prognosis. Designed via Biorender.

The four subtypes are also associated with different prognosis according to their aggressiveness. Luminal A and B are associated with the best prognosis since they are ER positive and normally respond well to hormonal treatments [15, 16]. HER2 is associated with a poor prognosis since the overexpression of HER2 is related with an aggressive phenotype of tumour cells, anti-hormonal cytotoxic resistance, and low survival [17, 16]. TNBC does not express any of the mentioned receptors. Thus, the lack of available effective treatments worsens the prognosis of patients diagnosed with this subtype [15].

1.1.2 Tumor microenvironment

The Tumour microenvironment (TME) is comprised of proliferating tumour cells and non-tumoral cells. These comprise fibroblasts, immune cells, infiltrating inflammatory cells, adipocytes, myoepithelial and endothelial cells. Components of the Extracellular matrix (ECM) and soluble factors such as cytokines, hormones, growth factors and enzymes, also comprise this microenvironment [18, 19, 20]. These elements trigger a state of constant change in the TME that varies with BC tumour type and is influenced by time and tumour progression.

The epithelial cells are influenced by the stromal cells through the secretion of many ECM proteins, chemokines, cytokines, and growth factors [21, 22]. TME is characterised by oxidative stress, hypoxia, and acidosis and by interactions between these different cell types, which will promote cellular genomic and biological differences. They also stimulate clonal evolution and, as a result, increase Intra-tumoral heterogeneity (ITH).

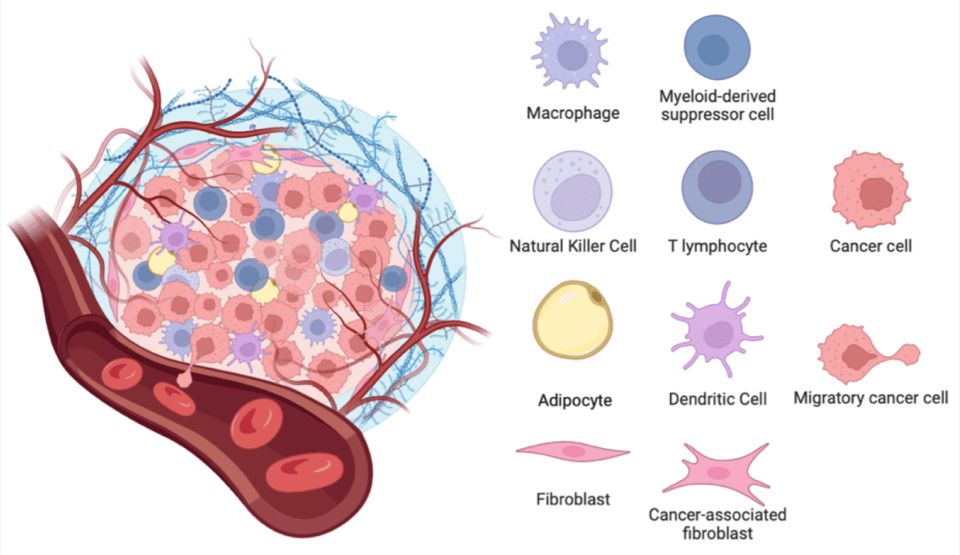

Figure 1.2: TME representation and the various cell it comprises. Designed via Biorender

Induction of angiogenesis, immune system modulation, and control over the survival, growth, and metastasis of cancer cells are the main effects of the interactions in the TME [23, 24, 25]. Furthermore, the mutagenic characteristic of tumour cells predisposes to epigenetic modifications in the non-tumorigenic cells that comprise the TME [23].

As BC, and cancer in general, is characterised by an uncontrolled proliferation of cells it is important to consider which cells are playing a pivotal role and how this environment impacts either the BC development or its progression [18]. Moreover, the presence of inflammatory cells and stromal cells in the TME can affect the therapeutic outcomes. The targeting of stromal fibroblasts, immune cells, vascular endothelial cells, or adipocytes can be important to prevent occurring epigenetic modifications, caused by tumour cells, and inhibit their tumour supporting role. Hence, this therapeutic strategy promotes a regularisation of the non-tumour cells of the TME while it also regulates the immune system and stimulates anti-tumour activity [23, 18, 26].

Thereby, the BC TME has been recognised as an important element for the prognosis of BC and therapeutic resistance [18]. To further improve research on this field, combining the targeting of tumour cells with the targeting of the TME has good potential for BC therapy, thus eventually improving treatment efficacy, especially for metastatic BC [25]. Hypoxia inducible factor 1 (HIF-1), Poly ADP ribose polymerase (PARP) [27], histone deacetylase [23], p53 [28], TME ambience characteristics (pH conditions) or angiogenesis [27] are possible targets for therapeutic approach.

Wu *et al.* employed $Fe(OH)_3$-modified Nanoparticle (NP) as an oxygen generator, while also promoting chemotherapy via hydroxyl radicals through the Fenton-like reaction. Utilising the strong oxygen production of the $Fe(OH)_3/H_2O_2$ reaction and the deep tissue penetration of 808 nm NPs excitation, they achieved effective near infra red-triggered breast tumour growth inhibition in live animal models [29, 30].

PARP inhibitors target faulty DNA repair pathways in Breast Cancer gene (BRCA) 1/2 mutated BC, inducing synthetic lethality. Olaparib, a PARP inhibitor, in phase 1-3 trials [27], demonstrated effectiveness in BRCA1 and 2-deficient breast and ovarian cancers [31, 32]. Hypoxia's impact on DNA repair and BRCA1 gene expression suggests PARP inhibitors' potential against hypoxic BC tumours, regardless of the BRCA status [32].

Other strategies aimed at the other listed above microenvironmentally induced therapeutic targets are also in clinical trial phases. Hence, recognising the microenvironment's impact on BC progression is driving new therapeutic approaches. Adaptations to hypoxic/acidic conditions in tumours foster aggressive cell populations, prompting these novel strategies in BC treatment [32, 23].

1.1.3 *In vitro* models

Given the importance of the TME and ITH in tumorigenesis, cell proliferation and cancer progression it is essential to include these factors in the development of novel therapeutic strategies and treatments. To achieve that it is important to recreate appropriate models that can mimic the tumour environment.

1.1.3.1 Two-dimensional *in vitro* models

2D models have been used for a long time in pre-clinical studies to research treatment approaches, through drug development based on the drug's *in vitro* cytotoxicity. The nearly exclusive usage of 2D *in vitro* models in the past has been due to the low complexity and cost of the model. The 2D models are also useful in initial nanomedicine studies and biological characterisation which include, for instance, cell toxicity, uptake, biochemical and functional studies, and biomarkers identification [33, 24, 34].

The 2D monolayer cell culture models are easier to use, to assess cell behaviour and to manipulate for in-depth mechanism study. However, they represent the most simplified tissue and cancer model [35], with several critical limitations. They possess random cell morphology [24], lack in specificity (e.g. absence of basement membrane, defective ECM, no stromal or inflammatory components) and are cultured in abnormal environment conditions (e.g. flat plastic surface and high medium concentrations) [35]. Several key features such as native signalling response in growth, morphology, metabolism, and differentiation are not well recapitulated in these models. These characteristics are important to predict the response to nanomedicines [24, 34].

Hence, it created the need of a better cancer model to conduct proper experiments in pre-clinical phases. Particularly by mimicking the TME, therefore allowing the development of effective treatment strategies. This paved the way for new cell culture strategies that have been greatly used in recent years such as cell co-cultures and advanced 3D cell models [34, 24].

1.1.3.2 Three-dimensional *in vitro* models

In *in vivo* tissues there are cell-to-cell and cell-to-ECM interactions which form a dynamic 3D system. The 3D *in vitro* models allow a proper outline of the TME providing cell interactions (cell-cell and cell-matrix), perfusion, and hypoxic conditions [24]. There are a great number of 3D cell culture systems, but they all share a lot of key characteristics, including multiple cell states: a more proliferative in the outer layers and quiescent or necrotic states in inner layers (Figure 1.3) [34]. The 3D models can also recapitulate different gradients present existing in tumours, i.e., the oxygen and nutrient, that decrease with the distance from tumour blood vessels. This results in varied environmental conditions dependent on the distance from the cell culture core and greatly influencing cell biology [36, 24, 34, 37].

Moreover, these models are able to represent important physiological barriers regarding the diffusion of nanomedicines through the ECM [34].

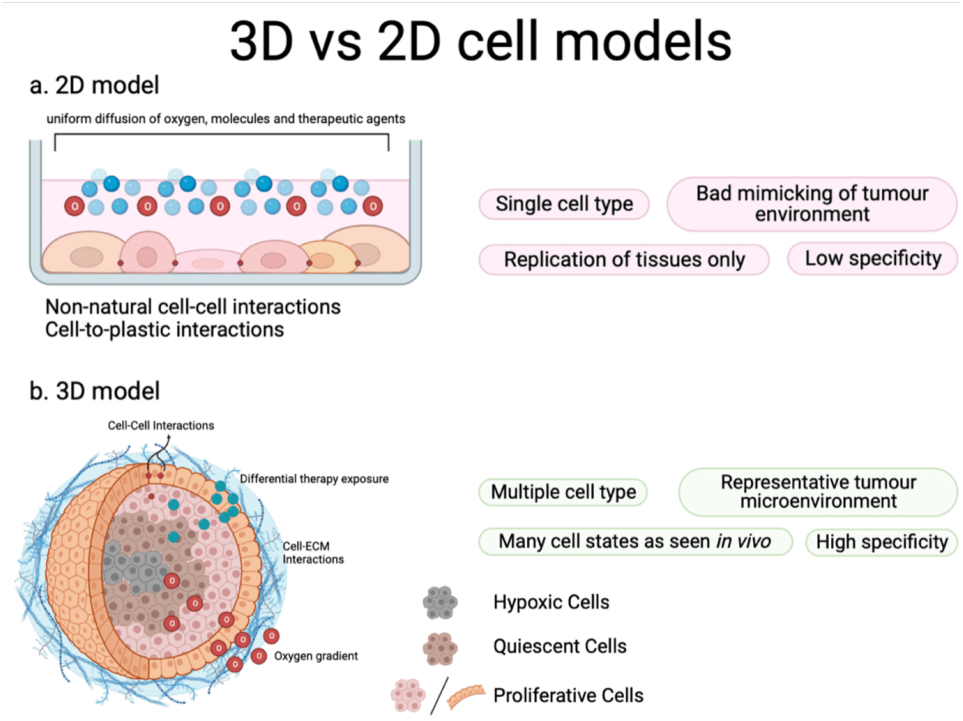

Figure 1.3: Schematic representation of 2D and 3D *in vitro* cell culture models. Adapted from Yarely *et al.* [38] and Sakalem *et al.* [39].

Since 3D BC models more accurately capture the multiple cells' states (proliferative, quiescent, and necrotic) and TME than 2D models, they are a more representative model that may be used to explore and investigate alternative approaches. With more trustworthy data, 3D BC cell culture models offer various therapeutic possibilities for nanomedicines development. These models enable innovative nanomedicines to target quiescent tumour cells, reveal their limitations against bulk proliferative cancer cells, facilitate novel combination techniques, and provide a holistic view of nanomedicines' tumour distribution.

They integrate data on cell uptake, penetration, and distribution while accounting for nanomedicines physicochemical properties [24, 34].

Gene expression, cell proliferation, cell migration or invasion [24], morphology [35], and heterogeneity [34] are considerably more similar in 3D *in vitro* models than in 2D *in vitro* models. Engineered 3D BC models use biomaterials and multi-cell arrangements, such as co-cultures, to mimic native cell morphology and foster cell-cell and cell-ECM interactions. Therefore, each of these elements contributes to the importance of 3D *in vitro* models as a cancer research tool and good alternative to 2D *in vitro* models [24].

1.1.4 BC treatment

The treatment for BC is dependent on numerous factors, such as the type of BC cells, gene expression profiles, tumour size, and disease prognosis [40, 10]. Conventional approved treatments are a combination of several strategies. Surgical resection with adjuvant postoperative radiotherapy and chemotherapy is generally the course of treatment [34]. Sometimes neoadjuvant chemotherapy is used prior to surgery to downstage the disease and facilitate breast conservation [41, 34].

The choice of chemotherapy is also dependent on whether it is intended to reduce tumour cell proliferation or minimise metastatic progression [42, 34]. Hence, standard HT with tamoxifen, toremifene or fluvestrant (oral antioestrogens), and exemestane, anastrozole or letrozole (aromatase inhibitors) are the most common administered ones for hormone expressing tumours (like Luminal A and B) [43, 44, 45, 46].

In HER2-enriched BC, ERBB2 overexpression is present in around 20 to 30% of early-stage BC. In this case, Targeted therapy (TT) or Immunotherapy (IT) are frequently employed in combination with chemotherapy to improve the survival of HER2-enriched diagnosed patients. Anti-HER2 therapies, such as Trastuzumab (humanised monoclonal antibody), pertuzumab (recombinant humanised monoclonal antibody) [40, 47, 48], trastuzumab-emtansine (trastuzumab linked to a cytotoxic agent), and Lapatinib (tyrosine kinase inhibitor for HER1 and HER2) [49, 50, 51] are currently used in the clinic to treat HER2+ tumours.

Up until recently, the sole therapeutic option for TNBC was chemotherapy. This subtype poses a great clinical challenge for the lack of targeted therapies and for not responding well to the current existing therapies (HT and chemotherapies) [15, 17, 16]. However, there have been developments in the field of IT for this subtype, which combine chemotherapy and IT [42, 34, 40]. Among the most popular ones are immune checkpoint inhibitors: pembrolizumab targeting Programmed death-1 (PD-1) inhibitor [27, 52, 53, 54], and tremelimumab Cytotoxic T lymphocyte-associated protein 4 (CTLA-4) blocking antibody [27, 55, 56].

BC presents a challenge due to its significant biological diversity, characterised by tumour heterogeneity, and rapid clonal evolution of cancer stem cells. The aforementioned therapies have been the gold standard for treating all BC subtypes. However, they come

with a number of drawbacks, including low solubility, poor tumour targeting, undesired toxicity in healthy cells, and even the development of drug resistance brought on by cancer cells' overexpression of specific proteins [57, 58, 20]. For example, Trastuzumab has shown toxicity accompanied by cardiac dysfunction in long term use [57, 59]. Owing to these limitations, nanomedicine and nanotechnology research have accelerated. The development of novel and targeted therapies, such as gene circuits delivered via multi-functional targeted nano-systems, have become ways to provide more effective and less toxic treatment options for BC patients in the future [57, 34, 40].

1.2 Nanomedicines and gene therapy for BC treatment

1.2.1 Nanocarriers: types and applications

Nanomedicine, an interdisciplinary fusion of nanotechnology, biotechnology, and information technology, has revolutionised the life sciences and marked significant departure from traditional cancer therapy's approaches, like chemotherapy and radiation [30].

Nanotechnology covers small materials, generally 10-1000nm [60, 61, 62]. Defining a broad research field, these nanomaterials can function as nanocarriers and overcome limitations associated with traditional medical strategies, addressing issues like drug stability, solubility, short half-life, cytotoxicity, narrow therapeutic range, and suboptimal pharmacokinetics and pharmacodynamics [63, 57]. Besides, they offer unique attributes like capillary and lymphatic passage, strong biomolecule binding, improved organ deposition, and reduced post-administration inflammation [63]. These benefits depend on the physicochemical properties of nanocarriers, including particle size, surface, and chemical composition, which significantly influence cellular uptake and distribution in the body [64, 58].

These characteristics are important to consider when developing TT for BC. The research for BC treatment is now centred on using cutting-edge methods such as gene therapy and NPs [65]. A wide range of NPs have been developed with specific targeting capabilities for BC tumours. The vast and different biomaterials available for such NP-based delivery systems ensures they can be tailored to have improved biocompatibility, and increased drug accumulation, higher stability in blood circulation and slower drug release. They are able to entrap multifunctional active agents and effectively deliver them, using target ligands to target specific cancer sites. These tuneable features result in NPs exhibiting reduced side effects [57, 58, 66]).

Nanocarriers offer two targeting approaches: passive or active targeting [66]. The tumour's incomplete vascular system leads to 100 nm to 2 μm gaps, causing vascular leakage [67]. Passive targeting capitalises on cancer vasculature changes [66]. It involves NP entrapment of small molecules for prolonged circulation, reducing side effects, without tissue-specific focus [30]. Vascular leakage and compromised lymphatic clearance lead to effective extravasation and persistence of small molecules in the tumour interstitium—the

Enhanced permeability and retention (EPR) effect [30, 66, 67, 68, 69]. Active NPs targeting entails incorporating a targeting moiety (e.g., aptamers, ligands, and antibodies) onto nanocarrier surfaces for specific tumour cell recognition. This involves NP recognising and binding to target cells through ligand-receptor interactions, followed by internalisation and controlled drug release within the cell. This approach minimises off-target drug release in contrast to passive targeting systems, enhancing the effectiveness of chemotherapeutic agents [70, 69, 67, 66, 30].

The nanocarriers that have been investigated for drug delivery can be divided in three main categories according to their constituent materials: Lipid-based NP (LbNp), Inorganic NP (INP), and Polymeric NP (PNP) (Figure 1.4). These specific types have notably emerged as the most promising nanocarriers in current literature [20].

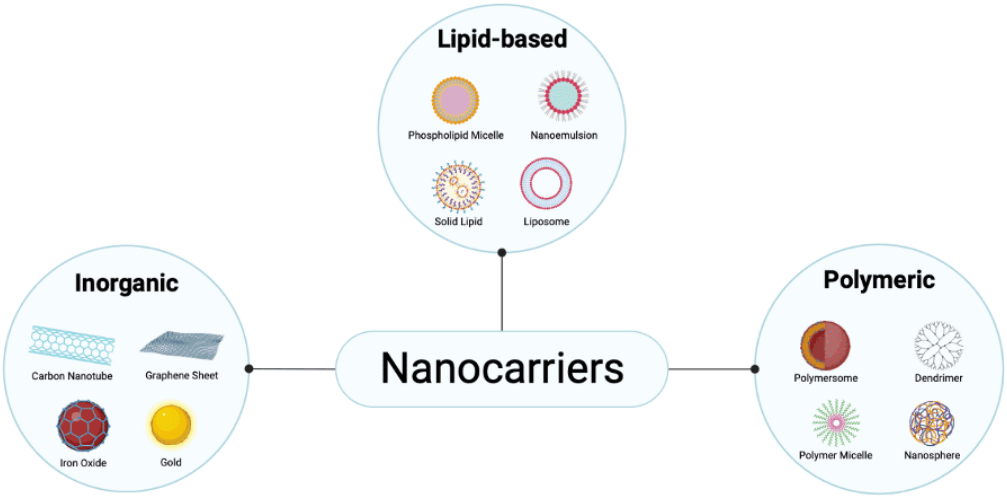

Figure 1.4: Existing nanocarriers for cancer nanomedicine-based therapy. Designed via Biorender

Liposomes are the most commonly used among the LbNps group. Due to their unique morphology (hydrophilic inner core surrounded by phospholipid bilayer) they are able to incorporate hydrophilic or amphiphilic agents therefore reducing the drugs' toxicity [57]. For example, the usage of Polyethylene glycol (PEG) for surface modification of Liposome NPs allows these to have longer half-lives along with increasing their targeting efficacy [71, 57]. In a study by Şalva *et al*. 2015 chitosan-coated liposomes were able to co-deliver a Small interfering NP (siRNA) system achieving lower cytotoxicity and higher silencing efficiency. They successfully proved the growth inhibition of two BC cell lines. Furthermore, they were able to increase the stability of siRNAs [72, 57].

Within the realm of INPs, Gold NP (AuNP)s stand out as a prominently employed entity in drug delivery. This is attributed to their modifiable attributes and a documented low toxicity [73, 74]. They can be coated with organic components that consequently allow the targeting of specific receptors or biomarkers. Kong *et al.* corroborated these claims through a study where functionalised AuNPs enhanced the radiotherapy effectiveness compared to non-functionalised AuNPs [75, 57].

Numerous other types of NPs are currently under investigation and being employed

as both drug delivery platforms and therapeutic agents. Examples include Superparamagnetic iron oxide NP (SPIONS), quantum dots, carbon-based NPs, dendrimers, protein-based viral NPs, and silica-based NPs. Each of these exhibit distinct attributes and adjustable properties. However, given the scope of this project, only polymeric NPs will be explored in more detail.

1.2.1.1 Polymeric NPs for BC treatment

PNPs have gained significant attention in recent years due to their unique properties. Two of the most important are their biocompatibility and biodegradability [76]. Biodegradable polymers experience degradation through both non-enzymatic and enzymatic processes, resulting in biocompatible by-products with limited adverse effects. Within the context of targeted drug delivery applications, biodegradable polymers exhibit a significant focus on their chemistry and integration with novel molecules [77]. Biocompatibility, simply put, is a material's capacity to elicit the appropriate host response in a specific application without adverse tissue reactions. This involves throughout *in vitro* and *in vivo* evaluations of nanomaterials, following standard protocols. Testing encompasses cytotoxicity, genotoxicity, carcinogenicity, reproductive toxicity, immunotoxicity, irritation, sensitisation, hemocompatibility, systemic toxicity, pyrogenicity, and implantation. These tests are essential for the safety of patients undergoing nanomaterials-based treatments [76, 78].

Other inherent traits encompass high loading capacity and straightforward surface functionalisation. These PNPs can protect Nucleic acid (NA)s from degradation and provide sustained release of the therapeutic payload. Furthermore, they can be modified with targeting ligands to enhance their specificity towards the tumour site [79].

Various types of PNPs have been explored for NA delivery in BC treatment. PNPs can be formulated using two main groups of polymers: natural and synthetic polymers.

1.2.1.1.1 Natural Polymers

Natural polymers encompass proteins and polysaccharides sourced from animals and plants, as well as polymers acquired from microbial origins. These substances are extensively employed in drug delivery research, primarily due to their distinctive characteristics. Including prevalent natural occurrence, biodegradability, biocompatibility, and low toxicity [77]. They undergo enzymatic degradation into metabolisable peptides or polysaccharides within the body. Furthermore, this degradation rate can be finely tuned to achieve a desired release profile. Among the most used ones are dextran, chitosan, Hyaluronic acid (HA), gelatin, alginate and albumin [79, 80, 81, 82, 83, 84].

For example, chitosan is derived from chitin which is a very abundant natural polymer among the arthropod family. It is a cationic polymer, resulting in electrostatically binding to negatively charged molecules such as NAs [83, 85, 81]. However, this natural polymer

possesses some limiting drawbacks (e.g. poor solubility in neutral and alkaline pH and low mechanical resistance) [86].

HA and its derivatives represent a class of PNPs categorised within the mucopolysaccharides group. Amino acid conjugation to HA's carboxyl or hydroxyl groups prolongs its blood circulation despite rapid body clearance. Notably, cancer cell-associated HA receptors, become activated, boosting cellular infiltration and tumour malignancy. HA facilitates NP internalisation by binding to these receptors [87, 83].

Zhao *et al.* reported a NP composed of Polyethylenimine (PEI)-grafted chitosan oligosaccharide integrated with HA and siRNA that adeptly transported the therapeutic gene to CD44-expressing cells. Furthermore, the researchers stated that it yielded a substantial mitigation of endometriosis clinical manifestations within tissues along with showing biocompatibility with reproductive organs [88, 89, 85, 83].

However, natural polymers are not free from limitations. Oftentimes they need chemical modifications to properly function as nanocarriers or even, need to be purified to avoid immunogenicity [85].

1.2.1.1.2 Synthetic Biopolymers

Synthetic polymers can be meticulously designed for charge, hydrophobicity, and degradation to align with specific cargos, routes, and targets. Precise synthesis minimises variability, and scalability suits large-scale manufacturing. This complements stability, flexibility, low immunogenicity, and biodegradability. Their resistance to hydrolysis and high-temperature tolerance allows effective heat sterilisation. Due to these advantages, synthetic biopolymers play pivotal roles in various applications. These include tissue engineering, gene therapy, and novel drug delivery systems, among other products [90, 85, 83].

Among the most used synthetic polymers for drug delivery, gene therapy and cancer treatment are poly-L-Lysine (PLL), PEI, Poly-amidoamine (PAMAM), poly(lactic-co-glycolic acid) (PLGA), and poly(ϵ-caprolactone) (PCL).

Some biodegradable polyesters with surface modifications englobing cationic surfactants, PEI or PLL can even be classified as cationic polymers. These are mostly used due to their positive surface charge. They can bind to NAs (that are negatively charged), forming a small and compact structure, through electrostatic interactions. In the preparation of PNPs for NA delivery, it is common to employ an excess of cationic polymer compared to oligonucleotide. This approach results in the formation of NPs with a positive surface charge, enabling efficient condensation of NAs into smaller particles. The NAs payload is entrapped within the polymer matrix and protected by the surrounding polymer chains, which act as a physical barrier that restricts access of nucleolytic enzymes [79].

PLGA and Poly-(Lactic Acid) (PLA) have received approval from the US Food and Drug Administration (FDA) for human use. Polyester-based NPs can be designed to entrap a diverse range of therapeutic agents, including low molecular weight drugs, as well as

macromolecules like proteins and plasmid DNA (pDNA). Biodegradable polymers are preferred for NA delivery due to their ability to degrade *in vivo*, eliminating the need for their removal from the body after treatment [91].

There are several examples of the use of synthetic biopolymers. Shenoy *et al.* reported a PEG-modified PCL NP for tamoxifen targeted delivery in BC. The researchers highlighted an increase of drug accumulation in the targeted BC cells with these NP [92, 57]. In another study, Pandey *et al.* employed tamoxifen-loaded PLGA-derived NPs. Their findings indicated heightened DNA cleavage within tumour cells, along with increased nuclear fragmentation, cytotoxicity, and bioavailability. This approach demonstrated superior performance compared to free tamoxifen, particularly through receptor-mediated endocytosis in MDA-MB-231 BC cells [93, 57]. Moreover, in a separate study, a complexation of triple-helix strands of microRNA (miRNA)s with PAMAM G5 dendrimer yielded a branched sponge-like architecture. This approach effectively controlled key genetic driver in BC TME, as documented by Conde *et al.* [94].

1.2.1.1.3 PLA NPs

Among the existing PNPs, PLA-based NPs are promising for the delivery of NAs since they confer several advantages, including sustained therapeutic drug release over extended periods, owing to their polymer matrix that enables regulation of drug release kinetics.

PLA is part of a family of aliphatic polyesters made from α-hydroxy acids (including polyglycolic acid and polymandelic acid). Lactic acid is the building block of PLA and can exist in optically active D- or L-enantiomers (Figure 1.5. PLA can be synthesised with different properties depending on the quantity of enantiomers used, consequently creating a broad range of PLA polymers to meet performance criteria [95]. These polymers are considered biocompatible and biodegradable [96, 97, 98, 99].

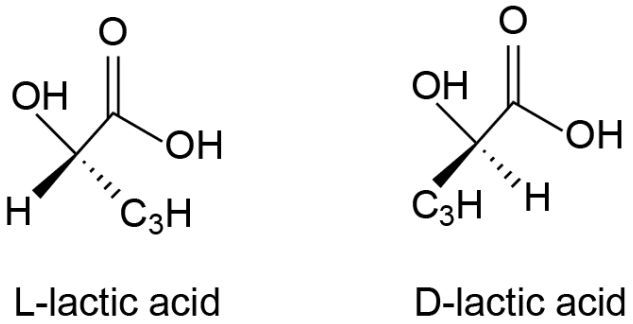

Figure 1.5: Optical monomers of lactic acid. Designed via ChemDraw version 19.0.0

PLA is easily degraded through hydrolysis of the ester bond not requiring activity of any enzyme to catalyse the reaction. The degradation of PLA is influenced by particle size, crystallinity, isomer ratio, water diffusion rate, and hydrolysis temperature. The products of this degradation are non-toxic. In biological settings, PLA undergoes hydrolysis, leading to the formation of its constituent α-hydroxy acid. Subsequently, it becomes integrated

into the tricarboxylic acid cycle and is ultimately excreted [100, 98]. The final products of this degradation include water [100] and carbon dioxide [101], lactic acid monomers [102] and oligomers [103]. Lactic acid is a by-product of anaerobic respiration, subsequently transformed into glucose by the liver through the Cori cycle [102].

Despite these advantages, PLA is hydrophobic and has poor cell recognition sites resulting in low cell affinity [98, 104]. Therefore, surface modifications of PLA play an important role in biomedical applications [105, 98]. The capacity to shape PLA properties, such as surface functionalities, hydrophilicity, roughness, and topography, to the desired needs make this polymer even more attractive in the nanomedicine field [98]. Hence, to enhance cell affinity, PLA can undergo coating with ECM proteins or other polymers. Additionally, incorporating molecules like alginate, gelatin, PLL, or PEG onto its surface contributes to the overall enhancement of PLA-cell affinity [98].

Owing to these desirable properties, PLA NPs gained recognition in the past decades and continue to raise interest as drug delivery systems [106, 107, 108]. The methods used for the preparation of PLA NPs can be divided into four categories: emulsion based, precipitation based, direct compositing, and other approaches. Within these categories, the single/double-emulsion, nanoprecipitation, salting-out, spray-drying and dialysis are the most common methods for formulation of PLA NPs.

Included in the emulsion-based category are single emulsion, double emulsion, and multiple emulsions methods. The single emulsion/solvent extraction technique is a straightforward approach that dissolves hydrophobic drugs and PLA within organic solvents. These solutions are emulsified in a water phase with a stabiliser. High-energy sources like ultrasound or homogenisers aid emulsification, and the oil phase is removed through methods like reduced pressure evaporation, vacuum, or solvent extraction with water. This leads to NPs formation in the aqueous phase, followed by purification through centrifugation or filtration and subsequent lyophilisation for long-term storage [109, 102, 83, 89, 84].

Double-emulsion/extraction methods improve entrapment efficiency for water soluble drugs, like peptides and proteins, which are challenging to entrap with single emulsion. This method is similar to the single emulsion but introduces a secondary emulsion. Common emulsifying agents, like gelatine and Polyvinyl alcohol (PVA) are used [102, 109, 83, 89, 84]. This method was the one used for the formulation of the PLA NPs in this project. Hence, this technique will be further described in detail in chapter 3. Figure 1.6 represents a general scheme for the double emulsion method.

The characteristics for the other methods along with advantages and some drawbacks are gathered in table A.1.

Several studies have shown the low cytotoxic effect of PLA NPs [110, 111, 112, 96] and their ability to deliver different loads of drug molecules (from small to large proteins and NAs) in a controlled manner. This further proves that PLA NPs can be used as nanocarriers for high therapeutic effect and potential delivery systems for gene therapy [113, 114, 108, 111, 112].

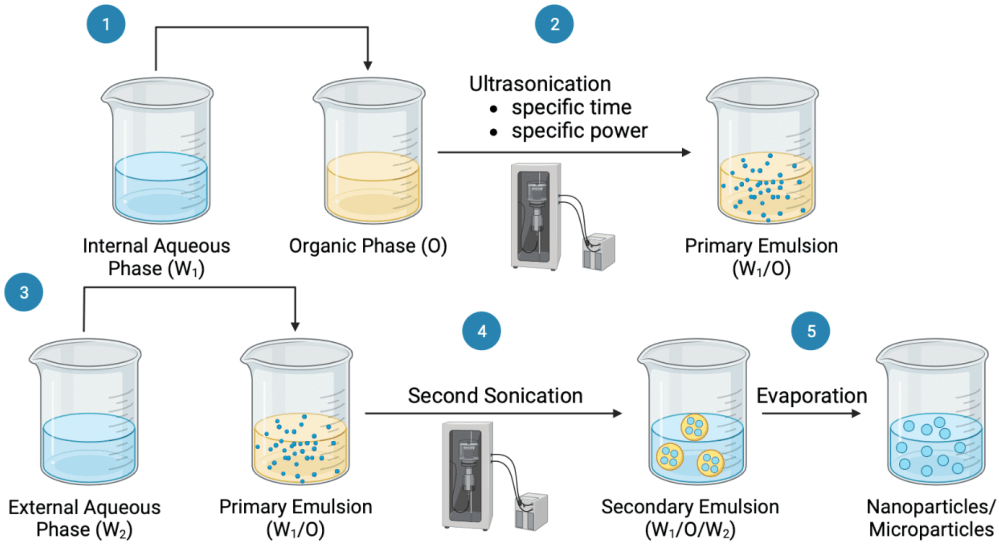

Figure 1.6: Basic principle of double-emulsion solvent evaporation technique (W/O/W type). Designed via Biorender.

1.2.2 Nano-based systems for gene therapy in BC

The success of clinical gene therapy largely relies on the chosen delivery methods, which can be classified into viral and non-viral delivery systems. Among the non-viral delivery systems, the use of NPs-based delivery has emerged as a promising approach due to several benefits over viral methodologies. These benefits include a relatively safer profile, reduced adverse immune responses, ease of large-scale production, and potential for ligand incorporation to facilitate specific targeting of cell types [58].

Gene therapy involving free NAs has the potential to strategically address up-regulated genes in cancer by delivering functional molecules to target cells. This modification of gene expression activates biological treatment [58]. The current global effort to elucidate the human genome, along with the recent discovery of RNA interference (RNAi) and Clustered Regularly Interspaced Short Palindromic Repeats (CRISPR)-based genome editing, has led to increased attention towards NAs [79, 115].

NAs have shown considerable advantages in comparison to traditional treatments (surgery, chemotherapy, and HT). Unlike the latter, NAs present high specificity, and their mechanism of action provides a promising approach for viral infections, a range of cancers, and genetic disorders that are currently difficult to treat. Furthermore, in theory, administering a genetic payload with NAs can lead to a lasting and potentially curative effect with just a single treatment [79].

The field of gene therapy can be classified into three main groups. The first one involves the CRISPR associated protein 9 (CRISPR-Cas9) technology to edit mutated genes to bring about a gain or loss of function. The second focuses on upregulating gene expression, which can be achieved by introducing a functional gene copy using various molecules, such as pDNA, minicircle DNA (mcDNA), synthetic Messenger RNA

(mRNA), circular RNA, and self-amplifying RNA (saRNA). The last one involves the down regulation of gene expression, which can be achieved with molecules such as siRNA, antisense oligonucleotides (ASOs), short hairpin RNA (shRNA), and microRNA (miRNA or microRNA (miR)) [79].

Despite potential of NA, therapy is hampered by issues like low cell uptake, reduced potency, instability in circulation, immune responses, off-target toxicity, and the risk of tumour-inducing mutations. Advances in synthetic biology and nanotechnology have greatly improved the bioavailability of NA-based therapeutics [58]. The use of nanotechnology, particularly involving PNPs, represents a solution to the challenges posed by delivering NAs alone. As said previously, NPs enhance solubility and stability, thereby increasing the therapeutic effectiveness of NAs [116, 117, 118, 119, 120]. Additionally, when NAs are entrappedd within NPs, they are safeguarded from degradation by enzymes, leading to an extended half-life in the bloodstream [121, 117, 118, 119, 120]. This nanotechnology-based approach enhances drug distribution and targeting through passive or active targeting [122, 117, 28, 119]. This possibility of tailoring their targeting delivery strategy leads to higher concentrations of NAs at tumour sites, while also reducing toxicity [116, 122, 117, 28, 118].

1.2.2.1 The potencial of miRNA potential for breast cancer

miRNA holds promise as an early detection tool for BC and is considered an ideal diagnostic biomarker. Furthermore, miRNA-based gene therapy has shown potential in restoring or repressing miRNA expression. However, current miRNA profiling techniques, such as RT-PCR and microarrays, are error-prone due to the small size of miRNA probes and dificult primer design. Alternatively, nanotechnology offers a sensitive and rigorous alternative for miRNA detection, with significant implications in cancer theranostics. NPs and nanopores have also demonstrated non-invasive delivery of therapeutic miRNA with high specificity to tumour targets [58].

In recent years, the study of miR expression, particularly through high-throughput profiling, has generated evidence linking the deregulation of miR expression to human BC. High-density microarray techniques have unveiled a significant set of deregulated miRNAs in breast tumours relative to normal breast tissue. Among these, miR-10b, miR-125b, miR-145, miR-21, miR-155 and miR-191 are the most frequently deregulated. The decreased expression of miR-10b, miR-125b and miR-145 and the increased expression of miR-21, miR-155 and miR-191 indicate their potential involvement in oncogenesis as either tumour suppressors or oncogenes [123]. The suppressor role involves miRNAs with tumour suppressive functions, which prevent tumorigenesis through the regulation of various cellular events, such as cell growth, apoptosis, and immune cell development. Down regulation of these miRNAs is frequently observed in different types of cancer. The oncogenic role of miRNAs involves the regulation of multiple tumour suppressor genes, leading to tumour initiation, progression, and metastasis in BC patients [119].

Certain cancer-associated miRNAs exhibit context-dependent behaviour, as they may exhibit either oncogenic or tumour suppressive roles depending on the specific tissue in which they are expressed [124].

HER2-amplified and HER2-overexpressing BC have been shown to exhibit decreased expression levels of miR-125a and miR-125b. Elevated expression levels of these miRNAs have been linked to the reduction of mRNA and protein levels of HER2 and HER3, leading to inhibited cell migration, invasion, and reduced anchorage-dependent growth [119]. Zhang *et al.* reported the development of solid lipid nanocarriers with paclitaxel and P53 mRNA showing an increased drug loading efficiency along with strong inhibition of tumour growth [125].

The therapeutic prospects of miRNAs are intriguing due to their innate biocompatibility. However, miRNAs exhibit water solubility and a negative charge, which limits their cellular uptake, resulting in sub-optimal targeting ability, low stability, and a short half-life. To circumvent these challenges, miRNAs must be formulated into carrier systems. One such system is the NP carrier, which has the potential to facilitate efficient delivery of miRNAs [119].

2

Aims

In this context, the primary goal of this thesis project was to develop multifunctional targeted nanosystems for gene circuit delivery aiming for treatment efficacy enhancing and characterising tumour heterogeneity. This will be achieved with help of several complementary proposed goals:

1. Formulation of the PLA-based NPs through the double emulsion-solvent evaporation method;
2. Characterisation of the nano-engineered platforms in terms of Hydrodynamic size (HS), Zeta potential (ZP), Polydispersity index (PI) and morphology, through methods like Dynamic light scattering (DLS) and Atomic force microscopy (AFM);
3. Formulation of fluorescently labelled PLA-based NPs with Rhodamine B;
4. Assessment of entrapment efficiency (EE) and loading capacity of the PLA/modified D-alpha-Tocopherol polyethylene glycol 1000 succinate (TPGS)-NPs with two NAs (pDNA and miR-125b – miR single stranded molecule from the miR 125 family) and consequent characterisation of the complexes' physical properties;
5. Establishing of a BC 2D monolayer cell culture and 3D microenvironment with cell culture techniques using three BC cell lines;
6. Assessment of cellular response to the PLA-based NPs by various therapeutic modalities, such as determination of cell viability, assessment of metabolic activity and cytotoxicity, using techniques like flow cytometry protocols, and fluorescence microscopy;
7. Analysis of cellular uptake of the fluorescently labelled PLA-based NPs using flow cytometry and fluorescence microscopy.

3

Materials And Methods

3.1 Plasmid DNA and microRNA assays

3.1.1 Plasmid DNA extraction

For this study, two different plasmids were extracted. Their development and quality assessment was done by the company Cyagen. Both plasmids have a human Cytomegalovirus (CMV) promoter that is expressed by most cells and a infrared fluorescent protein 713 (iRFP713) reporter. The fluorescent tag is used as a reporter gene to visualise and track gene expression and cellular localisation. In one of the plasmids the CMV promoter drives the expression of a construct containing miR-125b (gene of interest) and a translation initiation sequence (Kozak). The plasmids' constructs are present in the Table (3.1).

Both plasmids were extracted from *Escherichia coli* bacterial growth through the PureLink HiPure Plasmid Midiprep kit (Thermo Fisher Scientific).

Firstly, the bacteria were cultured in solid agar plates and then, after 24 hours, the colonies were collected and added to a liquid medium comprised of Luria Broth (LB) medium without antibiotic. The following day the plasmid was extracted using the aforementioned kit. The extraction of plasmid from the growth medium was done following the manufacturer's instructions. The purity and concentration of plasmid were read in NanoDrop 200 Spectrophotometer (Thermo Fisher Scientific).

Table 3.1: Plasmids' constructs used in the project

Plasmid	Species	microRNA	Promoter	Interest gene	Fluorescent tag
pDNA_CMV_RFP	Human	N/A	CMV	iRFP713	iRFP713
pDNA_miR125b_CMV_RFP	Human	miR-125b	CMV	miR-125b	iRFP713

3.1.2 microRNA-125b

The miR used for NPs complexation and subsequent *in vitro* studies was purchased from ATLAS Biolabs GmbH. It was obtained from BC cell lines of BC patients and was sequenced by the same company.

miR-125b was chosen as a potential therapeutic target due to its low expression in the BC cell lines previously investigated by the lab's group, indicating its role as a tumour-suppressing gene. This miR molecule possesses the fluorophore Atto 590 which serves as a means of measuring the promoter activity in the cells and, thus, evaluate the transfection efficiency.

Table 3.2: miR-125b sequence

Oligo name	*Length*	*MW (g/mol)*	*Sequence (5'-3')*	*Fluorescent tag*
Has-miR-125b-5p S	22 nucleotides	16021	UCCCUGAGACC-CUAACU	Atto590

3.2 Synthesis of TPGS modified with spermidine

TPGS was used as a surfactant in the formulation of the PLA-based NPs. It was modified with a spermidine. This modification was done according to the following procedure: firstly the alcohol molecules present in the PEG of TPGS must be activated with a reaction using para nitro benzyl (PNB). Once activated the alcohol molecules of PEG in TPGS react with the amines from spermidine and allow the appropriate entrapment of spermidine in TPGS. TPGS-para nitro benzyl (PNB) previously prepared (1.12 g, 0.63 mmol) was dissolved in dry Dichloromethane (DCM) (7 mL). The mixture was cooled to 0°C and triethylamine (TEA) (0.2 mL, 1.3 mmol) was added. Excess spermidine was then added. The reaction was stirred at Room temperature (RT) for 1.5 hours and was monitered by thin layer chromatography (TLC). After completion the reaction was dried over magnesium sulfate and the solvent was removed under reduced pressure. The product was purified by dialysis (MW cutoff 1kDa) to afford a TPGS-spermidine of 30%-50% modification. This was corroborated by Nuclear Magnetic Resonance (NMR) spectroscopy as seen in Figure I.1 of I.

3.3 Nanoparticles formulation and characterisation

The PLA NPs were formulated with the modified surfactant TPGS, described in the previous section 3.2. This modification was done to provide the final NPs with amines for NA binding.

3.3.1 Double emulsion-solvent evaporation

PLA/TPGS-NPs were formulated through the double emulsion-solvent evaporation method, as it is described by Alonso-Sande *et al.* [126] 10 mg of PLA (Mw = 1,600-2,400, Polysciences, Inc., USA) were weighed and added to a glass vial. Then, 200 μL of DCM (Sigma-Aldrich, cat. no.270997) were added to the same vial and vortex was preformed to dissolve the PLA. Afterwards, 100 μL of 10% (w/v) PVA (Mw = 13,000-23,000, Sigma-Aldrich, cat. no.363170) were added to the same vial. In this step, two phases were observed: one aqueous comprised of PVA and one oil phase comprised of PLA dissolved in DCM. Next, the mixture was sonicated with a microprobe sonicator (Fisher Scientific, cat. no.FB505220 & FB432B2), (sonication parameters previously optimised: 15 seconds, 20% amplitude) to obtain the first emulsion. Then, 400 μL of 2.5% (w/v) TPGS (Sigma-Aldrich, cat. no 9002-96-4) were added to the first emulsion and a second sonication cycle was performed to obtain the final double emulsion. The final emulsion was added dropwise with a Pasteur pipette to a beaker that contained 20 mL of 0.25% (w/v) PVA under stirring at 850 rpm, for an hour to evaporate the solvent.

To obtain the final suspension of NPs several washings were done. The suspension was added to a centrifuge tube (Thermo Scientific, cat. no.3119-0050) and centrifuged for 30 minutes at 20 000 G and 4°C (Gyrozen, 1686R). After the first washing, the NPs were resuspended in 2 mL of RNAse free Water (Thermo Scientific, cat. no.10977035) and centrifuged again at the same conditions. The final suspension of NPs was resuspended in 1 mL of Phosphate-buffered Saline (PBS) solution (1X – stored at 4°C). This procedure allowed the formation of 4 batches at a time.

The NPs were also fluorescently labelled with Rhodamine B (Fluorochem, cat. no F540175-25G). Rhodamine B was added to the PLA/modified TPGS-NPs in a 1:30 proportion. Rhodamine B was dissolved in DCM prior to the addition of PLA. The posterior steps were done as previously described, however protected from light due to the fluorescence of Rhodamine B.

3.3.2 Nanoparticle complexation with plasmid DNA and microRNA

The previously formulated NPs were complexed with the selected vectors for this project in different N/P ratios. N being the number of amine positive groups at the molecule's surface and P being the number of phosphates (negative groups) of the NA molecules. All ratios have the same quantity of NAs (1 μg).

Initially, based on the previously reported study from Walsh *et al.* [127], the N/P ratios decided for pDNA complexed NPs were 0.4, 1, 2, 4, 8, 15, 37 and 80. After optimisation processes through agarose gel electrophoresis complexation assessment, the ratios decided for pDNA NPs ranged from 15 to 44 in intervals of 7, approximately.

For miR NPs, since pDNA ones had already been optimised, the initially selected N/P ratios were based on the final ratios used for pDNA. Hence, it ranged from 15 to 44 (in increments of 7, approximately). Again, after optimisation, the final selected ratios ranged

from N/P 15 to 73, in intervals of 15, approximately. The NPs were mixed with pDNA and miR according to these ratios, vortexed and allowed to incubate under rotative agitation (IKA loopster) for 20 minutes at RT - ~25°C.

3.3.3 Hydrodynamic size and surface charge characterisation (by Dynamic Light Scattering and Electrophoretic Light Scattering)

DLS consists in the incidence of a monochromatic laser in a colloidal dispersion where the light will be scattered due to the particles present in suspension [128]. DLS enables the measuring of the HS of particles by this scattering light mechanism which analyses the modulation of intensity of scattered light as a function of time. The HS of particles is correlated with their Brownian motion: a smaller particle diffuses faster than a larger one. The equipment generates a correlation function, mathematically linked with the particle's size [129].

Electrophoretic light scattering (ELS) allows the determination of the ZP of the particles. ZP is characterised as the potential at the slipping plane of a colloidal particle flowing in an electric field. The effort required to bring a unit positive charge from infinity to the surface without accelerating it is known as the electric potential of a surface. With ELS the mobile particles during electrophoresis scatter the incident laser.

Mobile particles cause a Doppler shift in scattered light, which is detected by splitting the laser beam into a sample beam and a reference beam. The Doppler shift is determined by combining the scattered light with the reference beam. The particle velocity is determined from the Doppler shift, and the ZP is calculated using mathematical equations. In this case, the one used was the Schmoloski method [130].

After NPs' synthesis and for NA complexed NPs, their HS, (ZP) and PI were measured by DLS using the Anton Paar particle analyzer Litesizer 500 (Anton Paar, Austria). For each batch of NPs formulated and for each parameter three measurement cycles were performed. To measure the NPs, 1 mL of NPs diluted in 1:20 of KCL (10 mM) (Sigma-Aldrich, cat. No.P9333) was used. The size measurement was carried out in disposable polystyrene cuvettes (Alfagene, cat. No.6110349334) and the surface charge was measured in Omega Cuvettes (Anton Paar, cat. No.225288).

3.3.3.1 Temperature Stability Assay on the Nanoparticles

A thermal stability assay was also performed on the NPs to assess the physicochemical properties over a period of 30 days.

After the formulation, 3 batches of NPs were stored individually in each condition of temperature (4°C, RT, and 37°C). The HS, ZP and PI were measured by DLS at appropriate timepoints (0, 24, 48 and 72 hours, 7, 14, 21 and 30 days).

3.3.4 Morphology Characterisation

3.3.4.1 Atomic Force Microscopy

AFM, a type of scanning probe microscopy, was developed to measure non-electrically conductive materials like proteins [131], surpassing the limitations of older scanning microscopy instruments. It achieves sub-nanometer resolution for surface topography analysis of NPs on solid substrates (e.g. mica) in various environments [131, 132], providing both qualitative and quantitative data on physical properties (e.g. size, morphology, surface texture) and statistical characteristics (e.g. surface area and volume distributions) [133].

AFM offers high-resolution 3D visualisation for characterising a wide range of particle sizes within a single scan [133]. It employs a tip attached to a flexible cantilever, operating in various modes to measure the force between the tip and sample by monitoring cantilever deflection [131, 134].

Cantilever oscillation impacts vertical resolution, and tip diameter determines horizontal resolution. Measured forces rely on van der Waals interactions between NPs and the AFM tip [133].

The main AFM modes are contact and dynamic, which have further subdivisions. This thesis employed dynamic mode, specifically tapping mode (Acoustic (AC) mode) [131]. In AC AFM, the cantilever vibrates near the surface, potentially making brief contact. Interactions with the sample surface cause amplitude reduction and a phase shift. Amplitude modulation mode, often used in biomedical applications, offers high resolution, nearly non-destructive imaging, and suitability for both air and liquid environments [131].

Asylum Research MFP-3D Standalone system (Oxford Instruments) AFM was used to analyse the NPs' morphology, surface texture and size in AC mode at RT, at a resonance frequency of ~300 kHz and a spring constant of 26 N/m.

A drop of the NPs' samples was placed on a freshly cleaved mica and two ways were used to dry the sample: the pDNA-NPs were dried overnight and miR-NPs were dried 15 minutes prior to the reading with the help of pure N2 for about 2 seconds.

3.3.4.2 Quantification via agarose gel electrophoresis

Electrophoresis relies on the migration of charged species to separate the desired components resorting to the use of an electric field in a supporting medium, which can be a liquid or a hydrophilic gel. This technique allows the separation of a variety of charged molecules: small organic/inorganic ions, biopolymers (e.g. NAs), microorganisms, or even whole cells [135].

The successful complexation of the NPs aforesaid was evaluated through electrophoresis in a Tris-Borate EDTA (TBE) bath, with the complexes loaded in an agarose gel. 8 μL of each NPs complex was mixed in with 2 μL of loading buffer and 10 μL of this new mixture was loaded in each well of the agarose gel. The gel was previously prepared

in different concentrations according to the NA used: 1% for pDNA complexes and 3% for miR complexed NPs. The choice of agarose gel percentage is determined by the size range of the nucleic acid molecules under analysis [136]. For smaller molecules like miR, a 3% gel is utilised. This higher percentage provides a denser gel matrix, facilitating the separation of smaller molecules and resulting in enhanced resolution compared to a lower percentage gel (1%) [137]. The gel was then run at 70V for 110 minutes. The analysis was carried out under Ultraviolent (UV) light (Chemidoc®).

For pDNA conditions, a post-staining was performed in which the gel was incubated for 30 minutes under gentle agitation with a 3X GelRed™ solution in TBE in a container, protected from light. For miR complexes the staining was done prior to solidification of the agarose gel with a 1X GelRed™ solution.

3.4 *In vitro* studies

3.4.1 Cell culture

The *in vitro* studies were performed using BT-474, SK-BR-3 and MDA-MB-231 human BC cell lines (Japanese Collection of Research Bioresources Cell Bank – JCRB, cat. no. JCRB1450, JCRB1559 and JCRB1627.1) (Lasfargues EY, Coutinho WG, Redfield ES. Isolation of two human tumour epithelial cell lines from solid breast carcinomas. J Natl Cancer Inst. 1978 Oct;61(4):967-78 [138]). Cells were cultured in ventilated Tissue culture (TC) flasks in appropriate medium for each cell line:

- BT-474

  RPMI (1640) supplemented with 20% Foetal Bovine Serum (FBS), 2mM Glutamine, 1% Penicillin streptomycin (Pen-Strep), and Insulin in a concentration of 10 μ g/mL at 37°C in a 5% CO_2 atmosphere.

- SK-BR-3

  McCoy's 5A medium supplemented with 10% FBS and 1% Pen-Strep at 37°C in a 5% CO_2 atmosphere.

- MDA-MB-231

  L-15 medium supplemented with 15% FBS and 1% Pen-Strep at 37°C without CO_2.

Cell medium was changed every two to three days for nutrient renewal. At approximately 80% of cell confluence, cells were detached with trypsin-EDTA (0.25%) from the bottom of the flask. Cell culture medium was added to stop the trypsin's activity. Afterwards the cells were centrifuged for 5 minutes at 200 g. The cells were then diluted in TrypanBlue® that stain the cells which have a compromised membrane, allowing the appropriate counting of live cells. An aliquot of the cell suspension was taken out and TrypanBlue® was added in a 1:1 proportion ration. 10 μ L of the stained cells were added

to each side of a Neubauer chamber to count the cells. This is followed by the resuspension of the cells in the cell culture medium and the sub-culturing in new TC flasks.

3.4.2 3D Cell Culture

To obtain 3D cell culture models (spheroids), BT-474 cells were cultured in agar-coated plates. The agar coating was applied using the liquid overlay method [139, 140]. 1.5% agarose was prepared in PBS prior to the assay and then 50 μL were added to each well of 96-well untreated plates (Thermo Fisher Scientific, cat. no 168136). BT-474 cells were detached as explained previously. Cells were counted with a Neubauer chamber, and then these were diluted in new medium and 200 μL were added to each well. The 96-well plate was then centrifuged for 3 minutes at 100 G. Pictures of 9 wells were taken for each timepoint of the experiment (Days 0, 1, 2, 3 and 4). Finally, the plate was stored in an incubator at 37°C in a 5% CO_2 atmosphere.

3.4.3 Internalisation of pDNA- and miRNA- complexed NPs

After culturing the spheroids, PLA/modified TPGS-NPs complexed with NAs were internalised for subsequent assessment of the transfection efficiency of these carriers. The incubation of NA complexed NPs was done both in 2D cell culture and in 3D spheroids. For 2D cell culture, the pDNA- and miR-NPs were incubated 24 hours after cell seeding. For 3D spheroids, the NA complexed NPs were incubated after four days. In this case, four days after spheroids' formation, 50 μL of BT-474 medium + BT-474 spheroids were transferred to a new sterile untreated 96-well plate, already prepared with culture medium (100 μL), carefully placing one in each well. Then, another 50 μL of culture medium were added to each well.

The preparation of the NPs complexes followed a simple outline, identical for both 2D and 3D preparations: each type of complex (pDNA- and miR-NPs) were prepared in a flow chamber. Firstly, the naked NPs underwent a 15-minute period of sterilisation under UV light. The complexation of NPs with both NA is explained in section 3.3.2 and the same procedure was followed for this experiment. The cells were then incubated and afterwards they were put in the incubator at 37°C in a 5% CO_2 atmosphere for three timepoints (24-, 48- and 72h). The plates' layout with the conditions to be tested in the several assays used for assessment of cellular viability, internalisation, cytotoxicity and metabolic activity, and transfection efficiency (3D and 2D) are shown in Figures B.1, B.3, B.2, B.4, B.5, B.9, B.8, B.7, and B.6 respectively.

- 2D

  For each condition, 50 μL of NPs complexes were added to each well.

- 3D

  For the conditions tested, 10 μL of each one was added to each well.

After incubation with NA complexed NPs, the 2D cell culture and 3D BT-474 spheroids were submitted to different assays. These will be further explained in the following sections.

3.4.4 MTT (3-(4,5-Dimethylthiazol-2-yl)-2,5-Diphenyltetrazolium Bromide)

The Metabolic activity (MA) of the cells was analysed using CytoSelect™ 3-(4,5-dimethylthiazol-2-yl)-2,5-diphenyltetrazolium bromide (MTT) Cell Proliferation Assay following the manufacturer's instructions. By definition, this assay is a colorimetric method used to measure cell MA based on the reduction of a yellow tetrazolium salt, MTT, to purple formazan crystals [141, 142]. This reduction process is facilitated by Nicotinamide adenine dinucleotide phosphate (NADPH)-dependent cellular oxidoreductase enzymes [143]. These enzymes operate in the mitochondria of living cells, converting MTT into its insoluble formazan derivative, characterised by a purple colour [141].

The three control conditions present in the previously described plates (Figure B.7 and B.6) for the experiment are positive controls, containing 10% DMSO, BT-474 spheroids and cell culture medium, a negative control containing only spheroids in culture medium, and a blank control comprising only culture medium. Briefly, after the incubation of the NPs with spheroids, the medium from each well was discarded (200 μLL) and 100 μLL of fresh medium were added. This experiment was performed for three timepoints (24, 48 and 72h post-treatment). Then, 10 μLL of the CytoSelect™ MTT Cell Proliferation Assay Reagent were added to each well and the plate was incubated for 24 hours, at 37°C in a 5% CO_2 atmosphere. This step was done protected from light. After 24h, 100 μLL of Detergent Solution were added in the dark to each well and the plate was incubated at RT for another 24h. These procedures were performed in a flow chamber. The next day, the absorbance was measured at 540 nm in Synergy HT microplate reader (Biotek®).

The results were analysed using Microsoft Excel (version 2.71 MacOS).

3.4.5 Flow Cytometry

Single cells or particles in suspension in a buffered salt-based solution are swiftly analysed by flow cytometry as they pass through single or multiple lasers. For every particle and/or sample it is possible to analyse the visible light scatter, as well as fluorescence parameters. The first one can be measured in two directions, one being the forward scatter providing information regarding the relative size of the cell; and the other, at 90º, offering data for the internal complexity or granularity of the cell. After cell incubation, the signal registered by the cytometer comes from transfected cells, with expression of fluorescent proteins, or by staining the samples with fluorescent dyes or conjugated antibodies [144].

Flow cytometry was used to assess the efficacy of transfection and cell viability throughout the development of this project. All experiments followed the same basic procedure. pDNA-NPs and miR-NPs incubated 2D cell cultures were washed with PBS and then

trypsinized with 100 μL of Trypsin-EDTA and incubated at 37°C for 5-10 minutes. Afterwards, 100 μL of appropriate cell medium (according to each used cell line) were added to block the action of trypsin, and the samples were centrifuged for 5 minutes at 2500 G. The cells were washed with PBS after the removing of the supernatant. Zombie Violet (1:500 in PBS), a dye that stains cells with damaged membranes was used (100 μL). They were allowed to incubate for 15 minutes at RT, protected from light, before being washed with PBS a third time. They were fixed with a solution of PBS containing 4% Paraformaldehyde (PFA) and 2% sucrose and incubated for 20 minutes at RT. PBS (700 μL) was added again, and the cells were centrifuged under the same conditions as before. Finally, the supernatant was removed, and the pellet was resuspended in 200 μL of PBS containing 2% FBS.

The BT-474 spheroids were firstly transferred to microtubes (six per condition which are represented in Figures B.9, B.8) and then washed with PBS. After that, each microtube was loaded with 50 μL of Trypsin-EDTA and incubated at 37°C for 5-10 minutes. The following steps followed the same methodology as the 2D samples.

The samples were analysed in FACS Aria™ III (BioPROTECT) and the results were analysed with the software GraphPad Prism (version 9.5.1 (528) MacOS).

3.4.6 Fluorescence Microscopy

In fluorescence microscopy, the samples are excited through the incidence of a short wavelength light, generally blue light or UV. A barrier filter used to observe the sample transmits the fluorescence, which is seen as bright against a dark backdrop because it absorbs the high energy light. Since this occurs, fluorescence being seen as luminosity against a dark background, even small quantities of fluorescent compounds and particles can be seen within the examined samples [145].

3.4.6.1 Confocal Microscopy

Confocal fluorescence microscopy (CFM) is widely used in nanomedicine and biological laboratory context being a non-invasive optical method that allows *in vivo* imaging of untreated biological tissues at a cellular-level resolution. With CFM it is possible to visualise 3D high-resolution images due to the suppression of signal from the focus plane (detector covered by a pinhole). This technique provides the acquisition of images with auto-fluorescence that possess higher lateral and axial resolutions when compared to other fluorescence spectroscopy techniques (like wide field) [146].

In this thesis, CFM was used to assess whether the cultured cells had efficiently uptake the vehicles of gene delivery along with the therapy system. This technique was used following the NPs' internalisation in 2D cell culture. The conditons tested are shown in Figure B.5. Prior to the confocal sample analysis, the cells were transferred to a new non-sterile 96-well plate and fixed at the timepoints of each experiment (24, 48 and 72 hours) in 4% PFA and 2% sucrose for 20 minutes, protected from the light. The cells

were then washed with PBS, two times. Afterwards, 100 μL of 4',6'-diamino-2-fenil-indol (DAPI) staining solution in a 1:1000 PBS ratio was added to each condition and allowed to incubate, protected from light, for 5 minutes. The plate was stored at 4°C in 200 μL of PBS.

4

Results & Discussion

4.1 Nanoparticle formulation and characterisation

After the NPs formulation, the NPs physical properties were measured by DLS.

4.1.1 Size, surface charge and polydispersity index

The DLS analysis revealed an average HS of 231 ± 44 nm for the PLA/modified TPGS-NPs (Figure 4.1A). The HS for PLA/unmodified TPGS-NPs (PLA/TPGS-NPs) has an average value of 244.8 ± 6 nm (Figure 4.1A), which is similar to the PLA/modified TPGS-NPs. Figure 4.1B represents the ZP of PLA-based NPs. It shows and average ZP of 8.7 ± 2.3 mV for the PLA/modified TPGS-NPs. Whereas for the PLA/TPGS-NPs the average ZP is 0.1 ± 0.0 mV. A significantly difference in comparison to the PLA/modified TPGS-NPs. Relative to the PI, the average values for PLA/TPGS-NPs and PLA/modified TPGS-NPs are 0.13 ± 0.04 and 0.16 ± 0.06, respectively (Figure 4.1C).

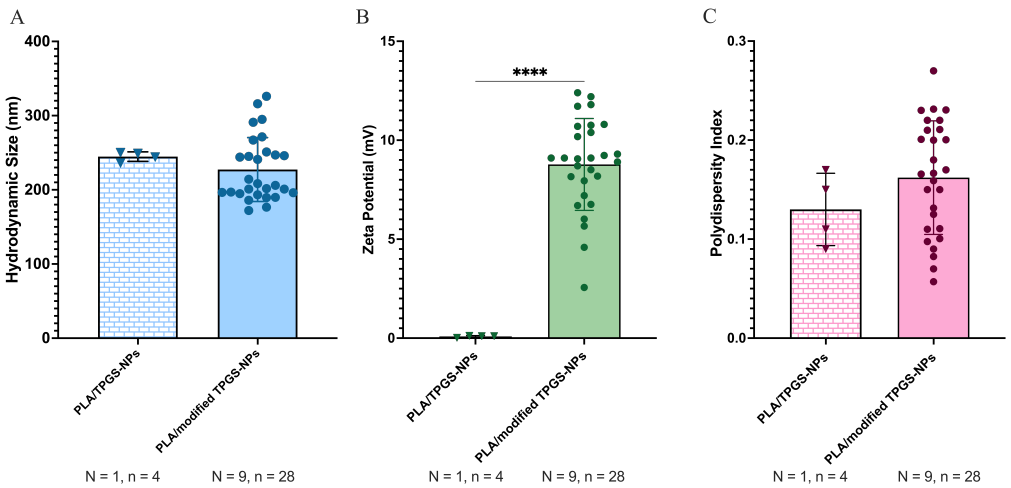

Figure 4.1: (A) HS, (B) ZP and (C) PI of PLA/TPGS-NPs and PLA/modified TPGS-NPs measured by DLS.

Accurate particle size determination is a crucial aspect of NPs characterisation. This metric holds significant importance as various secondary properties, including surface

area, toxicity, degradation, targeting, and uptake mechanism, are closely associated with the particle size [81]. Although the EPR effect highly influences NPs uptake into the tumour, this process is not uniform. NPs can enter through various mechanisms. These include Clathrin-mediated endocytosis (CME), caveolae-mediated endocytosis, and sometimes micropinocytosis, contingent on NPs size. According to the literature, NPs with a size of about 200 nm seem to perform well and have good permeability for biological barriers [147], therefore promoting tumour accumulation and cell adhesion.

Another important characteristic of NPs is their ZP. ZP holds importance as it correlates with the stability of NPs over both short and long terms as well as their cell adhesion, internalisation, and potential cytoxicity [148]. NPs possessing high ZP values (either negative or positive) are electrically stabilised in suspension. Conversely, NPs featuring low ZP values tend to undergo coagulation or flocculation, leading to compromised physical stability [149, 150]. Literature suggests that NPs with ZP values between −10 and +10 mV are considered approximately neutral [151] and even that ZP values in the range of −5 mV to +5 mV indicate rapid aggregation [148]. While if absolute ZP values are over 30 mV are considered strongly cationic or anionic [151, 152], showing also good stability [151].

Despite these reference values, they are applied to low molecular weight surfactants and pure electric stabilisation. Larger molecular weight stabilisers, mainly acting through steric stabilisation, necessitate different considerations. For such cases, absolute ZP values of 20 mV or even lower can offer sufficient stabilisation [148, 153]. Additionally, effectiveness of gene vector transfection may depend on ZP value. A system exhibiting either a positive surface charge density is preferable for accommodating DNA or miRNA molecules. Given that numerous proteins, DNA, and cell membrane surfaces possess an anionic nature, a positive ZP not only improves NA loading efficiency but also potentially facilitates effective accumulation within target cells [148].

The DLS results showing a significant difference in ZP values for PLA/modified TPGS-NPs in comparison to PLA/TPGS-NPs (Figure 4.1B) suggest that the formulation of NPs with modified TPGS introduces positive charges on the NPs surface. These charges are due to the amine groups of spermidine in modified TPGS provided by the modification of TPGS described in section 3.2.

Moreover, these ZP results, according to literature, may be considered relatively neutral [148]. However, positively charged amine groups may be enough to bind to the negatively charged phosphate groups of NAs and increase the interaction with the negatively charged cellular membranes. Consequently improving NPs loading and bioavailability [154].

Besides the size and ZP, the NPs suspension should have a population with low dispersity. That is given by the value of PI. When characterising NPs size distribution, the PI serves as a parameter to delineate the range of sizes within NP systems. This term quantifies the extent of non-uniformity in the distribution of NPs sizes. PI is dimensionless and it ranges from 0.0 (represents a perfectly uniform population) to 1.0 (highly polydisperse population comprising multiple sizes). In practice, values equal to

or below 0.2 are commonly considered suitable for polymer-based NPs [155]. According to the average PI of 0.16 ± 0.06 for the PLA-based NPs (Figure 4.1C), the NP population has a low dispersion.

The NPs were also analysed through AFM. Through this analysis is possible to assert the topographic feature of the NPs suspension along with the size. From Figure 4.2 it is possible to see the NPs have a spherical shape and smooth surface.

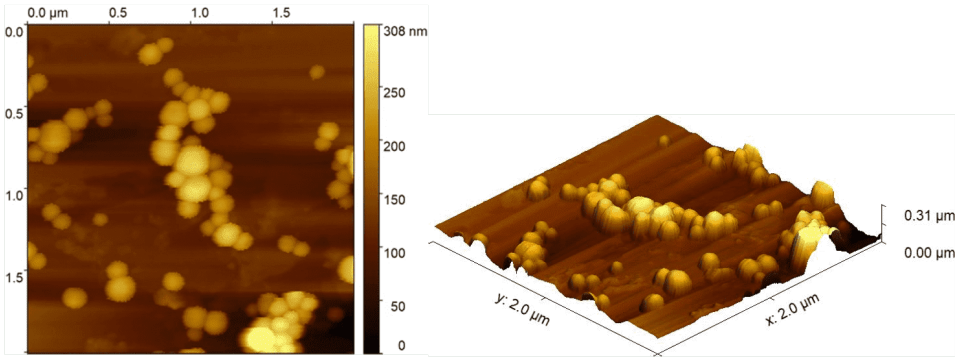

Figure 4.2: AFM images of PLA-based NPs.

Further measurements using the AFM analysis software Gwyddion (version 2.62 Windows 10) indicates an average value of 206 nm for the NPs size. The shape and surface of the NPs is in accordance with previously reported studies of PLA/TPGS-NPs [156, 157, 158]. It should also be noted that, even though similar, this value for NPs size is different from the one measured by DLS. This is due to the fact that DLS measures HS through NPs Brownian movements, not making distinction between a single dried NP and NPs that are hydrated in suspension. In AFM, it is possible to measure each NP individually.

4.1.2 Nanoparticle temperature stability

NPs were also submitted to a temperature stability assay by varying the temperature conditions in which the suspension was stored. Over a period of 30 days, NPs were kept at three different temperatures: 4°C, RT (25°C) and 37°C, and the HS, ZP and PI were measured periodically. The results from this assay are gathered in Figure 4.3.

At 37°C the NPs properties started to change over time. The HS of PLA/modified TPGS-NPs experiences a significant increase (Figure 4.3G) while the ZP experiences a significant decrease (Figure 4.3H), over time. The NPs also become more polydispersed, over time (Figure 4.3I).

At the other two temperature conditions, 4°C and RT, the NPs mostly maintained the properties along the 30 days. The HS was the least changed over time. At these two temperature conditions (4°C and RT) it is possible to see that the ZP values suffered some variations over time, but they are not significant.

The stability of NPs pertains to their ability to maintain their physicochemical characteristics over time. It encompasses the potential alteration in molecular arrangement,

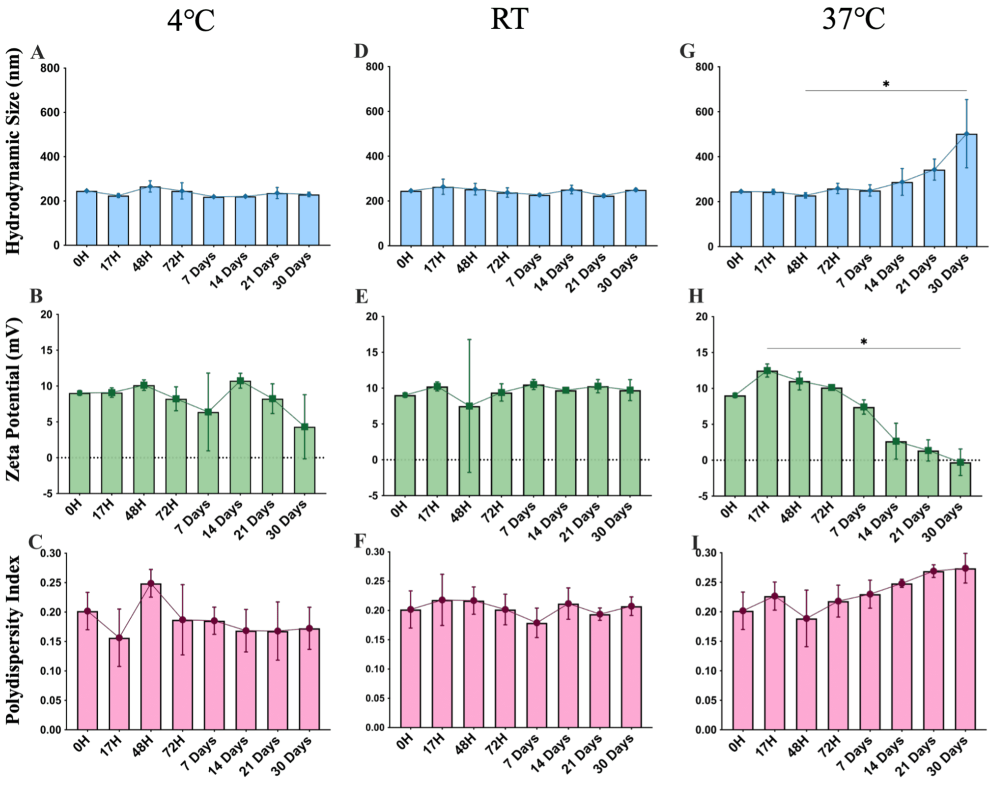

Figure 4.3: HS, ZP and PI of PLA NPs over a period time of 30 days at three different temperature conditions. A, D and G: 4ºC; B, E and H: RT; C, F and I: 37 ºC. N=1, n=3

not solely limited to chemical degradation, influenced by various environmental factors such as temperature, light, humidity, and pH. In cases where NPs serve as carriers for biomolecules *in vivo*, becomes crucial to understand their interaction stability with loaded biomolecules under diverse biophysical conditions, resembling the systemic circulation matrix [153, 159].

The difference in behaviour may be explained by the mechanisms which influence the degradation of PLA. The degradation of PLA is greatly dependent on pH and temperature [100]. PLA exhibits limited heat resistance attributed to its heightened molecular mobility near its glass transition temperature (Tg), typically around 45-60ºC. Elevated temperatures during processing can induce ester bond cleavage, generating carboxyl groups that subsequently undergo self-catalytic degradation during the thermal degradation process of PLA [160]. From existing literature, it is evident that PLA experience a degradation span of 100 hours under physiological pH of 7.4. Interestingly, in an acidic pH of 3, no noticeable degradation is observed even after 400 hours. The degradation rate of PLA accelerates by fourfold at 37°C compared to 25°C, leading to complete degradation within 400 hours. Further elevating the temperature to 60°C results in rapid degradation within 10 hours [100].

Hence, it is possible to conclude that the higher temperature of storage can change NPs properties over time and alter their stability in suspension. This factor may be favourable

for the goal of the study since in biological conditions the temperature is around 37°C. This instability is welcomed when the goal is for the NPs to degrade once they are inside the cells in order to release the NA cargo for the therapeutic purposes. However the higher temperature may also suggest that NPs watter diffusion increases, leading to the increase in HS registered by DLS at 37°C (Figure 4.3G)

4.2 Nanoparticle Complexation with nucleic acids

The PLA/modified TPGS-NPs were complexed with pDNA (pDNA-NPs) in several N/P ratios to evaluate the best ratio for future studies. The complexed pDNA-NPs were also analysed in terms of HS, ZP and PI through DLS and topography by AFM.

4.2.1 Complexation of NPs with Plasmid DNA

The HS, ZP, and PI were measured using the same procedure for the naked NPs (PLA/modifiedTPGS-NPs without NAs). The HS of NPs complexed with pDNA significantly increased with the N/P ratio (Figure 4.4A). Figure 4.4B represents the ZP of pDNA-NPs. ZP appears to become slightly less negative with an increase in the N/P ratio. However, this observation is not entirely definitive due to the similar ZP values across all N/P ratios, as indicated by the standard deviation. pDNA-NPs seem to have a more disperse population when compared to the control naked NPs, as it is visible from the PI results shown in Figure 4.4C. From the modal distribution of HS shown in Figure C.1 it is visible a highly polydispersed population for these pDNA-NPs.

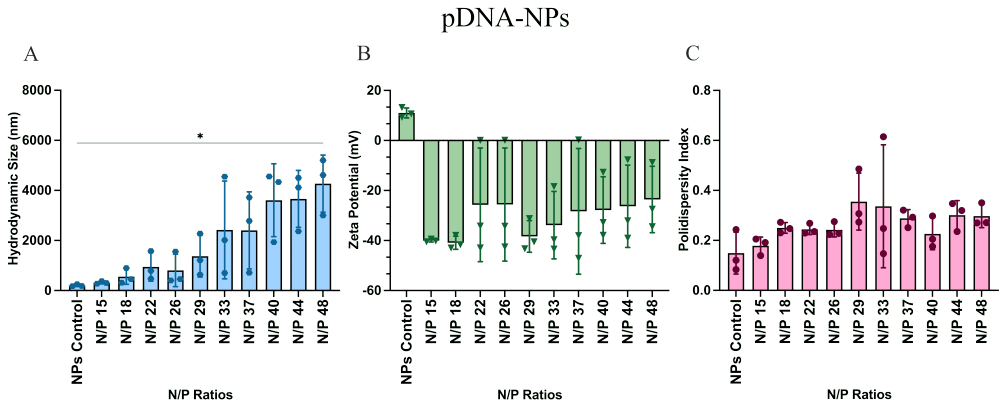

Figure 4.4: pDNA-NPs' HS (A), ZP (B) and PI (C) analysed by DLS. Statistical analysis was performed using One-way ANOVA.

Accompanying the DLS results, the pDNA-NPs were also analysed in terms of complexation by agarose gel electrophoresis (Figure 4.5). From Figure 4.5A, it is visible an increasing complexation from the disappearing bands along the N/P ratios in the gel shift. At N/P ratio 44 a complete complexation is observed due to the complete disappearing of the band on this ratio and the presence of a strong signal only in the sample well. Figure

4.5B, confirms this statement. The percentage of complexation is increasing with the N/P ratios, reaching 100% at 44 N/P ratio.

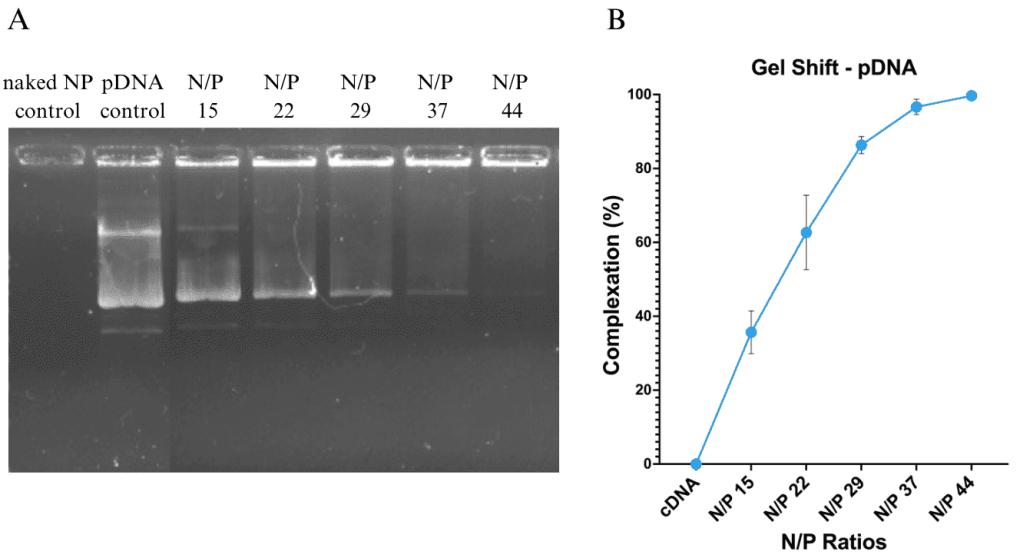

Figure 4.5: (A) Agarose gel electrophoresis bands of pDNA-NPs. (B) Gel shift curve of pDNA-NPs. N=2, n=3.

The results from topography and morphology analysis by AFM are shown in Figure 4.6A and B. From these, it is visible a great agglomeration of pDNA-NPs. In comparison to naked NPs, they remain spherical and with a smooth surface. Analysis of these results with the Gwyddion software shows an average size of approximately 332 nm for N/P ratio 44.

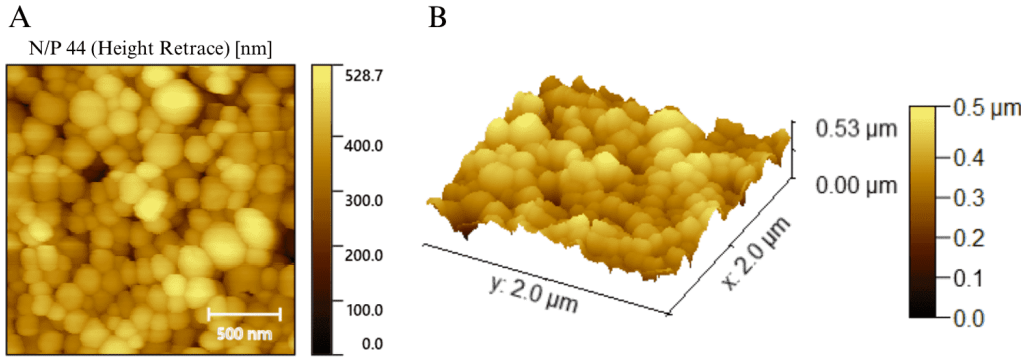

Figure 4.6: (A) 2D AFM images of N/P ratio 44 of pDNA-NPs. (B) 3D images of N/P ratio 44 of pDNA-NPs.

This value is slightly higher than the one registered for naked NPs (from 206 nm to 332 nm), which may indicate the pDNA complexation with PLA/modified TPGS-NPs. Although the measured size in AFM for pDNA-NPs is higher than the one for naked NPs, it is still lower than the HS measured by DLS for pDNA-NPs. Hence the pDNA-NPs follow the same trend as the naked NPs. The measured HS is higher than the one measured in AFM.

The increase in size can be explained in two ways. The first and more plausible one is the potential formation of a pDNA-NPs matrix. With increasing N/P ratios, a greater

number of NPs are introduced into the system. Consequently, more NPs are available to bind with the relatively large pDNA molecules (6195 base pairs). This binding may lead to the interaction of multiple NPs with the same pDNA molecule, resulting in the creation of a substantial matrix. It is also possible that pDNA molecules remain free in suspension. This also causes the dispersity of the suspension to increase. The increase of NPs connected with pDNA in suspension, along with free pDNA explains the increase in HS registered by DLS.

Another explanation, however less probable, is that the NPs did not successfully complex with pDNA. If it were the case, it could be because of insufficient amine groups, and therefore not enough positive charges. However, that appears to not be the case when visualising the results from the agarose gel electrophoresis (Figure 4.5A). As stated above, the NPs indeed demonstrate a successful complexation with pDNA.

Moreover, cationic polymers, equipped with protonable amine groups, effectively form complexes with NAs, strengthening transfection efficiency. Electrostatic attractions between positively charged amine groups and negatively charged phosphate groups in pDNA prompt rapid condensation, leading to spontaneous complex formation by polycations. The polycation/DNA ratio regulates the charge aspect [161]. The modified TPGS as a surfactant in the NPs provides them the necessary amine groups and charge for the interaction with pDNA. Therefore, a successful complexation of the PLA/modifiedTPGS NPs with pDNA should be observed. However, the ZP of pDNA-NPs remains negative. This is due to the connections made between the NPs and pDNA molecules. Since they bind electrostatically, and the N/P ratio is increasing it means that more NPs can bind to pDNA molecules. This connection can lead to various NPs binding to the same pDNA molecule, leaving some pDNA molecules free, which increases the overall negative charge of the suspension (registered by DLS). Further, the ZP values of pDNA-NPs (Figure 4.4B) are in accordance with previously registered ones for PLA pDNA-NPs [162]. Further proving a successful complexation of the NPs with pDNA.

Given the obtained results, the chosen N/P ratios to carry out in the *in vitro* studies were N/P 29 and 44. The obvious choice was of course the N/P 44 ratio. This is the ratio that reached 100% complexation and had the overall less negative charge of all the ratios tested. However, since the HS of this ratio was quite high it was decided that a ratio with smaller HS but still with a high percentage of complexation would be a good candidate to perform the *in vitro* studies. Hence, the N/P ratio 29 was also chosen for the *in vitro* assays. Furthermore, it was also decided that N/P ratio 15 would also be tested to evaluate the differences between these ratios with three different complexation percentages.

4.2.2 Complexation of NPs with miR125b

Similarly to pDNA-NPs, NPs complexed with miR (miR-NPs) were also characterised in terms of HS, ZP and PI, as well as percentage of complexation.

The miR-NPs had an increase in the HS, analogously to the pDNA-NPs (Figure 4.7A).

In terms of ZP, miR molecules do not differ much from pDNA ones (Figure 4.7B). miR are also negatively charged so to effectively bind these molecules the NPs must have a positive surface charge. As stated before, that was possible with the NPs being formulated with the modified TPGS that confers them the positive charges. Figure 4.7C represents the PI of miR-NPs also showing an increase in population dispersity, confirmed by the modal distribution of HS represented by Figure C.2 that shows a highly polydisperse population.

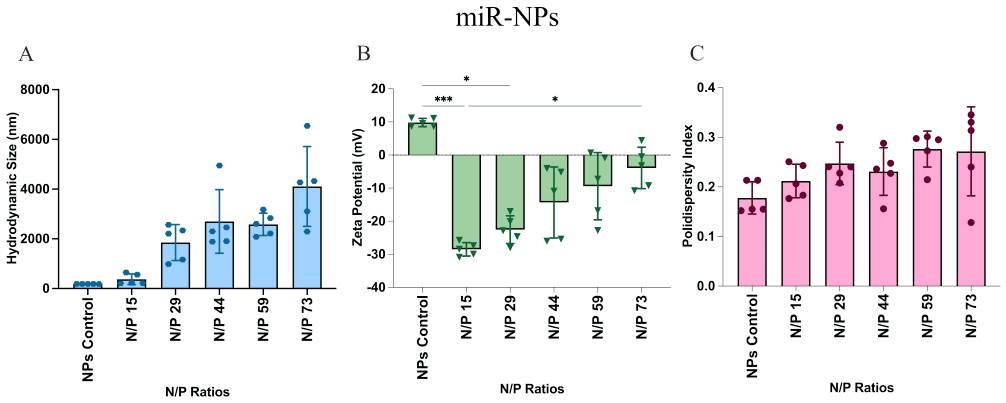

Figure 4.7: miR-NPs' HS (A), ZP (B) and PI (C) analysed by DLS. Statistical analysis was performed using t-test.

Looking at these results, it is possible to do the same extrapolation as in the previous section. The miR-NPs seem to form a matrix between the NPs and the miR molecules as well. This results in an increase in the HS measured by DLS. As the N/P ratio increases, there are more NPs in suspension to interact with the miR molecules. Several NPs can have multiple miR molecules interacting with their surface and other NPs can establish interactions with the free ends of miR molecules.

Further, the N/P ratios tested with miR were chosen according to the results obtained for pDNA-NPs. A complete complexation was verified at N/P ratio 44 for pDNA-NPs. Since pDNA is a much larger molecule, it was decided that higher N/P ratios should be tested to hypothetically achieve a complete complexation. The chosen ratios according to this reasoning are described in section 3.3.2.

However, from the agarose gel shift results is possible to conclude that a complete complexation was not verified in any of the tested N/P ratios (Figure 4.8A). With the increase in N/P ratio the agarose gel bands suffer a decrease in intensity. However no band disappears completely. From Figure 4.8B, this incomplete complexation is more visible since the percentage did not reach 100%. Furthermore, it can be stated that from N/P ratio 29 the complexation reached a kind of plateau and it did not surpass 65%. Considering these results, this may be an explanation as to why the miR-NPs experience an increase in size measured by DLS.

When examining the ZP of miR-NPs as shown in Figure 4.7B, a distinct trend becomes evident. There is a noticeable alteration in the ZP of the miR-NPs as the N/P ratio increases. The ZP appears to become less negatively charged with the rising N/P ratio. Given that the

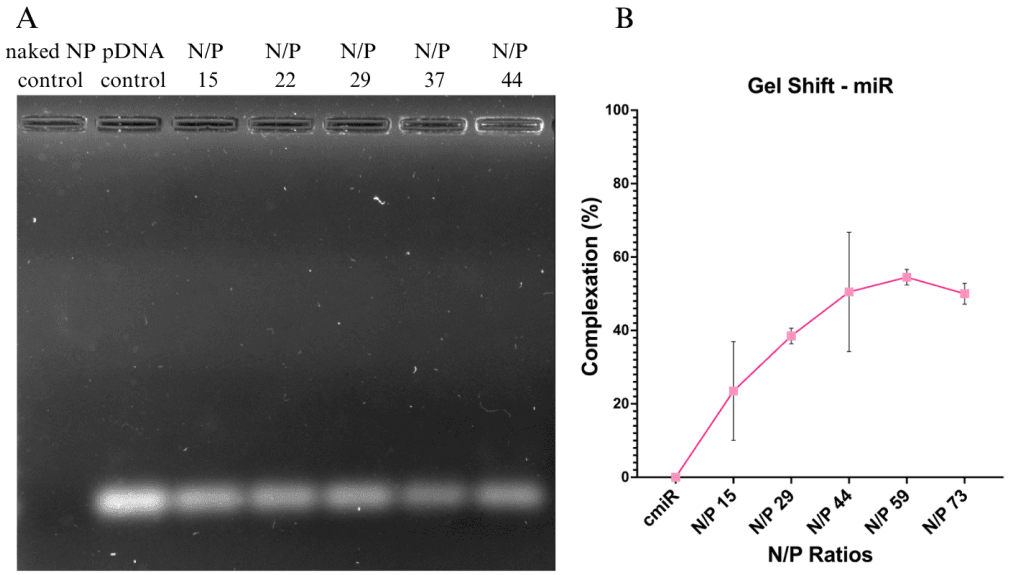

Figure 4.8: (A) Agarose gel electrophoresis bands of miR-NPs. (B) Gel shift curve of miR-NPs. N=4, n=5.

naked NPs possess a positive charge, it is anticipated that they form complexes with miR molecules, which are negatively charged. Successful complexation with miR molecules should then result in the absolute values of ZP of miR-NPs decreasing. This trend is indeed observed in the ZP results (Figure 4.7B).

In the same way as pDNA-NPs, the topography and morphology of miR-NPs were also analysed by AFM. The results from this analysis are shown in Figures 4.9A and B. The measured size was N/P 73. In both representations (2D and 3D AFM images) it is clear the miR-NPs remain spherical and with a smooth surface. The average size measured in AFM is approximately 389 nm.

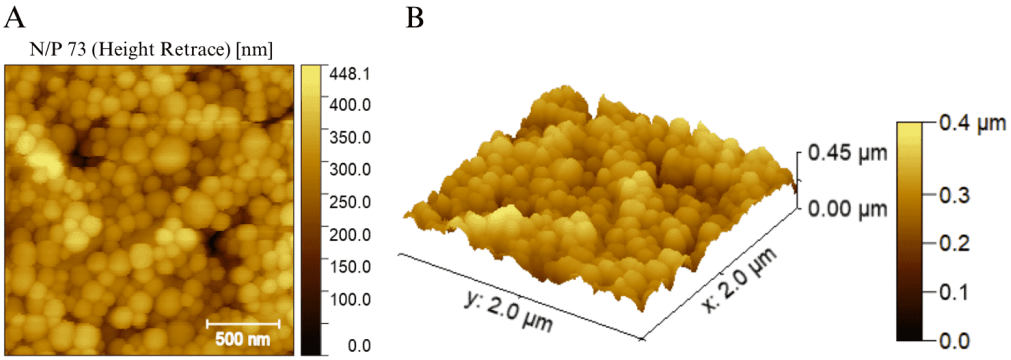

Figure 4.9: (A) 2D AFM images of N/P ratio 73.3 of miR-NPs. (B) 3D images of N/P ratio 73.3 of miR-NPs.

This size is, again, smaller than the one measured by DLS but higher than the naked NPs. Moreover, great density of NPs is also visible from these Figures 4.9A and B, which may explain the increase in size registered by DLS that measures the HS of miR-NPs in suspension. With higher density of complexed NPs in suspension the polydispersity also increases, consequently increasing the HS measured by DLS.

Combining all the results for miR-NPs, it was possible to infer that N/P ratio 73 would be the best suited for *in vitro* studies. Owing to the less negative charge along with the overall size of each individual NP it was expected that this ratio would perform better in the *in vitro* studies. Despite the higher HS caused by the NPs matrix, the less negative charge would possibly serve as an advantage for interaction with the cells. Nonetheless, in terms of comparison between pDNA-NPs and miR-NPs, it was also decided that N/P ratio of 15 and 29 would also be tested for the same reasons as in the pDNA-NPs.

4.2.3 *in vitro* Studies

4.2.3.1 Cellular viability in 2D monolayer cell culture

The *in vitro* cell viability assessment performed in 2D was carried out using three different BC cell lines: BT-474, SK-BR-3 and MDA-MB-231. These three cell lines were cultured in different experiments and incubated with the pDNA-NPs and miR-NPs in three timepoints: 24, 48, and 72 hours.

Figure 4.10 summarises the results from the cell viability evaluation on the three different cell lines for pDNA-NPs. The analysis was carried out with flow cytometry using FACS Aria III and the results were analysed in FlowJo (version 10.9.0 MacOS). This method was previously described in the methods section (3.4.5).

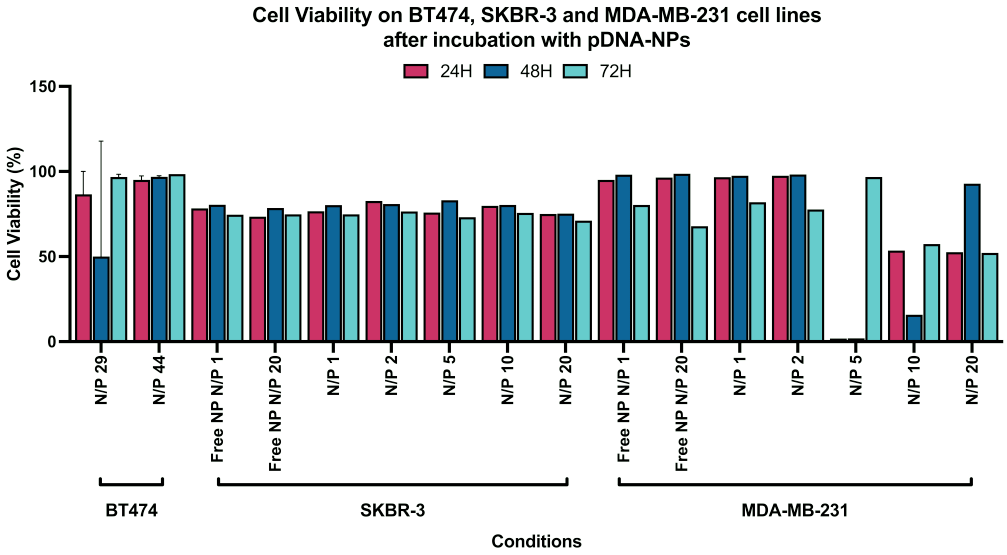

Figure 4.10: Cell viability of the three cell lines: BT-474, SK-BR-3 and MDA-MB-231 after pDNA-NPs delivery in 2D cell culture. BT-474: n=2; SK-BR-3 and MDA-MB-231: n=1.

In general, the incubated cells from the three cell lines exhibit high percentages of viability. However, higher N/P ratios on MDA-MB-231 cell line (N/P 5, 10 and 20) display on average a 50% viability. This appears to suggest higher vulnerability of the cell line to the pDNA-NPs, resulting in a decreased cell viability.

Figure 4.11 gathers the results from the cell viability assessment on the same three different cell lines but for miR-NPs. Across all conditions tested in the three cell lines

(BT-474, SK-BR-3 and MDA-MB-231), all show a high viability percentage on miR-NPs across the three timepoints.

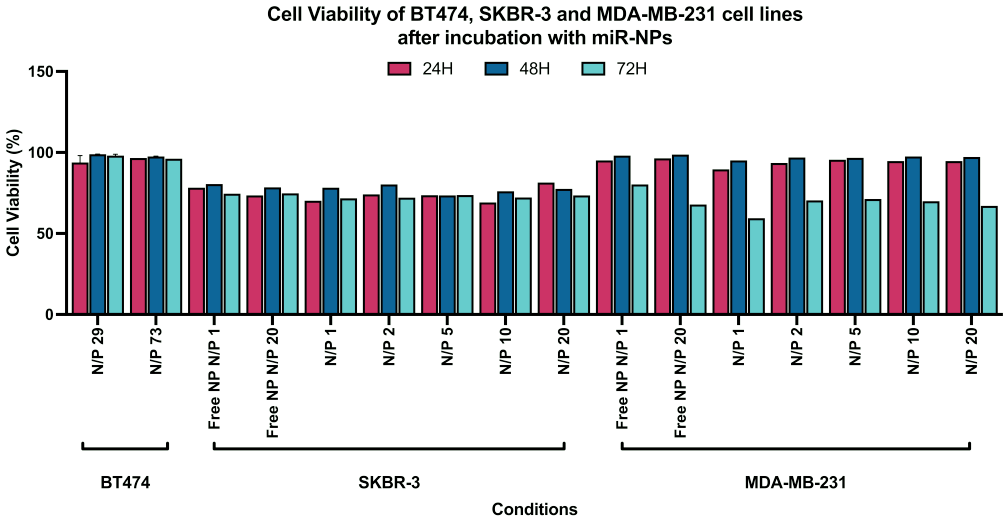

Figure 4.11: Cell viability of the three cell lines: BT-474, SK-BR-3 and MDA-MB-231 incubated with miR-NPs, in 2D cell culture. BT-474: n=2; SK-BR-3 and MDA-MB-231: n=1.

This is an important finding and crucial result to consider for further potential therapeutic applications. The negligible cytotoxicity observed in these results provide a good foundation to consider these miR-NPs for further *in vivo* studies and potential treatment without harming healthy cells.

Moreover, the high viability percentage found across the three cell lines suggest the miR-NPs have a broad applicability and are compatible with different cell types, responding well to variability.

In a parallel assay, MDA-MB-231 2D cells incubated with fluorescently labelled pDNA-NPs with Rhodamine B were also analysed in flow cytometry to assess cellular viability. The results from this experiment are presented in Figure 4.12. In all the three timepoints the percentage of viability remains above 80 in all conditions.

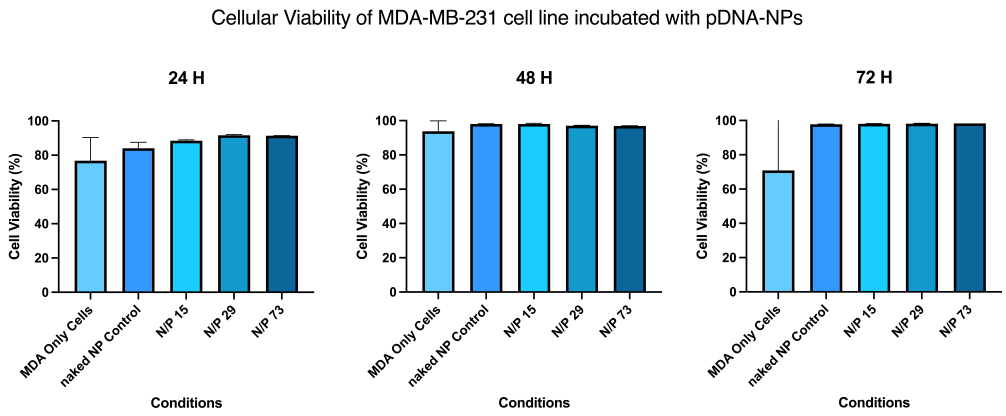

Figure 4.12: Cell viability of MDA-MB-231 2D cells incubated with pDNA-NPs fluorescently labelled with Rhodamine B at three timepoints (24-, 48-, and 72h). (n=3)

It is evident that the pDNA-NPs labelled with Rhodamine B do not seem to induce cytotoxic effects in the different N/P ratios tested and across the three timepoints (24-, 48-, and 72h).

Similar results were obtained for miR-NPs fluorescently labelled with Rhodamine B. These are mustered in Figure 4.13.

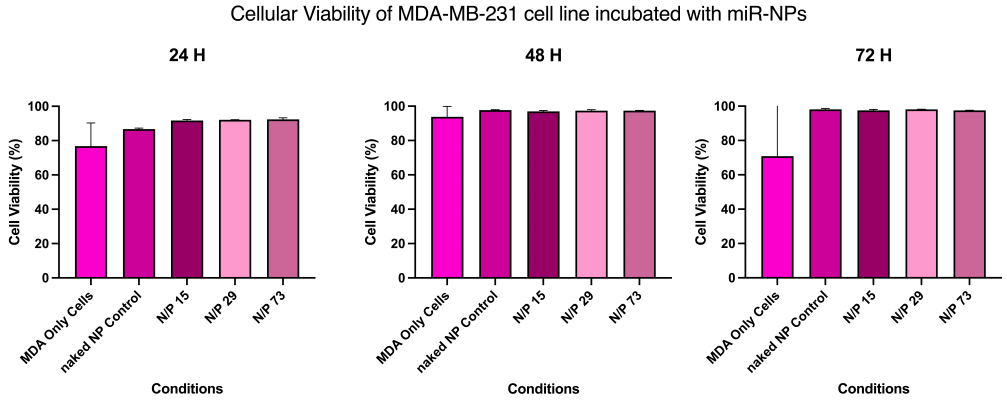

Figure 4.13: Cell viability of MDA-MB-231 2D cells incubated with miR-NPs fluorescently labelled with Rhodamine B at three timepoints (24-, 48-, and 72h). (n=3)

In every timepoint (24-, 48-, and 72h) the values of cellular viability percentage also remain over 80 for all N/P ratios, further proving the negligible toxicity of the NPs.

4.2.3.2 Cellular uptake of fluorescently labelled NPs

The naked NPs were functionalised with a fluorescent dye – Rhodamine B – to assess whether or not the NPs were being internalised by the cells. Therefore providing a background study for further transfection efficiency analysis with pDNA- and miR-NPs.

This experiment was carried out in 2D cell cultured MDA-MB-231 cell line with three ratios: N/P 15, 29 and 73. A NP control was also tested, corresponding to the higher amount of NP present in the highest N/P ratio 73. Figure 4.14 summarises the results of the internalisation evaluation of MDA-MB-231 cells incubated with pDNA-NPs.

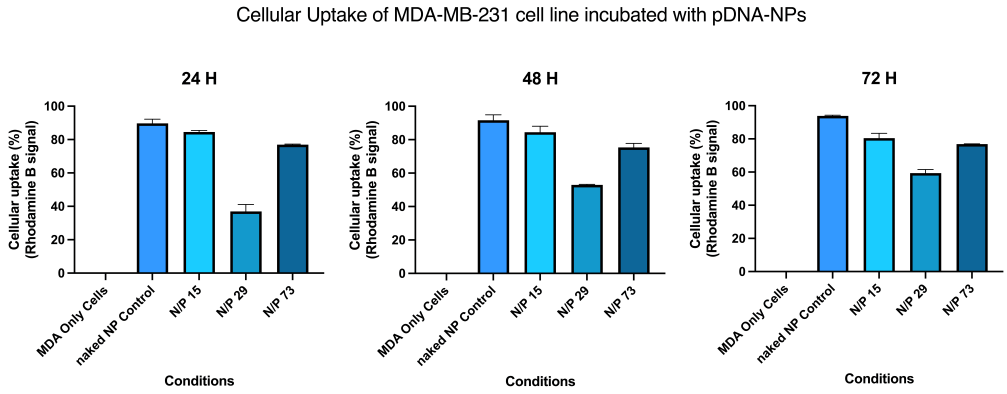

Figure 4.14: Cellular uptake of MDA-MB-231 2D cells incubated with Rhodamine B functionalised pDNA-NPs at three timepoints: 24, 48, and 72 hours. (n=3)

Regarding the internalisation of pDNA-NPs given by the detected signal of positive population for Rhodamine B , N/P 29 was the ratio that showed the lowest levels of uptake signal although with values around or above 40%. The other two ratios (N/P 15 and 73) show values around 80% for the three timepoints. Control NPs showed values of cellular uptake around 90%. Given that this condition consists of naked NPs, it is highly probable that they were uptake by the cells. This is due to the physical characteristics of the NPs alone, i.e., relatively small size (~200 nm) and positive charge (~10 mV). Nevertheless, values of 90% of uptake signal are extremely high, so some of the presented signal may be related to the expression of free Rhodamine B.

Figure 4.15 gathers the results from the internalisation assessment of MDA-MB-231 cells incubated with miR-NPs.

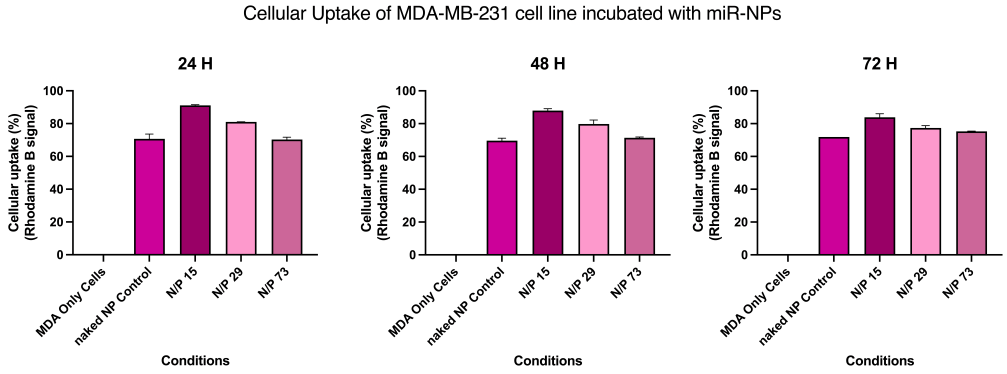

Figure 4.15: Cellular uptake of MDA-MB-231 2D cells incubated with Rhodamine B functionalised miR-NPs at three timepoints: 24, 48, and 72 hours. (n=3)

Similar results were obtained with miR-NPs functionalised with Rhodamine B. The internalisation efficiency of control NPs showed lower values than those of in the pDNA-NPs conditions (Figure 4.14), with values around 70%. The N/P ratios of miR-NPs displayed uptake signals around 80%. The explanation for these values could be the same as the pDNA-NPs.

To confirm the results obtained from flow cytometry analysis, the Rhodamine B labelled pDNA- and miR-NPs were also analysed in confocal microscopy.

The images represented by Figure 4.16A-O show the confocal images of only cells (Figure 4.16A – C), naked NPs control (Figure 4.16D – F), and pDNA conditions (Figure 4.16G – O).

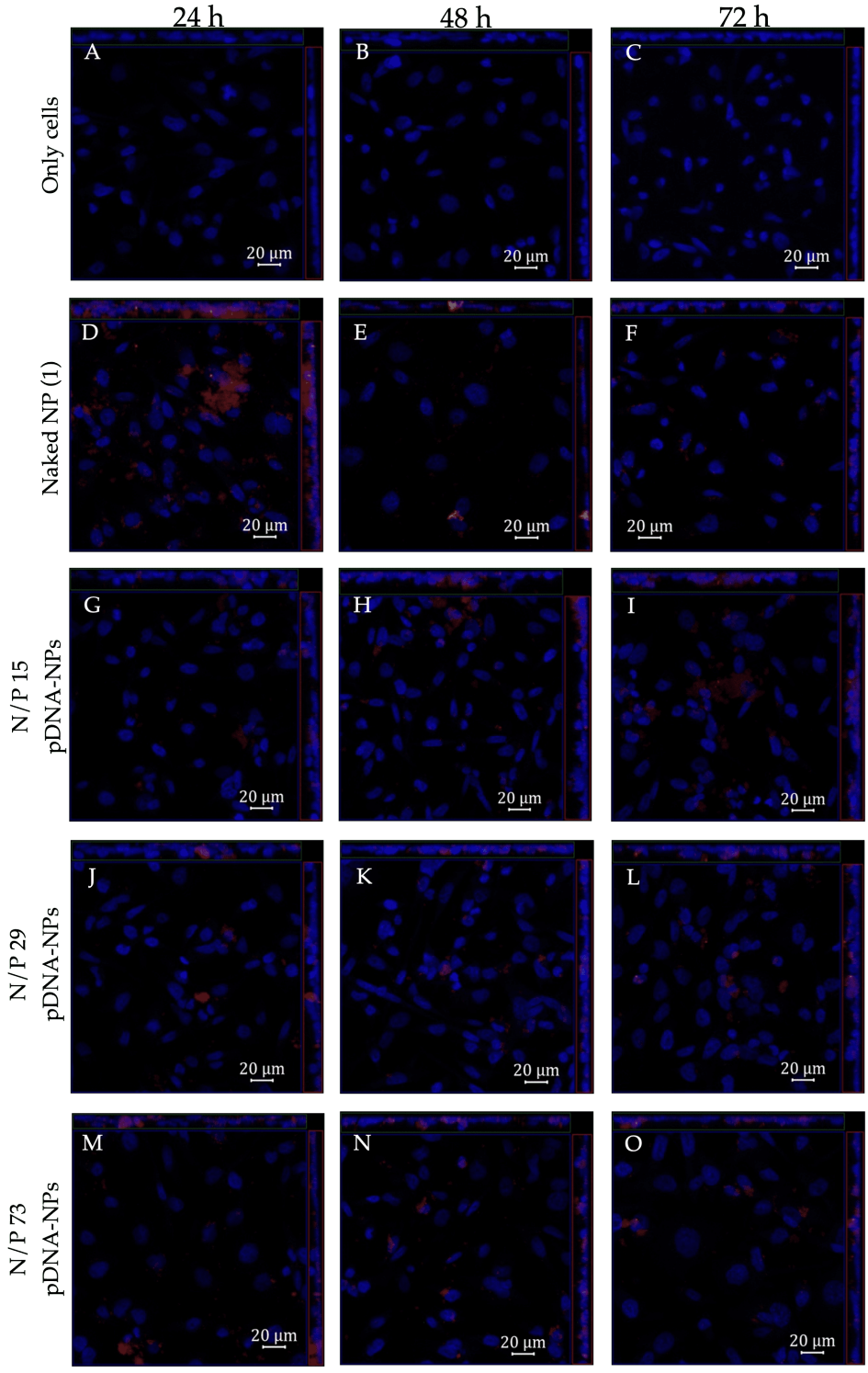

Figure 4.16: Confocal fluorescence microscopy images of cellular uptake in MDA-MB-231 cells incubated with pDNA-NPs labelled with Rhodamine B. (A–C) only cells; (D-F) naked NPs control for pDNA-NPs N/P 73.3; (E-G) pDNA-NPs N/P 15; (H-J) pDNA-NPs N/P 29; (K-M) pDNA-NPs N/P 73. All images are maximum projections of their z-stacks. Magnification: 40X.

While Figure 4.17A-L show the confocal images of naked NPs control (Figure 4.17A – C) and miR conditions (Figure 4.17D – L).

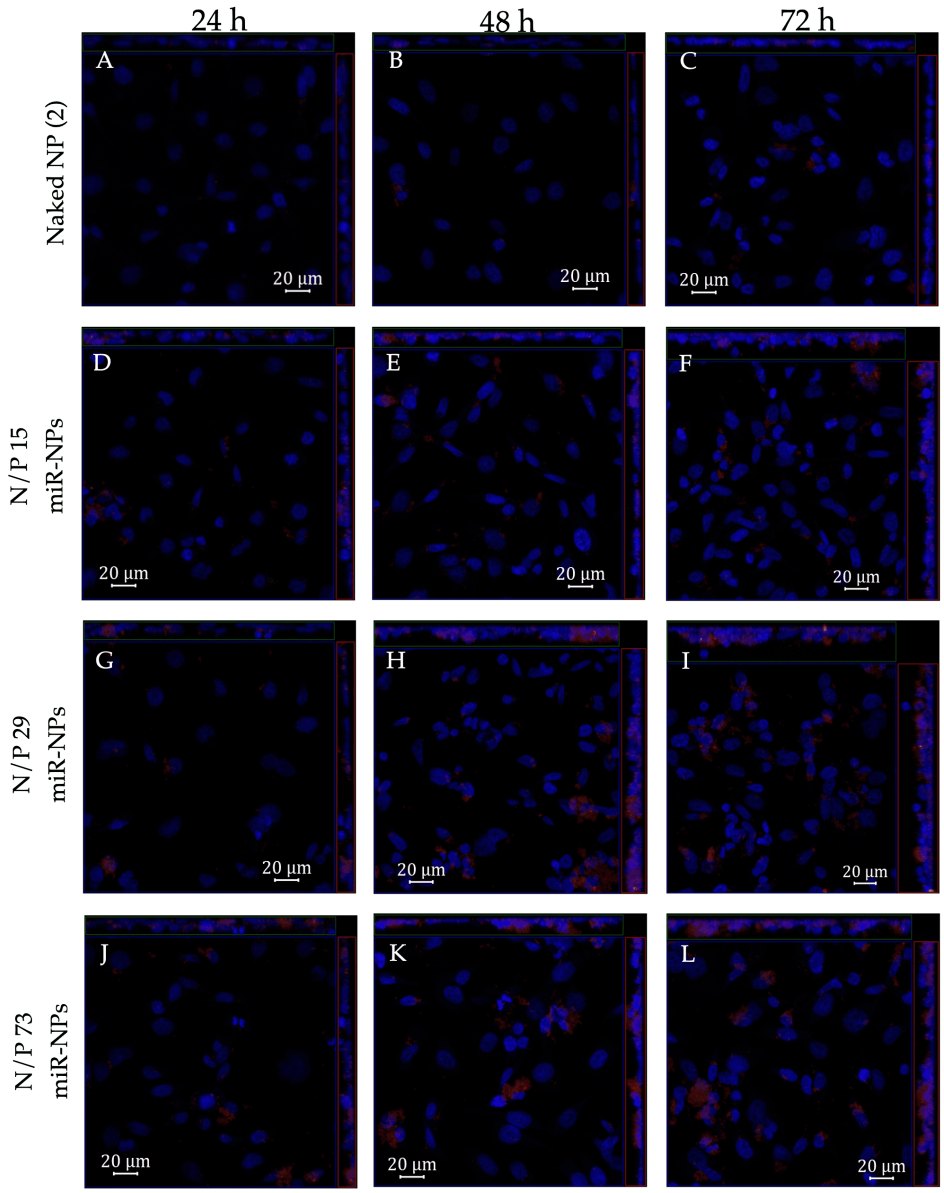

Figure 4.17: Confocal fluorescence microscopy images of cellular uptake in MDA-MB-231 cells incubated with miR-NPs labelled with Rhodamine B. (A-C) naked NPs control for miR-NPs N/P; (D-F) miR-NPs N/P 15; (G-I) miR-NPs N/P 29; (J-L) miR-NPs N/P 73. All images are maximum projections of their z-stack. Magnification: 40X.

The fluorescence signal represented in blue in all images is related to the expression of DAPI which stains the cells' nucleus. The red signal represents the fluorescence from Rhodamine B for both pDNA conditions and miR conditions.

It is clear the presence of cellular uptake by comparison between the negative control (only cells) and all the other conditions. Although at 24 hours, the NPs may be completely uptake by 2D cell culture, from these confocal images (Figures 4.16 and 4.17) is not clear whether they are inside the cells or just attached to the surface. However, these results still do not exclude the possibility of free Rhodamine B being expressed. This conclusion is drawn by the fact that it is not visible an increase in red fluorescence signal over time.

The signal remains somewhat the same for 24, 48, and 72 hours.

4.2.3.3 Spheroids morphology

In parallel to 2D cell culture *in vitro* studies, the goal was to also try establishing a 3D microenvironment of BC. The 3D cell culture model used was based on spheroids which were formed with the technique described in the methods section (3.4.2). Creating and characterising this 3D cell culture model holds paramount significance. It enhances the comprehension of TME attributes, notably factors like hypoxia. Furthermore, it aids in more accurately anticipating how the TME interacts with the therapeutic action of the developed NPs.

The developed spheroids comprise a single cell line (BT-474) representative of the subtype Luminal B of BC. Their development was carried out for four days. Figure 4.18A represents the brightfield images obtained for each day of the experiment. It is evident that BT-474 forms spheroids with an almost perfect spherical morphology. Immediately after day 0, it becomes evident that these spheroids begin to heavily cluster together, forming highly compact spheroids. Consequently, the diameter of these spheroids greatly decreases over the experiment's duration.

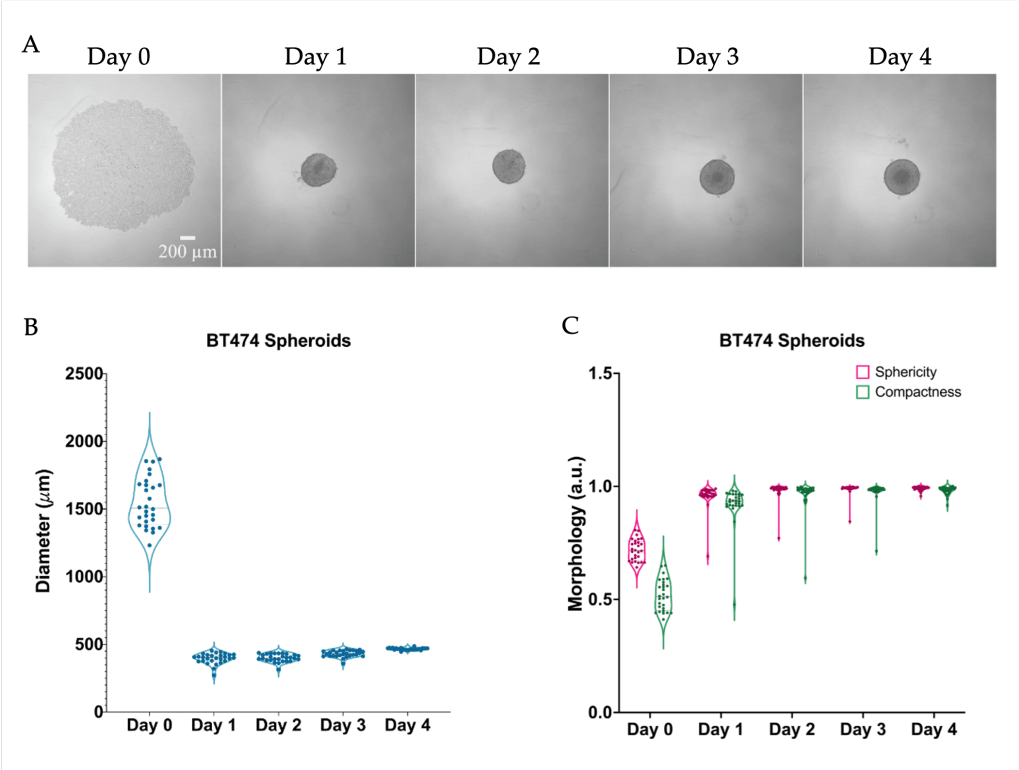

Figure 4.18: (A) Brightfield images of BT-474 spheroids in each day of development. At day 0 the spheroid is formed with 7500 cells. Magnification: 5x. Scale bar: 200 μm. (B) Spheroids diameter development over the 4-days experiment. (C) Compactness and sphericity evolution over the 4-days experiment. Number of experiments: 3; number of replicates in each experiment: 9

Furthermore, it is visible that the spheroids become darker in colour and actually

start to have two different tonalities: a darker core and a lighter outer layer. This might suggest an increase in the spheroids compactness and cell layers creation, resulting in a 3D structure. The darker inner core may also indicate the presence of cells in a senescent state due to existing hypoxic conditions and lack of nutrients [163].

Figure 4.18B and C, summarises the results observed in brightfield microscopy, corresponding to the spheroids diameter (Figure 4.18B), sphericity and compactness (Figure 4.18C). On day 0, the day of the cell seeding, the spheroids revealed an average diameter of 1547 ± 181 μm. On day 1, the diameter decreases to 396 ± 39 μm. This decrease suggests that the spheroids form 24 hours after cell seeding. Posteriorly, once the spheroid is formed and reaches a sort of equilibrium the cells start to proliferate, resulting in a slight increase in the spheroids diameter. However, this increase occurs at a slow rate. At day 2, 3 and 4 the diameters are 401 ± 29 μm, 431 ± 24 μm, 467 ± 8 μm, respectively.

With regards to the sphericity, it is obvious from both the brightfield images (Figure 4.18A) and the morphology graph (Figure 4.18C) that on day 0 the spheroids do not have a well-defined shape. However, on the remaining days, the spheroids gain clear spherical form, with this characteristic becoming more evident.

The compactness of the BT-474 spheroids is noticeable on Figures 4.18A (brightfield images) and is evident on Figure 4.18C (morphology graph). Compactness can be evaluated in terms of aggregation. Spheroids with spaces and gaps have loose aggregates while spheroids with a visible border around them and almost no loose cells have a great degree of compactness. The high degree of compactness is observable on the brightfield images (Figure 4.18A) of the spheroids for each day, except day 0. Compactness varies between 0 and 1, with the latter representing a perfectly compact spheroid. On days 1, 2, 3 and 4 the BT-474 spheroids' compactness are 0.92 ± 0.09, 0.96 ± 0.07, 0.98 ± 0.05, 0.98 ± 0.02, respectively (Figure 4.18C). These results are all close to 1, leading to the conclusion that this cell line forms spheroids with a high degree of compactness.

By definition, compactness pertains to the level of remodelling and density within a spheroid. A high degree of compactness translates to a pronounced hypoxic gradient extending from the surface to the core of the spheroid. Consequently, it also influences the spheroids interaction with small molecules [164].

These results suggest the rising of some challenges associated with the spheroids characteristics, namely with regards to compactness. Higher degree of compactness may affect affect treatment efficacy and, therefore, difficult the translation to *in vivo*[165].

4.2.3.4 Cellular viability and metabolic activity in 3D spheroids

The MTT assay was used to evaluate the MA of BT-474 spheroids incubated with NAs complexed NPs and therefore infer about the NPs' cytotoxicity. The incubated cells with a tetrazolium salt are cleaved into a coloured formazan product by metabolically active cells. This assay serves as a valuable tool for assessing cell viability and MA. The

formazan crystals are dissolved, and the absorbance of the solution can be measured by spectrophotometry at 570 nm.

The preparation of the spheroids incubated with NPs for the MTT assay was previously described in the methods section (3.4.3). The MTT assay was performed for three timepoints (24h, 48h and 72h). The conditions tested were previously described in the methods sections and are represented on Figures B.6 and B.7.

The results from this assay are summarised in the heatmaps represented by Figure 4.19A and B. Figure 4.19A shows the MA of BT-474 3D spheroids incubated with pDNA-NPs while Figure 4.19B demonstrates the MA of the same spheroids incubated with miR-NPs. In a preliminary analysis, in general NPs did not seem to greatly impact the viability of cells, showing a negligible toxicity. Moreover, in several conditions a darker green is observed, indicating the MA was higher than 100%.

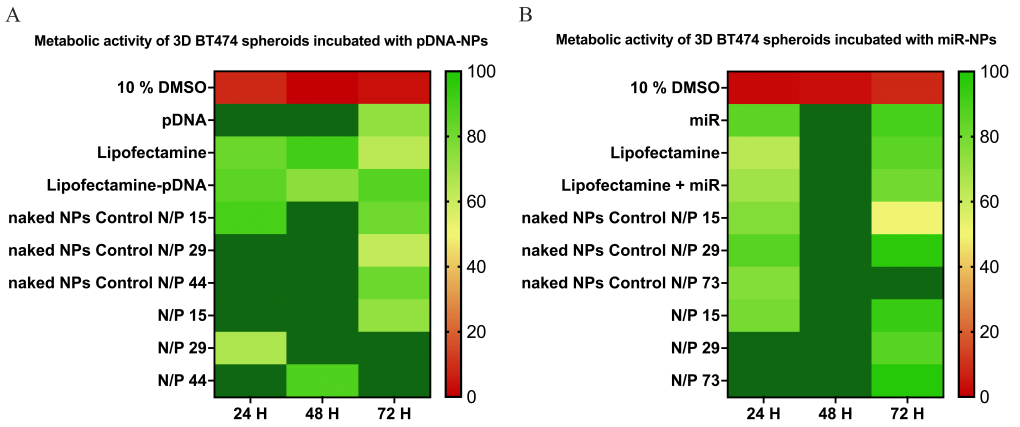

Figure 4.19: MA of NAs complexed NPs measured by MTT cell proliferation assay. (A) Heatmap of MA in 3D spheroids of BT-474 incubated with several controls and pDNA-NPs ratios. The controls correspond to the amount of non-complexed NPs used in each ratio. (B) Heatmap of MA in 3D spheroids of BT-474 incubated with several controls and miR-NPs ratios. The controls correspond to the amount of non-complexed NPs used in each ratio. n=3 in all conditions.

At 24 hours of incubation in Figure 4.19A, naked NPs controls and pDNA-NPs show high MA displaying values of 70% or higher, meaning the NPs did not induce strong cytotoxic effects. The same trend is noticeable in Figure 4.19B, with miR-NPs and naked NPs controls.

At 48 hours of incubation, there is an increase in MA on naked NPs controls, pDNA-NPs ratios 15 and 29 (Figure 4.19A) showing a metabolic percentage higher then 100%. This means BT-474 spheroids are proliferation wih a possible increase of their external layers. Once more, this tendency is also witnessed for miR conditions (Figure 4.19B). Moreover these suggest that NPs did not induce cytotoxic effects.

At 72 hours some changes become perceptible. A trend is noticeable in all pDNA conditions where the MA decreases, except N/P ratios 29 and 44 (Figure 4.19A). Even though this decline occurs the cells still remain metabolically active, with values over 70%. This suggest that with time the presence of NPs might induce cytotoxic effects. For the two N/P ratios that showed higher MA percentages (N/P 29 and 44), a possible explanation

might be the amount of NPs present in these ratios. Compared to N/P 15, since pDNA amount remains the same, the higher amount of NPs in N/P 29 and 44 might suggest a protective effect of PLA NPs from pDNA toxicity on the cells. Relative to miR conditions, a similar inclination is clear. The MA diminishes at this timepoint in almost every condition, apart from NPs control (6). Overall the percentage of MA remains above 50%, indicating that the cytotoxic effects of NPs on the cells are negligible and did not affect regular cell metabolism and proliferation.

The cause for the low overall decrease in MA might also be attributed to the type of cells used in the experiment. The 3D spheroids of BT-474 have a high degree of compactness, as previously discussed in section 4.2.3.4. Higher compactness degree promotes oxidative stress and nutrient deprivation, especially in the core of the spheroid. These factors influence mitochondrial activity, promoting cellular repair mechanisms and resulting in high values for MA.

Cellular viability of BT-474 spheroids incubated with pDNA-NPs and miR-NPs was also assessed by flow cytometry using FACS Aria III. The results from this assay were analysed with the help of FlowJo (version 10.9.0 MacOS). The cellular viability results are gathered in Figure 4.20A and B.

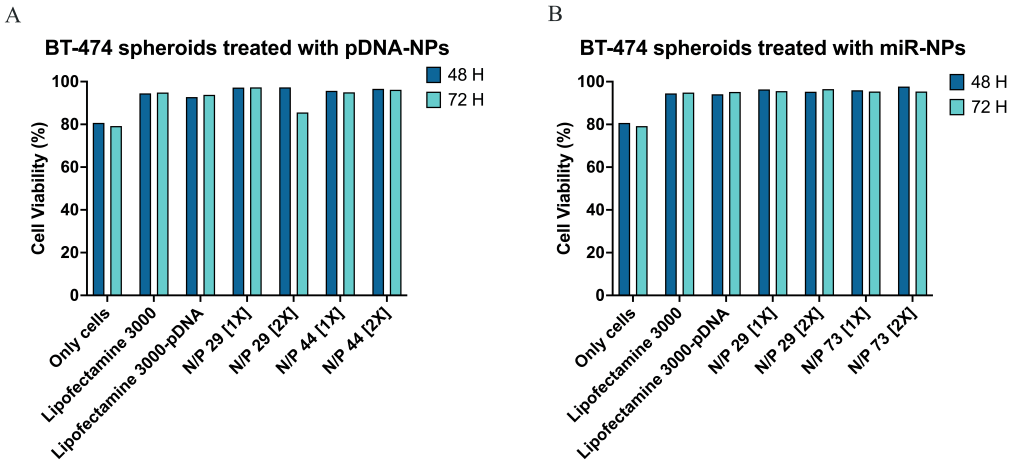

Figure 4.20: (A) Evaluation of cellular viability of BT-474 3D spheroids incubated with pDNA-NPs. n=1 (B) Evaluation of cellular viability of BT-474 3D spheroids incubated with miR-NPs. n=1

The cell viability is associated with the staining used. The cells were stained with Zombie Violet which is a dye that stains cells which have compromised membranes. From Figure 4.20A and B it is evident the high cell viability of both NPs conditions (pDNA-NPs and miR-NPs), with values around 95% of viability. These results also corroborate the MTT results (Figure 4.19A and B), exhibiting once more that these NPs have low toxicity.

4.2.3.5 Cellular uptake and transfection efficiency in 3D spheroids

Once concluded that the NPs had negligible toxicity, the transfection efficiency of the BT-474 spheroids incubated with pDNA-NPs and miR-NPs was assessed also through

flow cytometry using FACS Aria III and the results analysed in FlowJo. The results from the transfection efficiency are gathered in Figure 4.21A and B.

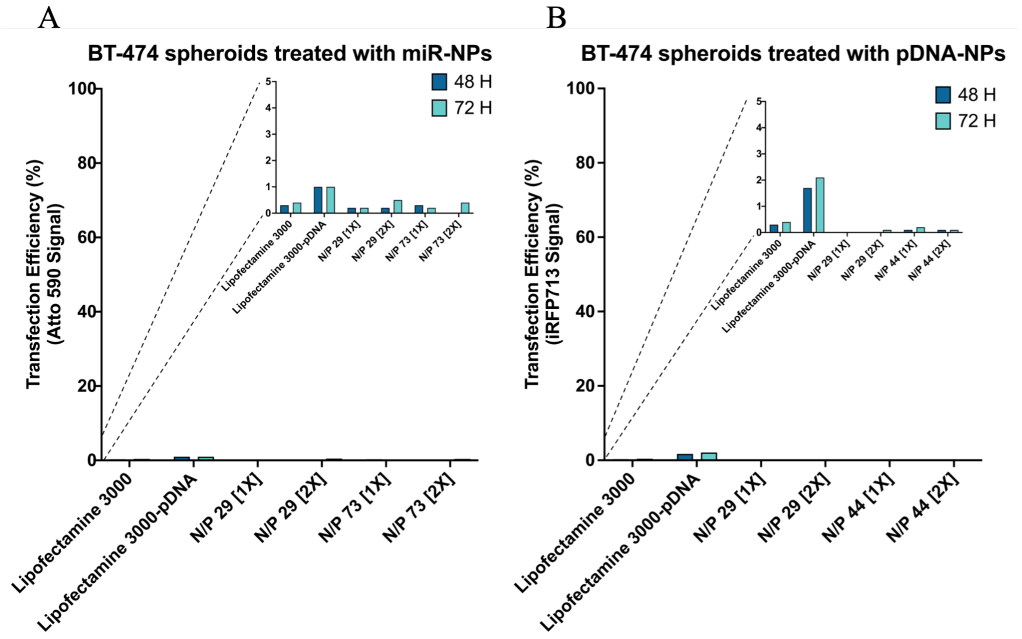

Figure 4.21: (A) Evaluation of transfection efficiency of BT-474 3D spheroids incubated with pDNA-NPs, through analysis of iRFP713 fluorescence signal. n=1 (B) Evaluation of transfection efficiency of BT-474 3D spheroids incubated with miR-NPs, through analysis of Atto 590 fluorescence signal. n=1

It is possible to infer about the transfection efficiency through the signal emitted by both pDNA and miR-125b. Once transfected and translated, the emission signal is directly related to the expression of iRFP713, in the case of pDNA, and of Atto 590 in miR.

Based on the results from Figure 4.21A and B, it is possible to see that the signal detected for iRFP713 corresponded to a very small population of cells. The percentage of positive population for each of the fluorophores (iRFP713 and Atto590) below 1% for all the conditions of pDNA-NPs and miR-NPs, which is considered not relevant. Moreover, pDNA- and miR-lipofectamine show a percentage of positive population for each fluorophore of around 2% and 1% at 72h, respectively. Lipofectamine 3000 was used as a positive control due to being recognised for its ability to yield substantial transfection efficiency and elevated transgene expression [166, 167]). Hence, it should be expected that the Lipofectamine conditions showed high levels of transfection efficiency. However, the 2% and 1% values of transfection efficiency detected correspond to a very low population of cells. This may be happening because of the inability of this vehicle to cross cell membranes or reach cell nuclei on these spheroids. In this case, the high degree of compactness of these BT-474 spheroids may pose a great challenge for the transfection. Percentage values below 2% in flow cytometry is considered background noise, hence these values of positive population for each fluorophore are not considered relevant.

Further, the previously chosen N/P ratios in sections 3.3.1 and 3.3.2 were also tested. It was also decided to test the ratios in two different concentrations: [1x] and [2x]. By

increasing the concentration ([2x]), the ratio remained the same, but the amount of amines and phosphates would be doubled. This increase would possibly promote transfection. However, as said previously, from the results shown on Figure 4.21A and B, the signal observed in any of the NPs conditions is not considered relevant.

Relating the transfection results with the cell viability it is possible to hypothesise the reason for this limited transfection signal. Since the NPs are biocompatible, the explanation for the limited transfection signal must rely on the connection between the positively charged PLA/modified TPGS-NPs and the negatively charged NAs. As seen in sections 4.2.1 and 4.2.2, the pDNA-NPs and miR-NPs are successfully complexed (Figures 4.4 and 4.6 – A and B). This grants the pDNA- and miR-NPs a certain stability that is difficult to revert. Therefore, it prevents the pDNA and miR to unbind from the NPs without occurring some degradation of the NPs. Owing to these reasons, the effective delivery might be hindered. Hence, a successful release of NA and, consequently efficient transfection might only occur upon a complete decomplexation of the NPs from NAs. Based on literature, release of pDNA is dependent on the molecular weight of PLA. Lower molecular weight means a more hydrophilic profile, therefore degradation should occur faster. However the studies' findings from Basarkar *et al.* demonstrated that the release of pDNA was not registered for lower molecular weight PLA, attributing it to the strong electrostatic connection of PLA/modified TPGS-NPs with pDNA [154].

Moreover, as stated previously in 4.1.2, these NPs have a slow degradation rate [168]. Therefore, to appropriately assess the success of this delivery, the assay would have to be carried out with longer timepoints. However, based on previously reported studies, PLA may take up to 400 hours to degrade in physiological conditions [100]. There is a possibility that the degradation can take longer than 400 hours in acidic conditions, since in previous reports PLA seems to not degrade in strong acidic pH (0142-9612/96/115.00). This is a major challenge since 400h, or more is far too long to maintain cells in culture. Nevertheless, longer experiment times would provide a good way to further analyse the transfection, since the ones tested proved not to be enough to gather favourable results.

5

Conclusions

The main aim of this thesis project was to develop targeted multifunctional nano-engineered platforms for gene circuit delivery to achieve enhanced treatment efficacy and at the same time characterise tumour heterogeneity. The work conducted with this project allowed interesting findings and it made significant strides in the development of targeted drug and gene delivery nanosystems, deepening the understanding of tumour heterogeneity.

This project involved the formulation and thorough characterisation of PLA/modified TPGS-NPs for potential applications in imaging and targeting of the BC microenvironment. Additionally, it also involved the assessment of the NPs complexation with genetic materials (pDNA and miR-125b), and extensive *in vitro* evaluations using 2D and 3D cell culture models. This work also delved into the cellular response to various therapeutic modalities and functionalised NPs for enhanced cellular uptake analysis.

Through meticulous experimentation and analysis, several significant milestones were achieved. The PLA/modified TPGS-NPs were developed through the double emulsion solvent evaporation method. The formulation of PLA/modified TPGS-NPs was successfully achieved along with their physical characterisation, yielding NPs with sizes of around 200 nm and positive surface charge. The obtained characteristics of NPs were crucial as they facilitate the interaction with NAs and adhesion to cell membranes.

The complexation of the PLA/modified TPGS-NPs with NAs was also accomplished. While the pDNA-NPs and miR-NPs displayed an interesting increasing trend in size, directly correlated with increase in the N/P ratio, the pDNA-NPs ZP transitioned into a strongly negative realm while remaining remarkably stable and the miR-NPs ZP gradually trended towards less negative charges with increase in N/P ratio. Importantly, these pDNA- and miR-NPs demonstrated overall great biocompatibility, as evidenced by their minimal cytotoxic effects in both flow cytometry and MTT assays.

The functionalisation of PLA/modified TPGS-NPs with Rhodamine B was also achieved. The developed NPs exhibited robust cellular uptake, as confirmed by confocal microscopy and flow cytometry.

Additionally, 3D BC spheroid models were successfully established, providing valuable insights into the behaviour of the developed NPs within a more physiologically relevant

microenvironment. However, the challenge of optimising transfection efficiency remains an ongoing quest and has prompted further exploration into the underlying factors affecting transfection outcomes.

5.1 Future Work

Despite the significant progress made in this study, several avenues for future research remained unexplored, offering the potential for further enhancing the understanding and application of PLA/TPGS NPs in BC research.

One avenue of future investigation involves comprehensive degradation studies, such as experiments related to water diffusion or crystallinity assessments, for instance, for both naked and complexed NPs. Such investigations could shed light on the long-term stability and effectiveness of these NPs. The optimisation of NPs characteristics is also a promising avenue. This includes efforts to fine-tune the NPs' size and ZP upon complexation. Achieving desired properties, such as a small sizes a cationic ZP, holds potential for enhancing cellular interactions and gene delivery.

Additionally, exploring stimuli-responsive functionalisation of NPs, particularly those responsive to pH, is an exciting prospect as it could affect the degradation of the NPs. Such functionalisation could enable controlled release of genetic materials within the BC microenvironment, potentially leading to more precise and effective treatments.

To gain a more comprehensive understanding of the NPs therapeutic potential, it would also be beneficial to extend incubation periods beyond the current 72-hour limit. This would allow for a thorough evaluation of transfection efficiency for pDNA and miR-125b within BC cells.

In summary, this work represents a critical step towards the development of nanoscale platforms for BC research. While the developed NPs have exhibited remarkable biocompatibility and cellular internalisation, further investigations are required to optimise their transfection capabilities. These findings contribute to the ongoing pursuit of innovative strategies for BC diagnosis and treatment within the complex tumour microenvironment.

Bibliography

1. Lourenço JM. The NOVAthesis LaTeX Template User's Manual. NOVA University Lisbon. 2021. Available from: https://github.com/joaomlourenco/novathesis/raw/main/template.pdf
2. Houghton SC and Hankinson SE. Cancer Progress and Priorities: Breast Cancer. Cancer Epidemiology, Biomarkers & Prevention 2021 May; 30:822–44. DOI: 10.1158/1055-9965.epi-20-1193. Available from: https://doi.org/10.1158/1055-9965.epi-20-1193
3. Katsura C, Ogunmwonyi I, Kankam HK, and Saha S. Breast cancer: presentation, investigation and management. British Journal of Hospital Medicine 2022; 83:1–7
4. M Braden A, V Stankowski R, M Engel J, and A Onitilo A. Breast cancer biomarkers: risk assessment, diagnosis, prognosis, prediction of treatment efficacy and toxicity, and recurrence. Current pharmaceutical design 2014; 20:4879–98
5. Kamińska M, Ciszewski T, Łopacka-Szatan K, Miotła P, and Starosławska E. Breast cancer risk factors. Menopause Review/Przegląd Menopauzalny 2015; 14:196–202
6. Kashyap D, Pal D, Sharma R, Garg VK, Goel N, Koundal D, Zaguia A, Koundal S, Belay A, et al. Global increase in breast cancer incidence: risk factors and preventive measures. BioMed research international 2022; 2022
7. Tamimi RM, Colditz GA, Hazra A, Baer HJ, Hankinson SE, Rosner B, Marotti J, Connolly JL, Schnitt SJ, and Collins LC. Traditional breast cancer risk factors in relation to molecular subtypes of breast cancer. Breast cancer research and treatment 2012; 131:159–67
8. Tan PH, Ellis I, Allison K, Brogi E, Fox SB, Lakhani S, Lazar AJ, Morris EA, Sahin A, Salgado R, Sapino A, Sasano H, Schnitt S, Sotiriou C, Diest P van, White VA, Lokuhetty D, and and IAC. The 2019 World Health Organization classification of tumours of the breast. Histopathology 2020 Jul; 77:181–5. DOI: 10.1111/his.14091. Available from: https://doi.org/10.1111/his.14091

9. Loibl S, Poortmans P, Morrow M, Denkert C, and Curigliano G. Breast cancer. The Lancet 2021 May; 397:1750–69. DOI: 10.1016/s0140-6736(20)32381-3. Available from: https://doi.org/10.1016/s0140-6736(20)32381-3

10. Gao JJ and Swain SM. Luminal A Breast Cancer and Molecular Assays: A Review. The Oncologist 2018 Feb; 23:556–65. DOI: 10.1634/theoncologist.2017-0535. Available from: https://doi.org/10.1634/theoncologist.2017-0535

11. Jacot W. 36th San Antonio Breast Cancer Symposium: focus on clinical trial results. Future Oncology 2014 Mar; 10:511–3. DOI: 10.2217/fon.14.11. Available from: https://doi.org/10.2217/fon.14.11

12. Barzaman K, Karami J, Zarei Z, Hosseinzadeh A, Kazemi MH, Moradi-Kalbolandi S, Safari E, and Farahmand L. Breast cancer: Biology, biomarkers, and treatments. International Immunopharmacology 2020 Jul; 84:106535. DOI: 10.1016/j.intimp.2020.106535. Available from: https://doi.org/10.1016/j.intimp.2020.106535

13. Waks AG and Winer EP. Breast Cancer Treatment. JAMA 2019 Jan; 321:288. DOI: 10.1001/jama.2018.19323. Available from: https://doi.org/10.1001/jama.2018.19323

14. Ades F, Zardavas D, Bozovic-Spasojevic I, Pugliano L, Fumagalli D, Azambuja E de, Viale G, Sotiriou C, and Piccart M. Luminal B Breast Cancer: Molecular Characterization, Clinical Management, and Future Perspectives. Journal of Clinical Oncology 2014 Sep; 32:2794–803. DOI: 10.1200/jco.2013.54.1870. Available from: https://doi.org/10.1200/jco.2013.54.1870

15. Stricker TP, Brown CD, Bandlamudi C, McNerney M, Kittler R, Montoya V, Peterson A, Grossman R, and White KP. Robust stratification of breast cancer subtypes using differential patterns of transcript isoform expression. PLOS Genetics 2017 Mar; 13. Ed. by Hunter KW:e1006589. DOI: 10.1371/journal.pgen.1006589. Available from: https://doi.org/10.1371/journal.pgen.1006589

16. Huber KE, Carey LA, and Wazer DE. Breast Cancer Molecular Subtypes in Patients With Locally Advanced Disease: Impact on Prognosis, Patterns of Recurrence, and Response to Therapy. Seminars in Radiation Oncology 2009 Oct; 19:204–10. DOI: 10.1016/j.semradonc.2009.05.004. Available from: https://doi.org/10.1016/j.semradonc.2009.05.004

17. Banin-Hirata BK, Oliveira CEC de, Losi-Guembarovski R, Ozawa PMM, Vitiello GAF, Almeida FC de, Derossi DR, André ND, and Watanabe MAE. The prognostic value of regulatory T cells infiltration in HER2-enriched breast cancer microenvironment. International Reviews of Immunology 2017 Dec; 37:144–50. DOI: 10.1080/08830185.2017.1401620. Available from: https://doi.org/10.1080/08830185.2017.1401620

18. Soysal SD, Tzankov A, and Muenst SE. Role of the Tumor Microenvironment in Breast Cancer. Pathobiology 2015; 82:142–52. DOI: 10.1159/000430499. Available from: https://doi.org/10.1159/000430499

19. Mittal S, Brown NJ, and Holen I. The breast tumor microenvironment: role in cancer development, progression and response to therapy. Expert Review of Molecular Diagnostics 2018 Feb; 18:227–43. DOI: 10.1080/14737159.2018.1439382. Available from: https://doi.org/10.1080/14737159.2018.1439382

20. Lôbo GCNB, Paiva KLR, Silva ALG, Simões MM, Radicchi MA, and Báo SN. Nanocarriers Used in Drug Delivery to Enhance Immune System in Cancer Therapy. Pharmaceutics 2021 Jul; 13:1167. DOI: 10.3390/pharmaceutics13081167. Available from: https://doi.org/10.3390/pharmaceutics13081167

21. Bhowmick NA, Neilson EG, and Moses HL. Stromal fibroblasts in cancer initiation and progression. Nature 2004 Nov; 432:332–7. DOI: 10.1038/nature03096. Available from: https://doi.org/10.1038/nature03096

22. Hu M and Polyak K. Molecular characterisation of the tumour microenvironment in breast cancer. European Journal of Cancer 2008 Dec; 44:2760–5. DOI: 10.1016/j.ejca.2008.09.038. Available from: https://doi.org/10.1016/j.ejca.2008.09.038

23. Bahrami A, Hassanian SM, Khazaei M, Hasanzadeh M, Shahidsales S, Maftouh M, Ferns GA, and Avan A. The Therapeutic Potential of Targeting Tumor Microenvironment in Breast Cancer: Rational Strategies and Recent Progress. Journal of Cellular Biochemistry 2017 Jul; 119:111–22. DOI: 10.1002/jcb.26183. Available from: https://doi.org/10.1002/jcb.26183

24. Bahcecioglu G, Basara G, Ellis BW, Ren X, and Zorlutuna P. Breast cancer models: Engineering the tumor microenvironment. Acta Biomaterialia 2020 Apr; 106:1–21. DOI: 10.1016/j.actbio.2020.02.006. Available from: https://doi.org/10.1016/j.actbio.2020.02.006

25. Tan K and Naylor MJ. Tumour Microenvironment-Immune Cell Interactions Influencing Breast Cancer Heterogeneity and Disease Progression. Frontiers in Oncology 2022 May; 12. DOI: 10.3389/fonc.2022.876451. Available from: https://doi.org/10.3389/fonc.2022.876451

26. Li JJ, Tsang JY, and Tse GM. Tumor Microenvironment in Breast Cancer—Updates on Therapeutic Implications and Pathologic Assessment. Cancers 2021 Aug; 13:4233. DOI: 10.3390/cancers13164233. Available from: https://doi.org/10.3390/cancers13164233

27. Li Y, Zhan Z, Yin X, Fu S, and Deng X. Targeted Therapeutic Strategies for Triple-Negative Breast Cancer. Frontiers in Oncology 2021 Oct; 11. DOI: 10.3389/fonc.2021.731535. Available from: https://doi.org/10.3389/fonc.2021.731535

28. McErlean EM, McCrudden CM, and McCarthy HO. Delivery of nucleic acids for cancer gene therapy: overcoming extra- and intra-cellular barriers. Therapeutic Delivery 2016 Sep; 7:619–37. DOI: 10.4155/tde-2016-0049. Available from: https://doi.org/10.4155/tde-2016-0049

29. Wu X, Yan P, Ren Z, Wang Y, Cai X, Li X, Deng R, and Han G. Ferric Hydroxide-Modified Upconversion Nanoparticles for 808 nm NIR-Triggered Synergetic Tumor Therapy with Hypoxia Modulation. ACS Applied Materials & Interfaces 2018 Dec; 11:385–93. DOI: 10.1021/acsami.8b18427. Available from: https://doi.org/10.1021/acsami.8b18427

30. Mendes BB, Sousa DP, Conniot J, and Conde J. Nanomedicine-based strategies to target and modulate the tumor microenvironment. Trends in Cancer 2021 Sep; 7:847–62. DOI: 10.1016/j.trecan.2021.05.001. Available from: https://doi.org/10.1016/j.trecan.2021.05.001

31. Fong PC, Boss DS, Yap TA, Tutt A, Wu P, Mergui-Roelvink M, Mortimer P, Swaisland H, Lau A, O'Connor MJ, Ashworth A, Carmichael J, Kaye SB, Schellens JH, and Bono JS de. Inhibition of Poly(ADP-Ribose) Polymerase in Tumors from BRCA Mutation Carriers. New England Journal of Medicine 2009 Jul; 361:123–34. DOI: 10.1056/nejmoa0900212. Available from: https://doi.org/10.1056/nejmoa0900212

32. Ward C, Langdon SP, Mullen P, Harris AL, Harrison DJ, Supuran CT, and Kunkler IH. New strategies for targeting the hypoxic tumour microenvironment in breast cancer. Cancer Treatment Reviews 2013 Apr; 39:171–9. DOI: 10.1016/j.ctrv.2012.08.004. Available from: https://doi.org/10.1016/j.ctrv.2012.08.004

33. Roberts S, Peyman S, and Speirs V. Current and Emerging 3D Models to Study Breast Cancer. *Advances in Experimental Medicine and Biology*. Springer International Publishing, 2019 :413–27. DOI: 10.1007/978-3-030-20301-6_22. Available from: https://doi.org/10.1007/978-3-030-20301-6_22

34. Boix-Montesinos P, Soriano-Teruel PM, Armiñán A, Orzáez M, and Vicent MJ. The past, present, and future of breast cancer models for nanomedicine development. Advanced Drug Delivery Reviews 2021 Jun; 173:306–30. DOI: 10.1016/j.addr.2021.03.018. Available from: https://doi.org/10.1016/j.addr.2021.03.018

35. Ellem SJ, De-Juan-Pardo EM, and Risbridger GP. In vitro modeling of the prostate cancer microenvironment. Advanced Drug Delivery Reviews 2014 Dec; 79-80:214–21. DOI: 10.1016/j.addr.2014.04.008. Available from: https://doi.org/10.1016/j.addr.2014.04.008

36. Fisher MF and Rao SS. Three-dimensional culture models to study drug resistance in breast cancer. Biotechnology and Bioengineering 2020 Apr; 117:2262–78. DOI: 10.1002/bit.27356. Available from: https://doi.org/10.1002/bit.27356

37. Kim JB, Stein R, and O'Hare MJ. Three-dimensional in vitro tissue culture models of breast cancer — a review. Breast Cancer Research and Treatment 2004 Jun; 85:281–91. DOI: 10.1023/b:brea.0000025418.88785.2b. Available from: https://doi.org/10.1023/b:brea.0000025418.88785.2b

38. Salinas-Vera YM, Valdés J, Pérez-Navarro Y, Mandujano-Lazaro G, Marchat LA, Ramos-Payán R, Nuñez-Olvera SI, Pérez-Plascencia C, and López-Camarillo C. Three-Dimensional 3D Culture Models in Gynecological and Breast Cancer Research. Frontiers in Oncology 2022 May; 12. DOI: 10.3389/fonc.2022.826113. Available from: https://doi.org/10.3389/fonc.2022.826113

39. Sakalem ME, Sibio MTD, Silva da Costa FA da, and Oliveira M de. Historical evolution of spheroids and organoids, and possibilities of use in life sciences and medicine. Biotechnology Journal 2021 Jan; 16. DOI: 10.1002/biot.202000463. Available from: https://doi.org/10.1002/biot.202000463

40. Ahmad A, ed. Breast Cancer Metastasis and Drug Resistance. Springer International Publishing, 2019. DOI: 10.1007/978-3-030-20301-6. Available from: https://doi.org/10.1007/978-3-030-20301-6

41. Moo TA, Sanford R, Dang C, and Morrow M. Overview of Breast Cancer Therapy. PET Clinics 2018 Jul; 13:339–54. DOI: 10.1016/j.cpet.2018.02.006. Available from: https://doi.org/10.1016/j.cpet.2018.02.006

42. McDonald ES, Clark AS, Tchou J, Zhang P, and Freedman GM. Clinical Diagnosis and Management of Breast Cancer. Journal of Nuclear Medicine 2016 Feb; 57:9S–16S. DOI: 10.2967/jnumed.115.157834. Available from: https://doi.org/10.2967/jnumed.115.157834

43. Sayed RE, Jamal LE, Iskandarani SE, Kort J, Salam MA, and Assi H. Endocrine and Targeted Therapy for Hormone-Receptor-Positive, HER2-Negative Advanced Breast Cancer: Insights to Sequencing Treatment and Overcoming Resistance Based on Clinical Trials. Frontiers in Oncology 2019 Jun; 9. DOI: 10.3389/fonc.2019.00510. Available from: https://doi.org/10.3389/fonc.2019.00510

44. Morales MAG, Rodríguez RB, Cruz JRS, and Teran LM. Overview of New Treatments with Immunotherapy for Breast Cancer and a Proposal of a Combination Therapy. Molecules 2020 Dec; 25:5686. DOI: 10.3390/molecules25235686. Available from: https://doi.org/10.3390/molecules25235686

45. Burstein HJ, Somerfield MR, Barton DL, Dorris A, Fallowfield LJ, Jain D, Johnston SRD, Korde LA, Litton JK, Macrae ER, Peterson LL, Vikas P, Yung RL, and Rugo HS. Endocrine Treatment and Targeted Therapy for Hormone Receptor–Positive, Human Epidermal Growth Factor Receptor 2–Negative Metastatic Breast Cancer: ASCO Guideline Update. Journal of Clinical Oncology 2021 Dec; 39:3959–77. DOI: 10.1200/jco.21.01392. Available from: https://doi.org/10.1200/jco.21.01392

46. Finn RS, Martin M, Rugo HS, Jones S, Im SA, Gelmon K, Harbeck N, Lipatov ON, Walshe JM, Moulder S, Gauthier E, Lu DR, Randolph S, Diéras V, and Slamon DJ. Palbociclib and Letrozole in Advanced Breast Cancer. New England Journal of Medicine 2016 Nov; 375:1925–36. DOI: 10.1056/nejmoa1607303. Available from: https://doi.org/10.1056/nejmoa1607303

47. Ishii K, Morii N, and Yamashiro H. Pertuzumab in the treatment of HER2-positive breast cancer: an evidence-based review of its safety, efficacy, and place in therapy. Core Evidence 2019 Oct; Volume 14:51–70. DOI: 10.2147/ce.s217848. Available from: https://doi.org/10.2147/ce.s217848

48. Maughan KL, Lutterbie MA, and Ham PS. Treatment of breast cancer. en. Am. Fam. Physician 2010 Jun; 81:1339–46

49. Martínez-Sáez O and Prat A. Current and Future Management of HER2-Positive Metastatic Breast Cancer. JCO Oncology Practice 2021 Oct; 17:594–604. DOI: 10.1200/op.21.00172. Available from: https://doi.org/10.1200/op.21.00172

50. Pernas S and Tolaney SM. HER2-positive breast cancer: new therapeutic frontiers and overcoming resistance. Therapeutic Advances in Medical Oncology 2019 Jan; 11:175883591983351. DOI: 10.1177/1758835919833519. Available from: https://doi.org/10.1177/1758835919833519

51. Kunte S, Abraham J, and Montero AJ. Novel HER2–targeted therapies for HER2–positive metastatic breast cancer. Cancer 2020 Jul; 126:4278–88. DOI: 10.1002/cncr.33102. Available from: https://doi.org/10.1002/cncr.33102

52. Kong X, Qi Y, Wang X, Jiang R, Wang J, Fang Y, Gao J, and Hwang KC. Nanoparticle drug delivery systems and their applications as targeted therapies for triple negative breast cancer. Progress in Materials Science 2023 Apr; 134:101070. DOI: 10.1016/j.pmatsci.2023.101070. Available from: https://doi.org/10.1016/j.pmatsci.2023.101070

53. Schmid P, Cortes J, Pusztai L, McArthur H, Kümmel S, Bergh J, Denkert C, Park YH, Hui R, Harbeck N, Takahashi M, Foukakis T, Fasching PA, Cardoso F, Untch M, Jia L, Karantza V, Zhao J, Aktan G, Dent R, and O'Shaughnessy J. Pembrolizumab for Early Triple-Negative Breast Cancer. New England Journal of Medicine 2020 Feb; 382:810–21. DOI: 10.1056/nejmoa1910549. Available from: https://doi.org/10.1056/nejmoa1910549

54. Cortes J et al. Pembrolizumab plus chemotherapy versus placebo plus chemotherapy for previously untreated locally recurrent inoperable or metastatic triple-negative breast cancer (KEYNOTE-355): a randomised, placebo-controlled, double-blind, phase 3 clinical trial. The Lancet 2020 Dec; 396:1817–28. DOI: 10.1016/s0140-6736(20)32531-9. Available from: https://doi.org/10.1016/s0140-6736(20)32531-9

55. Keam SJ. Tremelimumab: First Approval. Drugs 2022 Dec; 83:93–102. DOI: 10.1007/s40265-022-01827-8. Available from: https://doi.org/10.1007/s40265-022-01827-8

56. Vikas P, Borcherding N, and Zhang W. The clinical promise of immunotherapy in triple-negative breast cancer. Cancer Management and Research 2018 Dec; Volume 10:6823–33. DOI: 10.2147/cmar.s185176. Available from: https://doi.org/10.2147/cmar.s185176

57. Liyanage PY, Hettiarachchi SD, Zhou Y, Ouhtit A, Seven ES, Oztan CY, Celik E, and Leblanc RM. Nanoparticle-mediated targeted drug delivery for breast cancer treatment. Biochimica et Biophysica Acta (BBA) - Reviews on Cancer 2019 Apr; 1871:419–33. DOI: 10.1016/j.bbcan.2019.04.006. Available from: https://doi.org/10.1016/j.bbcan.2019.04.006

58. Mirza Z and Karim S. Nanoparticles-based drug delivery and gene therapy for breast cancer: Recent advancements and future challenges. Seminars in Cancer Biology 2021 Feb; 69:226–37. DOI: 10.1016/j.semcancer.2019.10.020. Available from: https://doi.org/10.1016/j.semcancer.2019.10.020

59. Zeglinski M, Ludke A, Jassal DS, and Singal PK. Trastuzumab-induced cardiac dysfunction: A 'dual-hit'. en. Exp. Clin. Cardiol. 2011; 16:70–4

60. MEI XG and YANG MY. Drug delivery system for active brain targeting. *Artificial Cells, Cell Engineering and Therapy*. Elsevier, 2007 :404–23. DOI: 10.1533/9781845693077.4.404. Available from: https://doi.org/10.1533/9781845693077.4.404

61. Calzoni E, Cesaretti A, Polchi A, Michele AD, Tancini B, and Emiliani C. Biocompatible Polymer Nanoparticles for Drug Delivery Applications in Cancer and Neurodegenerative Disorder Therapies. Journal of Functional Biomaterials 2019 Jan; 10:4. DOI: 10.3390/jfb10010004. Available from: https://doi.org/10.3390/jfb10010004

62. Sahoo SK and Labhasetwar V. Nanotech approaches to drug delivery and imaging. Drug Discovery Today 2003 Dec; 8:1112–20. DOI: 10.1016/s1359-6446(03)02903-9. Available from: https://doi.org/10.1016/s1359-6446(03)02903-9

63. Abdel-Mageed HM, AbuelEzz NZ, Radwan RA, and Mohamed SA. Nanoparticles in nanomedicine: a comprehensive updated review on current status, challenges and emerging opportunities. Journal of Microencapsulation 2021 Jul; 38:414–36. DOI: 10.1080/02652048.2021.1942275. Available from: https://doi.org/10.1080/02652048.2021.1942275

64. Doane TL and Burda C. The unique role of nanoparticles in nanomedicine: imaging, drug delivery and therapy. Chemical Society Reviews 2012; 41:2885. DOI: 10.1039/c2cs15260f. Available from: https://doi.org/10.1039/c2cs15260f

65. Xia W, Tao Z, Zhu B, Zhang W, Liu C, Chen S, and Song M. Targeted Delivery of Drugs and Genes Using Polymer Nanocarriers for Cancer Therapy. International Journal of Molecular Sciences 2021 Aug; 22:9118. DOI: 10.3390/ijms22179118. Available from: https://doi.org/10.3390/ijms22179118

66. Clemons TD, Singh R, Sorolla A, Chaudhari N, Hubbard A, and Iyer KS. Distinction Between Active and Passive Targeting of Nanoparticles Dictate Their Overall Therapeutic Efficacy. Langmuir 2018 Nov; 34:15343–9. DOI: 10.1021/acs.langmuir.8b02946. Available from: https://doi.org/10.1021/acs.langmuir.8b02946

67. Shi P, Cheng Z, Zhao K, Chen Y, Zhang A, Gan W, and Zhang Y. Active targeting schemes for nano-drug delivery systems in osteosarcoma therapeutics. Journal of Nanobiotechnology 2023 Mar; 21. DOI: 10.1186/s12951-023-01826-1. Available from: https://doi.org/10.1186/s12951-023-01826-1

68. Patel JK and Patel AP. Passive Targeting of Nanoparticles to Cancer. *Surface Modification of Nanoparticles for Targeted Drug Delivery*. Springer International Publishing, 2019 :125–43. DOI: 10.1007/978-3-030-06115-9_6. Available from: https://doi.org/10.1007/978-3-030-06115-9_6

69. Vaughan HJ, Green JJ, and Tzeng SY. Cancer-Targeting Nanoparticles for Combinatorial Nucleic Acid Delivery. Advanced Materials 2019 Jun; 32. DOI: 10.1002/adma.201901081. Available from: https://doi.org/10.1002/adma.201901081

70. Pérez-Herrero E and Fernández-Medarde A. Advanced targeted therapies in cancer: Drug nanocarriers, the future of chemotherapy. European Journal of Pharmaceutics and Biopharmaceutics 2015 Jun; 93:52–79. DOI: 10.1016/j.ejpb.2015.03.018. Available from: https://doi.org/10.1016/j.ejpb.2015.03.018

71. Yang T, Cui FD, Choi MK, Cho JW, Chung SJ, Shim CK, and Kim DD. Enhanced solubility and stability of PEGylated liposomal paclitaxel: In vitro and in vivo evaluation. International Journal of Pharmaceutics 2007 Jun; 338:317–26. DOI: 10.1016/j.ijpharm.2007.02.011. Available from: https://doi.org/10.1016/j.ijpharm.2007.02.011

72. Şalva E, Turan SÖ, Eren F, and Akbuğa J. The enhancement of gene silencing efficiency with chitosan-coated liposome formulations of siRNAs targeting HIF-1α and VEGF. International Journal of Pharmaceutics 2015 Jan; 478:147–54. DOI: 10.1016/j.ijpharm.2014.10.065. Available from: https://doi.org/10.1016/j.ijpharm.2014.10.065

73. GHOSH P, HAN G, DE M, KIM C, and ROTELLO V. Gold nanoparticles in delivery applications. Advanced Drug Delivery Reviews 2008 Aug; 60:1307–15. DOI: 10.1016/j.addr.2008.03.016. Available from: https://doi.org/10.1016/j.addr.2008.03.016

74. Giljohann D, Seferos D, Daniel W, Massich M, Patel P, and Mirkin C. Gold Nanoparticles for Biology and Medicine. Angewandte Chemie International Edition 2010 Apr; 49:3280–94. DOI: 10.1002/anie.200904359. Available from: https://doi.org/10.1002/anie.200904359

75. Kong T, Zeng J, Wang X, Yang X, Yang J, McQuarrie S, McEwan A, Roa W, Chen J, and Xing JZ. Enhancement of Radiation Cytotoxicity in Breast-Cancer Cells by Localized Attachment of Gold Nanoparticles. Small 2008 Sep; 4:1537–43. DOI: 10.1002/smll.200700794. Available from: https://doi.org/10.1002/smll.200700794

76. Kyriakides TR, Raj A, Tseng TH, Xiao H, Nguyen R, Mohammed FS, Halder S, Xu M, Wu MJ, Bao S, and Sheu WC. Biocompatibility of nanomaterials and their immunological properties. Biomedical Materials 2021 Mar; 16:042005. DOI: 10.1088/1748-605x/abe5fa. Available from: https://doi.org/10.1088/1748-605x/abe5fa

77. Idrees H, Zaidi SZJ, Sabir A, Khan RU, Zhang X, and Hassan Su. A Review of Biodegradable Natural Polymer-Based Nanoparticles for Drug Delivery Applications. Nanomaterials 2020 Oct; 10:1970. DOI: 10.3390/nano10101970. Available from: https://doi.org/10.3390/nano10101970

78. Anderson J. Biocompatibility. *Polymer Science: A Comprehensive Reference*. Elsevier, 2012 :363–83. DOI: 10.1016/b978-0-444-53349-4.00229-6. Available from: https://doi.org/10.1016/b978-0-444-53349-4.00229-6

79. Mendes BB, Conniot J, Avital A, Yao D, Jiang X, Zhou X, Sharf-Pauker N, Xiao Y, Adir O, Liang H, Shi J, Schroeder A, and Conde J. Nanodelivery of nucleic acids. Nature Reviews Methods Primers 2022 Apr; 2. DOI: 10.1038/s43586-022-00104-y. Available from: https://doi.org/10.1038/s43586-022-00104-y

80. Zielińska A, Carreiró F, Oliveira AM, Neves A, Pires B, Venkatesh DN, Durazzo A, Lucarini M, Eder P, Silva AM, Santini A, and Souto EB. Polymeric Nanoparticles: Production, Characterization, Toxicology and Ecotoxicology. Molecules 2020 Aug; 25:3731. DOI: 10.3390/molecules25163731. Available from: https://doi.org/10.3390/molecules25163731

81. Sur S, Rathore A, Dave V, Reddy KR, Chouhan RS, and Sadhu V. Recent developments in functionalized polymer nanoparticles for efficient drug delivery system. Nano-Structures & Nano-Objects 2019 Oct; 20:100397. DOI: 10.1016/j.nanoso.2019.100397. Available from: https://doi.org/10.1016/j.nanoso.2019.100397

82. Madej M, Kurowska N, and Strzalka-Mrozik B. Polymeric Nanoparticles - Tools in a Drug Delivery System in Selected Cancer Therapies. Applied Sciences 2022 Sep; 12:9479. DOI: 10.3390/app12199479. Available from: https://doi.org/10.3390/app12199479

83. Gagliardi A, Giuliano E, Venkateswararao E, Fresta M, Bulotta S, Awasthi V, and Cosco D. Biodegradable Polymeric Nanoparticles for Drug Delivery to Solid Tumors. Frontiers in Pharmacology 2021 Feb; 12. DOI: 10.3389/fphar.2021.601626. Available from: https://doi.org/10.3389/fphar.2021.601626

84. Pulingam T, Foroozandeh P, Chuah JA, and Sudesh K. Exploring Various Techniques for the Chemical and Biological Synthesis of Polymeric Nanoparticles. Nanomaterials 2022 Feb; 12:576. DOI: 10.3390/nano12030576. Available from: https://doi.org/10.3390/nano12030576

85. Karlsson J, Vaughan HJ, and Green JJ. Biodegradable Polymeric Nanoparticles for Therapeutic Cancer Treatments. Annual Review of Chemical and Biomolecular Engineering 2018 Jun; 9:105–27. DOI: 10.1146/annurev-chembioeng-060817-084055. Available from: https://doi.org/10.1146/annurev-chembioeng-060817-084055

86. Garg U, Chauhan S, Nagaich U, and Jain N. Current Advances in Chitosan Nanoparticles Based Drug Delivery and Targeting. Advanced Pharmaceutical Bulletin 2019 Jun; 9:195–204. DOI: 10.15171/apb.2019.023. Available from: https://doi.org/10.15171/apb.2019.023

87. Mainini F and Eccles MR. Lipid and Polymer-Based Nanoparticle siRNA Delivery Systems for Cancer Therapy. Molecules 2020 Jun; 25:2692. DOI: 10.3390/molecules25112692. Available from: https://doi.org/10.3390/molecules25112692

88. Zhao M, Cheng JL, Yan JJ, Chen FY, Sheng JZ, Sun DL, Chen J, Miao J, Zhang RJ, Zheng C, and Huang HF. Hyaluronic acid reagent functional chitosan-PEI conjugate with AQP2-siRNA suppressed endometriotic lesion formation. International Journal of Nanomedicine 2016 Mar :1323. DOI: 10.2147/ijn.s99692. Available from: https://doi.org/10.2147/ijn.s99692

89. Rai R, Alwani S, and Badea I. Polymeric Nanoparticles in Gene Therapy: New Avenues of Design and Optimization for Delivery Applications. Polymers 2019 Apr; 11:745. DOI: 10.3390/polym11040745. Available from: https://doi.org/10.3390/polym11040745

90. Rahman M and Hasan MR. Synthetic Biopolymers. *Polymers and Polymeric Composites: A Reference Series*. Springer International Publishing, 2019 :1–43. DOI: 10.1007/978-3-319-95990-0_1. Available from: https://doi.org/10.1007/978-3-319-95990-0_1

91. VASIR J and LABHASETWAR V. Biodegradable nanoparticles for cytosolic delivery of therapeutics. Advanced Drug Delivery Reviews 2007 Aug; 59:718–28. DOI: 10.1016/j.addr.2007.06.003. Available from: https://doi.org/10.1016/j.addr.2007.06.003

92. Shenoy DB and Amiji MM. Poly(ethylene oxide)-modified poly(ε-caprolactone) nanoparticles for targeted delivery of tamoxifen in breast cancer. International Journal of Pharmaceutics 2005 Apr; 293:261–70. DOI: 10.1016/j.ijpharm.2004.12.010. Available from: https://doi.org/10.1016/j.ijpharm.2004.12.010

93. Pandey SK, Patel DK, Maurya AK, Thakur R, Mishra DP, Vinayak M, Haldar C, and Maiti P. Controlled release of drug and better bioavailability using poly(lactic acid-co-glycolic acid) nanoparticles. International Journal of Biological Macromolecules 2016 Aug; 89:99–110. DOI: 10.1016/j.ijbiomac.2016.04.065. Available from: https://doi.org/10.1016/j.ijbiomac.2016.04.065

94. Conde J, Oliva N, Atilano M, Song HS, and Artzi N. Self-assembled RNA-triple-helix hydrogel scaffold for microRNA modulation in the tumour microenvironment. Nature Materials 2015 Dec; 15:353–63. DOI: 10.1038/nmat4497. Available from: https://doi.org/10.1038/nmat4497

95. Lim LT, Auras R, and Rubino M. Processing technologies for poly(lactic acid). Progress in Polymer Science 2008 Aug; 33:820–52. DOI: 10.1016/j.progpolymsci.2008.05.004. Available from: https://doi.org/10.1016/j.progpolymsci.2008.05.004

96. Luz CM da, Boyles MSP, Falagan-Lotsch P, Pereira MR, Tutumi HR, Oliveira Santos E de, Martins NB, Himly M, Sommer A, Foissner I, Duschl A, Granjeiro JM, and Leite PEC. Poly-lactic acid nanoparticles (PLA-NP) promote physiological modifications in lung epithelial cells and are internalized by clathrin-coated pits and lipid rafts. Journal of Nanobiotechnology 2017 Jan; 15. DOI: 10.1186/s12951-016-0238-1. Available from: https://doi.org/10.1186/s12951-016-0238-1

97. Garlotta D. Journal of Polymers and the Environment 2001; 9:63–84. DOI: 10.1023/a:1020200822435. Available from: https://doi.org/10.1023/a:1020200822435

98. Rasal RM, Janorkar AV, and Hirt DE. Poly(lactic acid) modifications. Progress in Polymer Science 2010 Mar; 35:338–56. DOI: 10.1016/j.progpolymsci.2009.12.003. Available from: https://doi.org/10.1016/j.progpolymsci.2009.12.003

99. Coolen AL, Lacroix C, Mercier-Gouy P, Delaune E, Monge C, Exposito JY, and Verrier B. Poly(lactic acid) nanoparticles and cell-penetrating peptide potentiate mRNA-based vaccine expression in dendritic cells triggering their activation. Biomaterials 2019 Mar; 195:23–37. DOI: 10.1016/j.biomaterials.2018.12.019. Available from: https://doi.org/10.1016/j.biomaterials.2018.12.019

100. Silva D da, Kaduri M, Poley M, Adir O, Krinsky N, Shainsky-Roitman J, and Schroeder A. Biocompatibility, biodegradation and excretion of polylactic acid (PLA) in medical implants and theranostic systems. Chemical Engineering Journal 2018 May; 340:9–14. DOI: 10.1016/j.cej.2018.01.010. Available from: https://doi.org/10.1016/j.cej.2018.01.010

101. Zaaba NF and Jaafar M. A review on degradation mechanisms of polylactic acid: Hydrolytic, photodegradative, microbial, and enzymatic degradation. Polymer Engineering & Science 2020 Sep; 60:2061–75. DOI: 10.1002/pen.25511. Available from: https://doi.org/10.1002/pen.25511

102. Mahapatro A and Singh DK. Biodegradable nanoparticles are excellent vehicle for site directed in-vivo delivery of drugs and vaccines. Journal of Nanobiotechnology 2011; 9:55. DOI: 10.1186/1477-3155-9-55. Available from: https://doi.org/10.1186/1477-3155-9-55

103. Gorrasi G and Pantani R. Hydrolysis and Biodegradation of Poly(lactic acid). *Synthesis, Structure and Properties of Poly(lactic acid)*. Springer International Publishing, 2017 :119–51. DOI: 10.1007/12_2016_12. Available from: https://doi.org/10.1007/12_2016_12

104. Castañeda-Rodríguez S, González-Torres M, Ribas-Aparicio RM, Prado-Audelo MLD, Leyva-Gómez G, Gürer ES, and Sharifi-Rad J. Recent advances in modified poly (lactic acid) as tissue engineering materials. Journal of Biological Engineering 2023 Mar; 17. DOI: 10.1186/s13036-023-00338-8. Available from: https://doi.org/10.1186/s13036-023-00338-8

105. Maharana T, Mohanty B, and Negi YS. Preparation of Poly(Lactic Acid) Nanoparticles and Optimization of the Particle Size. International Journal of Green Nanotechnology: Physics and Chemistry 2010 Dec; 2:P100–P109. DOI: 10.1080/19430876.2010.532462. Available from: https://doi.org/10.1080/19430876.2010.532462

106. Nobs L, Buchegger F, Gurny R, and Allémann E. Poly(lactic acid) nanoparticles labeled with biologically active Neutravidin™ for active targeting. European Journal of Pharmaceutics and Biopharmaceutics 2004 Nov; 58:483–90. DOI: 10.1016/j.ejpb.2004.04.006. Available from: https://doi.org/10.1016/j.ejpb.2004.04.006

107. Zambaux M. Influence of experimental parameters on the characteristics of poly(lactic acid) nanoparticles prepared by a double emulsion method. Journal of Controlled Release 1998 Jan; 50:31–40. DOI: 10.1016/s0168-3659(97)00106-5. Available from: https://doi.org/10.1016/s0168-3659(97)00106-5

108. Elmowafy EM, Tiboni M, and Soliman ME. Biocompatibility, biodegradation and biomedical applications of poly(lactic acid)/poly(lactic-co-glycolic acid) micro and nanoparticles. Journal of Pharmaceutical Investigation 2019 Apr; 49:347–80. DOI: 10.1007/s40005-019-00439-x. Available from: https://doi.org/10.1007/s40005-019-00439-x

109. Lee BK, Yun Y, and Park K. PLA micro- and nano-particles. Advanced Drug Delivery Reviews 2016 Dec; 107:176–91. DOI: 10.1016/j.addr.2016.05.020. Available from: https://doi.org/10.1016/j.addr.2016.05.020

110. Mattu C, Pabari R, Boffito M, Sartori S, Ciardelli G, and Ramtoola Z. Comparative evaluation of novel biodegradable nanoparticles for the drug targeting to breast cancer cells. European Journal of Pharmaceutics and Biopharmaceutics 2013 Nov; 85:463–72. DOI: 10.1016/j.ejpb.2013.07.016. Available from: https://doi.org/10.1016/j.ejpb.2013.07.016

111. Liu Y, Zhu YH, Mao CQ, Dou S, Shen S, Tan ZB, and Wang J. Triple negative breast cancer therapy with CDK1 siRNA delivered by cationic lipid assisted PEG-PLA nanoparticles. Journal of Controlled Release 2014 Oct; 192:114–21. DOI: 10.1016/j.jconrel.2014.07.001. Available from: https://doi.org/10.1016/j.jconrel.2014.07.001

112. Zhao ZX, Gao SY, Wang JC, Chen CJ, Zhao EY, Hou WJ, Feng Q, Gao LY, Liu XY, Zhang LR, and Zhang Q. Self-assembly nanomicelles based on cationic mPEG-PLA-b-Polyarginine(R15) triblock copolymer for siRNA delivery. Biomaterials 2012 Oct; 33:6793–807. DOI: 10.1016/j.biomaterials.2012.05.067. Available from: https://doi.org/10.1016/j.biomaterials.2012.05.067

113. Xu Z, Wang D, Cheng Y, Yang M, and Wu LP. Polyester based nanovehicles for siRNA delivery. Materials Science and Engineering: C 2018 Nov; 92:1006–15. DOI: 10.1016/j.msec.2018.05.031. Available from: https://doi.org/10.1016/j.msec.2018.05.031

114. Yang XZ, Dou S, Sun TM, Mao CQ, Wang HX, and Wang J. Systemic delivery of siRNA with cationic lipid assisted PEG-PLA nanoparticles for cancer therapy. Journal of Controlled Release 2011 Dec; 156:203–11. DOI: 10.1016/j.jconrel.2011.07.035. Available from: https://doi.org/10.1016/j.jconrel.2011.07.035

115. Mirza Z and Karim S. Advancements in CRISPR/Cas9 technology—Focusing on cancer therapeutics and beyond. Seminars in Cell & Developmental Biology 2019 Dec; 96:13–21. DOI: 10.1016/j.semcdb.2019.05.026. Available from: https://doi.org/10.1016/j.semcdb.2019.05.026

116. Tran P, Lee SE, Kim DH, Pyo YC, and Park JS. Recent advances of nanotechnology for the delivery of anticancer drugs for breast cancer treatment. Journal of Pharmaceutical Investigation 2019 Aug; 50:261–70. DOI: 10.1007/s40005-019-00459-7. Available from: https://doi.org/10.1007/s40005-019-00459-7

117. Navya PN, Kaphle A, Srinivas SP, Bhargava SK, Rotello VM, and Daima HK. Current trends and challenges in cancer management and therapy using designer nanomaterials. Nano Convergence 2019 Jul; 6. DOI: 10.1186/s40580-019-0193-2. Available from: https://doi.org/10.1186/s40580-019-0193-2

118. Hattab D and Bakhtiar A. Bioengineered siRNA-Based Nanoplatforms Targeting Molecular Signaling Pathways for the Treatment of Triple Negative Breast Cancer: Preclinical and Clinical Advancements. Pharmaceutics 2020 Sep; 12:929. DOI:

10.3390/pharmaceutics12100929. Available from: https://doi.org/10.3390/pharmaceutics12100929

119. Shinde SS, Ahmed S, Malik JA, Hani U, Khanam A, Bhat FA, Mir SA, Ghazwani M, Wahab S, Haider N, and Almehizia AA. Therapeutic Delivery of Tumor Suppressor miRNAs for Breast Cancer Treatment. Biology 2023 Mar; 12:467. DOI: 10.3390/biology12030467. Available from: https://doi.org/10.3390/biology12030467

120. Charbe NB, Amnerkar ND, Ramesh B, Tambuwala MM, Bakshi HA, Aljabali AA, Khadse SC, Satheeshkumar R, Satija S, Metha M, Chellappan DK, Shrivastava G, Gupta G, Negi P, Dua K, and Zacconi FC. Small interfering RNA for cancer treatment: overcoming hurdles in delivery. Acta Pharmaceutica Sinica B 2020 Nov; 10:2075–109. DOI: 10.1016/j.apsb.2020.10.005. Available from: https://doi.org/10.1016/j.apsb.2020.10.005

121. Xie Z and Zeng X. DNA/RNA-based formulations for treatment of breast cancer. Expert Opinion on Drug Delivery 2017 Apr; 14:1379–93. DOI: 10.1080/17425247.2017.1317744. Available from: https://doi.org/10.1080/17425247.2017.1317744

122. Polymeric Nanoparticles for Breast Cancer Therapy: A Comprehensive Review. Biointerface Research in Applied Chemistry 2020 Dec; 11:11151–71. DOI: 10.33263/briac114.1115111171. Available from: https://doi.org/10.33263/briac114.1115111171

123. MAR-AGUILAR F, LUNA-AGUIRRE CM, MORENO-ROCHA JC, ARAIZA-CHÁVEZ J, TREVINO V, RODRÍGUEZ-PADILLA C, and RESÉNDEZ-PÉREZ D. Differential expression of miR-21, miR-125b and miR-191 in breast cancer tissue. Asia-Pacific Journal of Clinical Oncology 2012 Jul; 9:53–9. DOI: 10.1111/j.1743-7563.2012.01548.x. Available from: https://doi.org/10.1111/j.1743-7563.2012.01548.x

124. Fridrichova I and Zmetakova I. MicroRNAs Contribute to Breast Cancer Invasiveness. Cells 2019 Oct; 8:1361. DOI: 10.3390/cells8111361. Available from: https://doi.org/10.3390/cells8111361

125. Zhang C, Zhang X, Zhao W, Zeng C, Li W, Li B, Luo X, Li J, Jiang J, Deng B, McComb DW, and Dong Y. Chemotherapy drugs derived nanoparticles encapsulating mRNA encoding tumor suppressor proteins to treat triple-negative breast cancer. Nano Research 2019 Feb; 12:855–61. DOI: 10.1007/s12274-019-2308-9. Available from: https://doi.org/10.1007/s12274-019-2308-9

126. Alonso-Sande M, Rieux A des, Fievez V, Sarmento B, Delgado A, Evora C, Remuñán-López C, Préat V, and Alonso MJ. Development of PLGA-Mannosamine Nanoparticles as Oral Protein Carriers. Biomacromolecules 2013 Oct; 14:4046–52. DOI: 10.1021/bm401141u. Available from: https://doi.org/10.1021/bm401141u

127. Walsh DP, Murphy RD, Panarella A, Raftery RM, Cavanagh B, Simpson JC, O'Brien FJ, Heise A, and Cryan SA. Bioinspired Star-Shaped Poly(l-lysine) Polypeptides: Efficient Polymeric Nanocarriers for the Delivery of DNA to Mesenchymal Stem Cells. Molecular Pharmaceutics 2018 Mar; 15:1878–91. DOI: 10.1021/acs.molpharmaceut.8b00044. Available from: https://doi.org/10.1021/acs.molpharmaceut.8b00044

128. Wang X, Ramström O, and Yan M. Dynamic light scattering as an efficient tool to study glyconanoparticle–lectin interactions. The Analyst 2011; 136:4174. DOI: 10.1039/c1an15469a. Available from: https://doi.org/10.1039/c1an15469a

129. Raval N, Maheshwari R, Kalyane D, Youngren-Ortiz SR, Chougule MB, and Tekade RK. Importance of Physicochemical Characterization of Nanoparticles in Pharmaceutical Product Development. *Basic Fundamentals of Drug Delivery*. Elsevier, 2019 :369–400. DOI: 10.1016/b978-0-12-817909-3.00010-8. Available from: https://doi.org/10.1016/b978-0-12-817909-3.00010-8

130. Bhattacharjee S. DLS and zeta potential – What they are and what they are not? Journal of Controlled Release 2016 Aug; 235:337–51. DOI: 10.1016/j.jconrel.2016.06.017. Available from: https://doi.org/10.1016/j.jconrel.2016.06.017

131. Maver U, Velnar T, Gaberšček M, Planinšek O, and Finšgar M. Recent progressive use of atomic force microscopy in biomedical applications. TrAC Trends in Analytical Chemistry 2016 Jun; 80:96–111. DOI: 10.1016/j.trac.2016.03.014. Available from: https://doi.org/10.1016/j.trac.2016.03.014

132. Takechi-Haraya Y, Goda Y, and Sakai-Kato K. Imaging and size measurement of nanoparticles in aqueous medium by use of atomic force microscopy. Analytical and Bioanalytical Chemistry 2017 Dec; 410:1525–31. DOI: 10.1007/s00216-017-0799-3. Available from: https://doi.org/10.1007/s00216-017-0799-3

133. Farré M and Barceló D. Introduction to the Analysis and Risk of Nanomaterials in Environmental and Food Samples. *Comprehensive Analytical Chemistry*. Elsevier, 2012 :1–32. DOI: 10.1016/b978-0-444-56328-6.00001-3. Available from: https://doi.org/10.1016/b978-0-444-56328-6.00001-3

134. Binnig G, Quate CF, and Gerber C. Atomic Force Microscope. Physical Review Letters 1986 Mar; 56:930–3. DOI: 10.1103/physrevlett.56.930. Available from: https://doi.org/10.1103/physrevlett.56.930

135. Gas B. ELECTROPHORESIS | Principles. *Encyclopedia of Analytical Science*. Elsevier, 2005 :363–70. DOI: 10.1016/b0-12-369397-7/00121-7. Available from: https://doi.org/10.1016/b0-12-369397-7/00121-7

136. Lee PY, Costumbrado J, Hsu CY, and Kim YH. Agarose Gel Electrophoresis for the Separation of DNA Fragments. Journal of Visualized Experiments 2012 Apr. DOI: 10.3791/3923. Available from: https://doi.org/10.3791/3923

137. Koontz L. Agarose Gel Electrophoresis. *Methods in Enzymology*. Elsevier, 2013 :35–45. DOI: 10.1016/b978-0-12-418687-3.00004-5. Available from: https://doi.org/10.1016/b978-0-12-418687-3.00004-5

138. Visser D, Xue D, Ronsky JL, Harder J, and Zernicke RF. Computer-aided optimal design of custom scoliosis braces considering clinical and patient evaluations. en. Comput. Methods Programs Biomed. 2012 Sep; 107:478–89

139. Friedrich J, Seidel C, Ebner R, and Kunz-Schughart LA. Spheroid-based drug screen: considerations and practical approach. Nature Protocols 2009 Feb; 4:309–24. DOI: 10.1038/nprot.2008.226. Available from: https://doi.org/10.1038/nprot.2008.226

140. Carlsson J and Yuhas JM. Liquid-Overlay Culture of Cellular Spheroids. *Spheroids in Cancer Research*. Springer Berlin Heidelberg, 1984 :1–23. DOI: 10.1007/978-3-642-82340-4_1. Available from: https://doi.org/10.1007/978-3-642-82340-4_1

141. Wachsmann P and Lamprecht A. Polymeric Nanoparticles for the Selective Therapy of Inflammatory Bowel Disease. *Methods in Enzymology*. Elsevier, 2012 :377–97. DOI: 10.1016/b978-0-12-391860-4.00019-7. Available from: https://doi.org/10.1016/b978-0-12-391860-4.00019-7

142. Berridge M and Tan A. Characterization of the Cellular Reduction of 3-(4, 5-dimethylthiazol-2-yl)-2, 5-diphenyltetrazolium bromide (MTT): Subcellular Localization, Substrate Dependence, and Involvement of Mitochondrial Electron Transport in MTT Reduction. Archives of Biochemistry and Biophysics 1993 Jun; 303:474–82. DOI: 10.1006/abbi.1993.1311. Available from: https://doi.org/10.1006/abbi.1993.1311

143. Kuete V, Karaosmanoğlu O, and Sivas H. Anticancer Activities of African Medicinal Spices and Vegetables. *Medicinal Spices and Vegetables from Africa*. Elsevier, 2017 :271–97. DOI: 10.1016/b978-0-12-809286-6.00010-8. Available from: https://doi.org/10.1016/b978-0-12-809286-6.00010-8

144. McKinnon KM. Flow Cytometry: An Overview. Current Protocols in Immunology 2018 Jan; 120. DOI: 10.1002/cpim.40. Available from: https://doi.org/10.1002/cpim.40

145. Rost F. Fluorescence Microscopy, Applications. *Encyclopedia of Spectroscopy and Spectrometry*. Elsevier, 2017 :627–31. DOI: 10.1016/b978-0-12-803224-4.00147-3. Available from: https://doi.org/10.1016/b978-0-12-803224-4.00147-3

146. Melanthota SK, Kistenev YV, Borisova E, Ivanov D, Zakharova O, Boyko A, Vrazhnov D, Gopal D, Chakrabarti S, K SP, and Mazumder N. Types of spectroscopy and microscopy techniques for cancer diagnosis: a review. Lasers in Medical Science 2022 Jul; 37:3067–84. DOI: 10.1007/s10103-022-03610-3. Available from: https://doi.org/10.1007/s10103-022-03610-3

147. Mazumdar S, Chitkara D, and Mittal A. Exploration and insights into the cellular internalization and intracellular fate of amphiphilic polymeric nanocarriers. Acta Pharmaceutica Sinica B 2021 Apr; 11:903–24. DOI: 10.1016/j.apsb.2021.02.019. Available from: https://doi.org/10.1016/j.apsb.2021.02.019

148. Honary S and Zahir F. Effect of Zeta Potential on the Properties of Nano-Drug Delivery Systems - A Review (Part 2). Tropical Journal of Pharmaceutical Research 2013 May; 12. DOI: 10.4314/tjpr.v12i2.20. Available from: https://doi.org/10.4314/tjpr.v12i2.20

149. Lu GW and Gao P. Emulsions and Microemulsions for Topical and Transdermal Drug Delivery. *Handbook of Non-Invasive Drug Delivery Systems*. Elsevier, 2010 :59–94. DOI: 10.1016/b978-0-8155-2025-2.10003-4. Available from: https://doi.org/10.1016/b978-0-8155-2025-2.10003-4

150. Gaikwad VL, Choudhari PB, Bhatia NM, and Bhatia MS. Characterization of pharmaceutical nanocarriers: in vitro and in vivo studies. *Nanomaterials for Drug Delivery and Therapy*. Elsevier, 2019 :33–58. DOI: 10.1016/b978-0-12-816505-8.00016-3. Available from: https://doi.org/10.1016/b978-0-12-816505-8.00016-3

151. Clogston JD and Patri AK. Zeta Potential Measurement. *Methods in Molecular Biology*. Humana Press, 2010 Oct :63–70. DOI: 10.1007/978-1-60327-198-1_6. Available from: https://doi.org/10.1007/978-1-60327-198-1_6

152. Samimi S, Maghsoudnia N, Eftekhari RB, and Dorkoosh F. Lipid-Based Nanoparticles for Drug Delivery Systems. *Characterization and Biology of Nanomaterials for Drug Delivery*. Elsevier, 2019 :47–76. DOI: 10.1016/b978-0-12-814031-4.00003-9. Available from: https://doi.org/10.1016/b978-0-12-814031-4.00003-9

153. Kumar A and Dixit CK. Methods for characterization of nanoparticles. *Advances in Nanomedicine for the Delivery of Therapeutic Nucleic Acids*. Elsevier, 2017 :43–58. DOI: 10.1016/b978-0-08-100557-6.00003-1. Available from: https://doi.org/10.1016/b978-0-08-100557-6.00003-1

154. BASARKAR A, DEVINENI D, PALANIAPPAN R, and SINGH J. Preparation, characterization, cytotoxicity and transfection efficiency of poly(dl-lactide-co-glycolide) and poly(dl-lactic acid) cationic nanoparticles for controlled delivery of plasmid DNA. International Journal of Pharmaceutics 2007 Oct; 343:247–54. DOI: 10.1016/j.ijpharm.2007.05.023. Available from: https://doi.org/10.1016/j.ijpharm.2007.05.023

155. Danaei M, Dehghankhold M, Ataei S, Davarani FH, Javanmard R, Dokhani A, Khorasani S, and Mozafari M. Impact of Particle Size and Polydispersity Index on the Clinical Applications of Lipidic Nanocarrier Systems. Pharmaceutics 2018 May; 10:57. DOI: 10.3390/pharmaceutics10020057. Available from: https://doi.org/10.3390/pharmaceutics10020057

156. Zhang Z, Lee SH, Gan CW, and Feng SS. In Vitro and In Vivo Investigation on PLA–TPGS Nanoparticles for Controlled and Sustained Small Molecule Chemotherapy. Pharmaceutical Research 2008 May; 25:1925–35. DOI: 10.1007/s11095-008-9611-6. Available from: https://doi.org/10.1007/s11095-008-9611-6

157. Tan GR, Feng SS, and Leong DT. The reduction of anti-cancer drug antagonism by the spatial protection of drugs with PLA–TPGS nanoparticles. Biomaterials 2014 Mar; 35:3044–51. DOI: 10.1016/j.biomaterials.2013.12.033. Available from: https://doi.org/10.1016/j.biomaterials.2013.12.033

158. ZHANG Z and FENG S. Nanoparticles of poly(lactide)/vitamin E TPGS copolymer for cancer chemotherapy: Synthesis, formulation, characterization and in vitro drug release. Biomaterials 2006 Jan; 27:262–70. DOI: 10.1016/j.biomaterials.2005.05.104. Available from: https://doi.org/10.1016/j.biomaterials.2005.05.104

159. Schubert J and Chanana M. Coating Matters: Review on Colloidal Stability of Nanoparticles with Biocompatible Coatings in Biological Media, Living Cells and Organisms. Current Medicinal Chemistry 2018 Dec; 25:4553–86. DOI: 10.2174/0929867325666180601101859. Available from: https://doi.org/10.2174/0929867325666180601101859

160. Jin FL, Hu RR, and Park SJ. Improvement of thermal behaviors of biodegradable poly(lactic acid) polymer: A review. Composites Part B: Engineering 2019 May; 164:287–96. DOI: 10.1016/j.compositesb.2018.10.078. Available from: https://doi.org/10.1016/j.compositesb.2018.10.078

161. Prokop A and Davidson JM. Nanovehicular Intracellular Delivery Systems. Journal of Pharmaceutical Sciences 2008 Sep; 97:3518–90. DOI: 10.1002/jps.21270. Available from: https://doi.org/10.1002/jps.21270

162. Senapati S, Upadhyaya A, Dhruw S, Giri D, and Maiti P. Controlled DNA Delivery Using Poly(lactide) Nanoparticles and Understanding the Binding Interactions. The Journal of Physical Chemistry B 2021 Aug; 125:10009–17. DOI: 10.1021/acs.jpcb.1c06520. Available from: https://doi.org/10.1021/acs.jpcb.1c06520

163. Cavaco M, Fraga P, Valle J, Andreu D, Castanho MARB, and Neves V. Development of Breast Cancer Spheroids to Evaluate Cytotoxic Response to an Anticancer Peptide. Pharmaceutics 2021 Nov; 13:1863. DOI: 10.3390/pharmaceutics13111863. Available from: https://doi.org/10.3390/pharmaceutics13111863

164. Leung BM, Lesher-Perez SC, Matsuoka T, Moraes C, and Takayama S. Media additives to promote spheroid circularity and compactness in hanging drop platform. Biomaterials Science 2015; 3:336–44. DOI: 10.1039/c4bm00319e. Available from: https://doi.org/10.1039/c4bm00319e

165. Carver K, Ming X, and Juliano RL. Multicellular Tumor Spheroids as a Model for Assessing Delivery of Oligonucleotides in Three Dimensions. Molecular Therapy - Nucleic Acids 2014 Jan; 3:e153. DOI: 10.1038/mtna.2014.5. Available from: https://doi.org/10.1038/mtna.2014.5

166. Shi B, Xue M, Wang Y, Wang Y, Li D, Zhao X, and Li X. An improved method for increasing the efficiency of gene transfection and transduction. en. Int. J. Physiol. Pathophysiol. Pharmacol. 2018 Apr; 10:95–104

167. Wang T, Larcher L, Ma L, and Veedu R. Systematic Screening of Commonly Used Commercial Transfection Reagents towards Efficient Transfection of Single-Stranded Oligonucleotides. Molecules 2018 Oct; 23:2564. DOI: 10.3390/molecules23102564. Available from: https://doi.org/10.3390/molecules23102564

168. Hussein AS, Abdullah N, and Ahmadun FR. In vitro degradation of poly (D, L-lactide-co-glycolide) nanoparticles loaded with linamarin. IET Nanobiotechnology 2013 Jun; 7:33–41. DOI: 10.1049/iet-nbt.2012.0012. Available from: https://doi.org/10.1049/iet-nbt.2012.0012

A

NPs formulation

Table A.1: Methods for the formulation of polymeric NPs

Method	*Characteristics*	*Advantages*	*Drawbacks*	*Ref*
Precipitation-based	Polymer and drug solution combined with a salting-out agent and colloidal stabiliser under high-speed stirring; Dilution with water leads to NPs formation; NPs harvested via centrifugation or cross-flow filtration.	Reduced tension on loaded proteins; Suitable for heat-sensitive drugs.	Complexity; Process variability; Low drug loading.	[102, 109, 83, 89, 84]
• *Salting-out*				
• *Nanoprecipitation*	Several implementation methods: direct pouring of water into organic solution or vice-versa, gradual drop-wise addition of water into organic solution, and dilution of polymeric dispersed phase. Essential factors: injection rate of organic phase, mixing rate, and organic solvent type.	Easy process; Uniform size; Eco-friendly and non-toxic solvents; Low energy process.	Solvent residues;	[102, 109, 105, 83, 89, 84]
• *Dialysis*	Polymer aggregation by replacing organic solvent with non-solvent.	Uniform size distribution; Biocompatibility; Versatility.	Time consuming; Risk of contamination; Solvent removal.	[109, 89]
Direct compositing	Dissolving or dispersing of drug in an organic phase mixed with the polymer; Suspension sprayed as ultra-fine droplets in dry air flow.	Easy set-up process.	Control of drug distribution.	[109]
• *Spray-drying*				
• *Melting technique*	Drug dispersed within a polymer melt; Drug/polymer melt solidifies through cooling; Cooled melt ground/milled into NPs.	Uniform size and shape distribution.	Drug thermal exposure; Process complexity.	[109]
• *Supercritical fluid*	Two main processes: rapid expansion of supercritical solution (RESS) and rapid expansion of supercritical solution into liquid solvent (RESOLV).	Eco-friendly; High purity NPs; No residual solvents.	RESS: low PLA concentrations; Challenging NPs size and morphology control.	[109, 83, 89]
Other approaches	In microfluidics devices: polymers dissolved in organic solvent, followed by droplet solidification by solvent evaporation, diffusion, or extraction.	Precise process; Uniform and biodegradable NPs; Precise control of drug release.	Complex equipment; Low throughput; Contamination risk; Device clogging.	[109]
• *Microfluidics*				

B

Plate conditions for *in vitro* assays

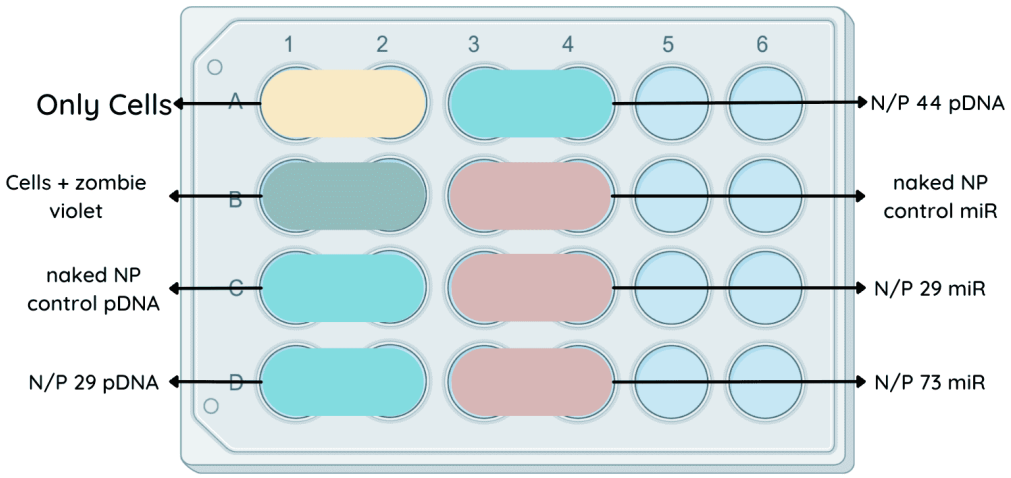

Figure B.1: Plate with the tested conditions in BT-474 2D cell culture for flow cytometry

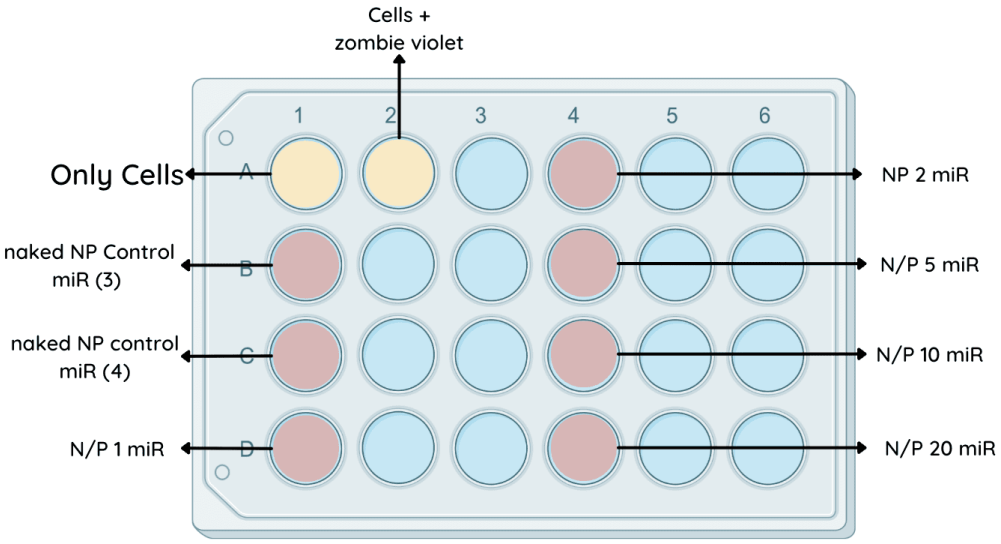

Figure B.2: Plate with tested conditions in SK-BR-3 and MDA-MB-231 2D cell culture of miR-NPs for flow cytometry.

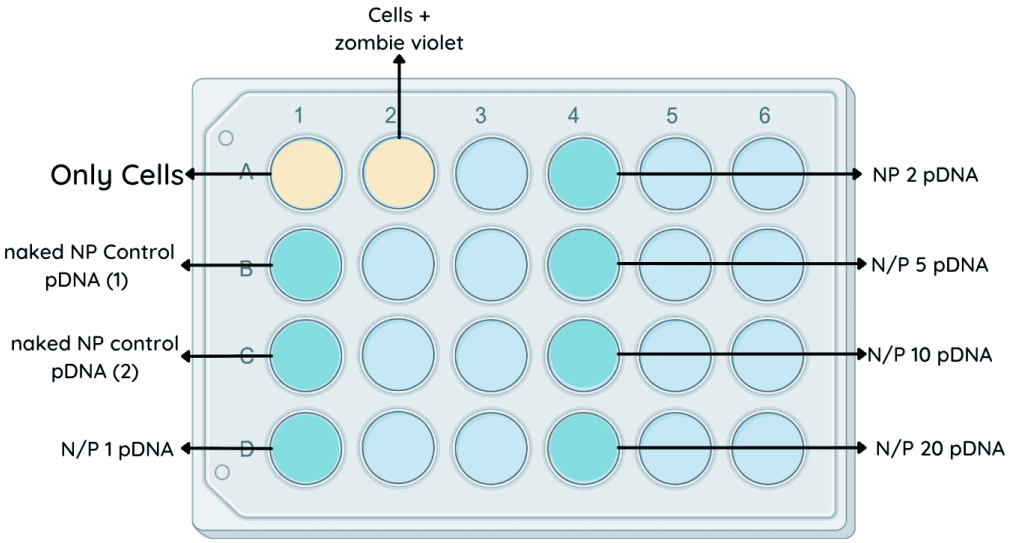

Figure B.3: Plate with the tested conditions in SK-BR-3 and MDA-MB-231 2D cell culture of pDNA-NPs for flow cytometry.

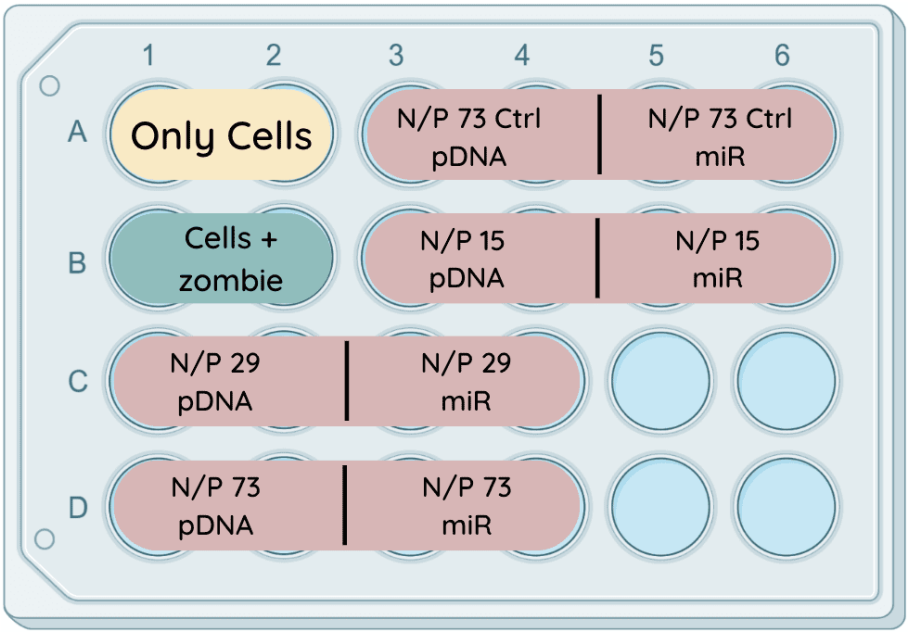

Figure B.4: Plate with the tested conditions in MDA-MB-231 2D cell culture of pDNA- and miR-NPs fluorescently labelled with Rhodamine B for flow cytometry

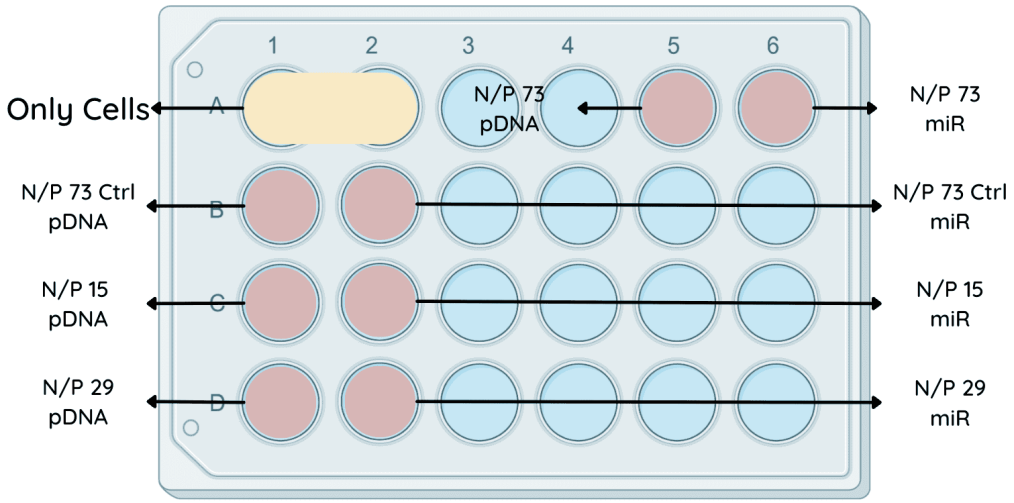

Figure B.5: Plate with the tested conditions in MDA-MB-231 2D cell culture of pDNA- and miR-NPs fluorescently labelled with Rhodamine B for confocal microscopy

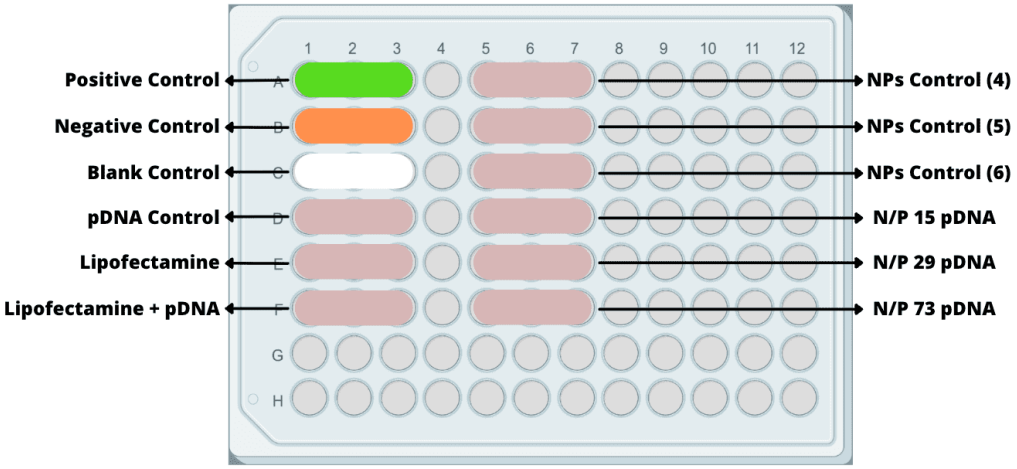

Figure B.6: Plate with the tested conditions in BT-474 3D spheroids of pDNA-NPs for MTT cytotoxic assay.

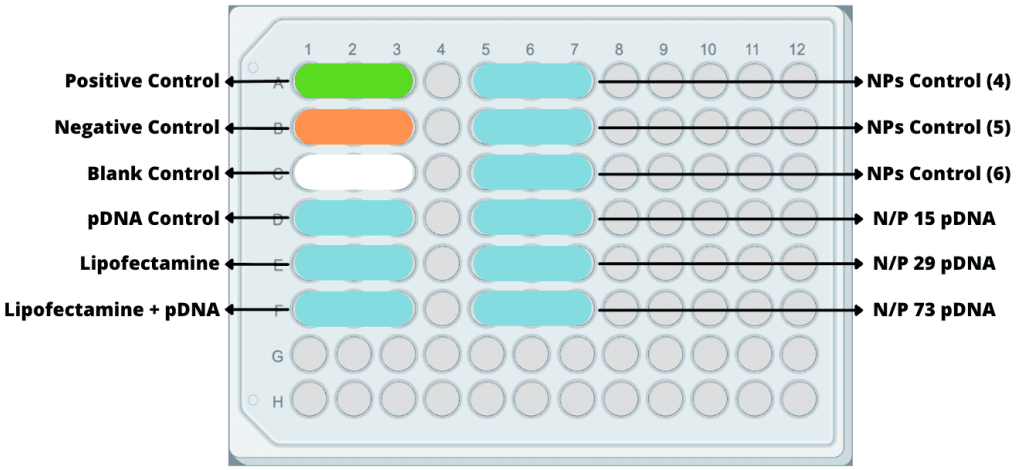

Figure B.7: Plate with the tested conditions in BT-474 3D spheroids of miR-NPs for MTT cytotoxic assay.

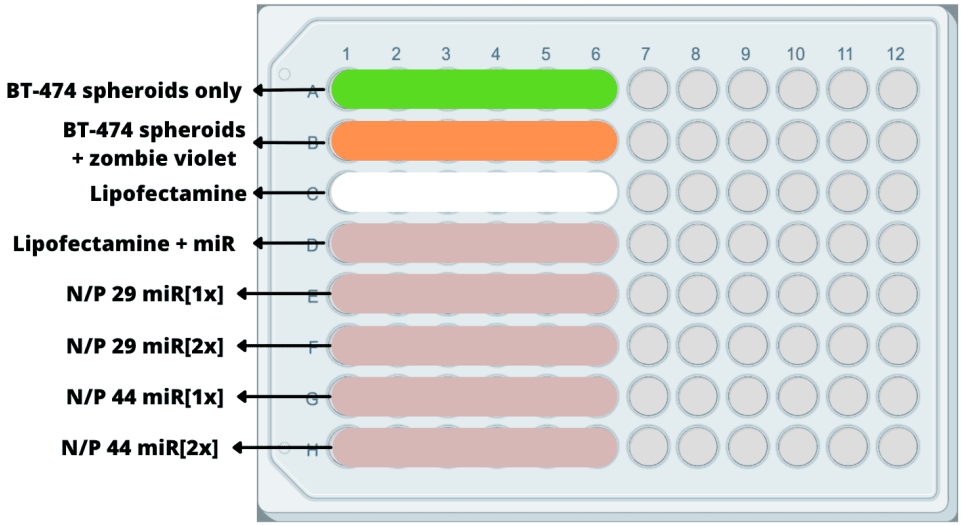

Figure B.8: Plate with the tested conditions in BT-474 3D spheroids of pDNA-NPs for flow cytometry.

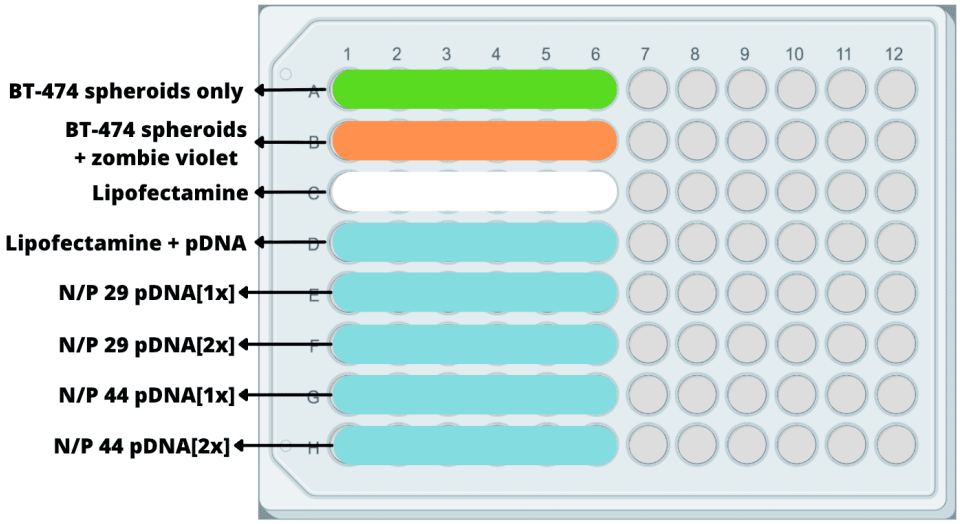

Figure B.9: Plate with the tested conditions in BT-474 3D spheroids of miR-NPs for flow cytometry.

C

Modal distributions of sizes

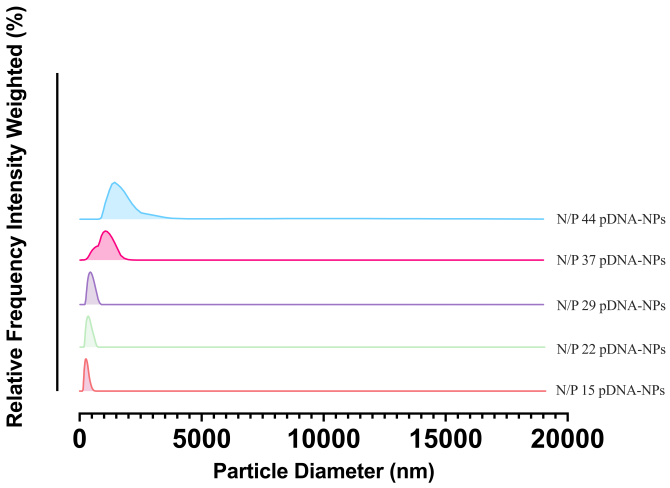

Figure C.1: Modal distribution of sizes of pDNA-NPs in the several ratios tested: N/P 15, N/P 22, N/P 29, 37, and 44

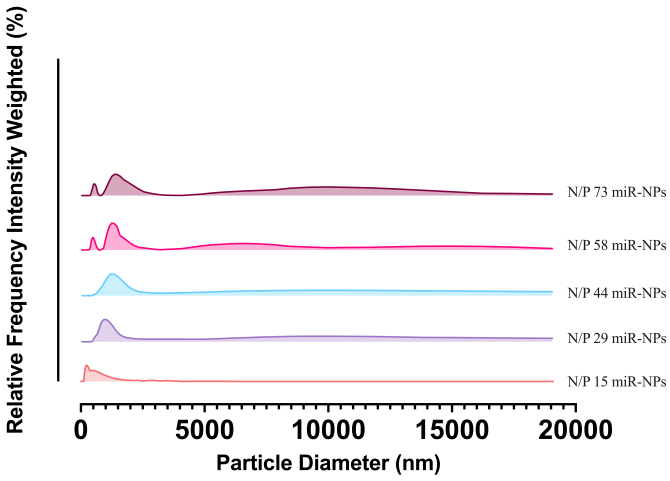

Figure C.2: Modal distribution of sizes of miR-NPs in the several ratios tested: N/P 15, N/P 29, N/P 44, 59, and 73

I

NMR spectroscopy of TPGS-spermidine

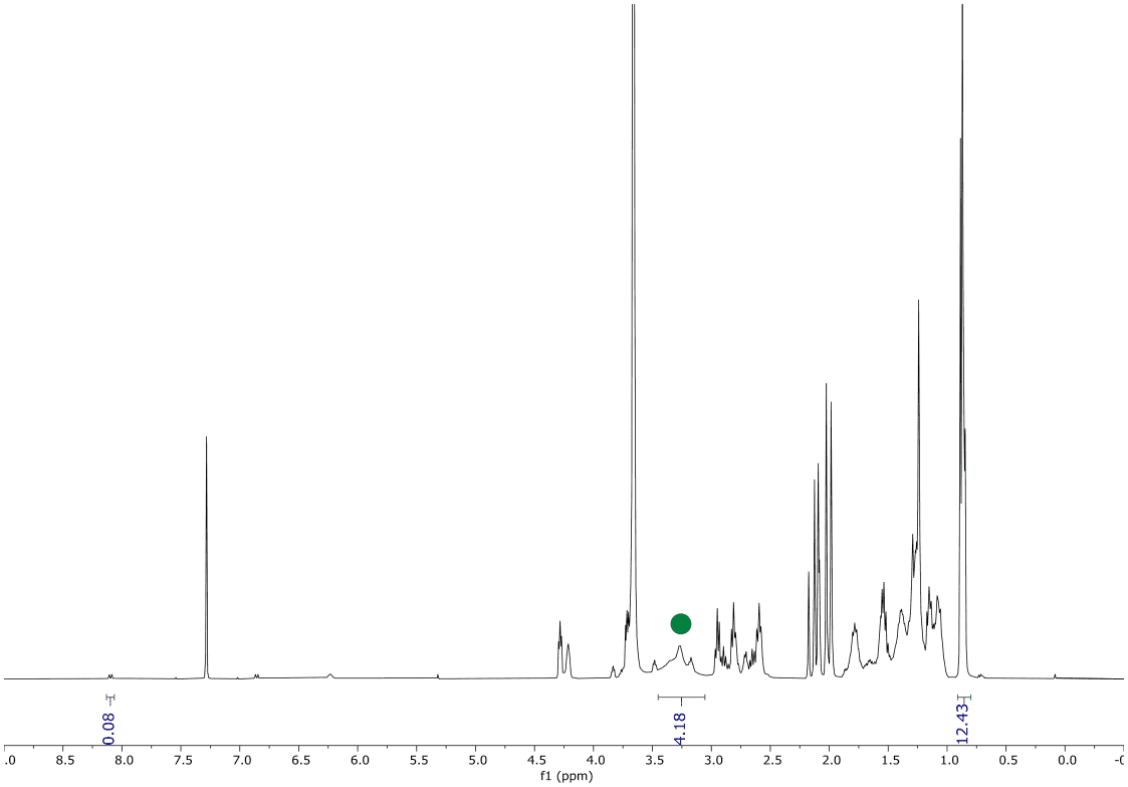

Figure I.1: ^{1}H-NMR spectrum of TPGS-Spermidine